

Electronic Thesis and Dissertation Repository

7-11-2023 2:00 PM

Water-fat magnetic resonance imaging for the assessment of human fetal adipose tissue

Stephanie A. Giza, *Western University*

Supervisor: McKenzie, Charles A., *The University of Western Ontario*

Joint Supervisor: de Vrijer, Barbra, *The University of Western Ontario*

A thesis submitted in partial fulfillment of the requirements for the Doctor of Philosophy degree in Medical Biophysics

© Stephanie A. Giza 2023

Follow this and additional works at: <https://ir.lib.uwo.ca/etd>



Part of the [Medical Biophysics Commons](#)

Recommended Citation

Giza, Stephanie A., "Water-fat magnetic resonance imaging for the assessment of human fetal adipose tissue" (2023). *Electronic Thesis and Dissertation Repository*. 9396.
<https://ir.lib.uwo.ca/etd/9396>

This Dissertation/Thesis is brought to you for free and open access by Scholarship@Western. It has been accepted for inclusion in Electronic Thesis and Dissertation Repository by an authorized administrator of Scholarship@Western. For more information, please contact wlsadmin@uwo.ca.

Abstract

Adipose tissue is crucial for providing heat and energy to infants, especially at transitions such as birth and therefore must begin developing *in utero*. This development may be altered due to an adverse uterine environment, increasing the risk of developing later-life metabolic diseases such as obesity. An early assessment of fetal adipose tissue development through lipid accumulation could be key to understanding metabolic programming and minimizing this risk.

Water-fat magnetic resonance imaging (MRI) can non-invasively measure the lipid concentration of tissues and can therefore monitor the development of adipose tissue via tissue lipid concentration. This work demonstrated the feasibility of measuring fetal adipose tissue volumes and lipid concentrations in the third trimester. Both measures increased with gestational age, indicating this technique is sensitive to the tissue expansion and accumulation of lipids within the adipose tissue, an important improvement over previous MRI techniques limited to volume measures only.

Two water-fat MRI techniques were compared for measuring fetal adipose tissue lipid concentration; modified two-point Dixon and chemical-shift encoded MRI. It was found that the two techniques produced reliable fetal adipose tissue lipid concentration measures; however, only chemical-shift encoded MRI is suitable for assessing the lipid concentration of the fetal liver.

A regional variability of fetal adipose tissue lipid concentrations was found, reflecting the different gestational ages that adipose tissue compartments begin developing. Two compartments that begin development simultaneously but contain one of the two main types of adipose tissue, brown (generates heat) and white (stores energy), also had different lipid concentrations. This is an encouraging result suggesting that water-fat MRI could be used to differentiate fetal brown and white adipose tissues.

In conclusion, this dissertation contains applications of water-fat MRI techniques to assess the lipid concentration of fetal adipose tissue. It highlights factors that affect lipid

concentration, including gestational age and adipose tissue region and type. These factors, and the choice of water-fat MRI technique, are important considerations for future studies aiming to use fetal tissue lipid concentrations to assess fetal metabolic programming.

Keywords

Magnetic resonance imaging, adipose tissue, development, water-fat MRI, chemical-shift encoded MRI, two-point Dixon, proton density fat fraction, pregnancy, fetus

Summary for Lay Audience

Babies born to mothers with diseases like obesity and diabetes that affect how their body processes food are at an increased risk of developing these diseases later in life. Since increases in fat tissue are associated with these diseases, investigating the development of fat tissue before birth may provide information about a baby's risk of developing these diseases. This thesis uses a special magnetic resonance imaging (MRI) technique, water-fat MRI, to measure the amount of fat tissue and the amount of fats within that tissue (fatty content).

Previous ultrasound and MRI techniques only measured the volume of fetal fat tissue, but with water-fat MRI, measuring the fatty content of the fetal fat was also possible. This fatty content increases through pregnancy, as one of the last parts of fetal fat tissue development includes the accumulation of fats in the fat tissue cells.

There are a few ways that water-fat MRI can be performed, and a comparison of two popular techniques is included. Both techniques can be used in the fetal fat tissue, but only one can be used in the fetal liver because of the effects of fetal liver blood cell production on the fatty content measurement.

During fetal fat tissue development, the accumulation of fats in different areas begins at different times during pregnancy. As a result, there was a higher fatty content in areas that begin developing earlier in pregnancy than in those that develop later in pregnancy.

The two main types of fat tissue are brown fat, which produces heat, and white fat, which stores energy. The fatty content was different between these two types of fat tissue.

The research in this thesis highlights the factors that will affect fatty content measurements, including the time during pregnancy and the area and type of fat tissue being measured. These results provide the information necessary to design future studies using water-fat MRI to study fetal fat tissue development, which may eventually provide insight into the development of early risks for later-life diseases affecting how the body processes food.

Co-Authorship Statement

Some sections of Chapter 1 are adapted from “The application of in utero magnetic resonance imaging in the study of the metabolic and cardiovascular consequences of the developmental origins of health and disease” which is published in the Journal of Developmental Origins of Health and Disease and is co-authored by Simran Sethi, Lauren M. Smith, Mary-Ellen E.T. Empey, Lindsay E. Morris, and Charles A. McKenzie. Stephanie Giza was responsible for performing literature reviews and writing the Introduction, Assessment of fetal growth and organ development, Adipose tissue and body composition, and Conclusion Sections, as well as critically revising the manuscript. Simran Sethi was responsible for performing literature reviews and writing the Fetal and placental oximetry section. Lauren Smith was responsible for performing literature reviews and writing the Metabolic MRI section. Mary-Ellen Empey and Lindsay Morris performed literature reviews and contributed to writing the Diffusion, perfusion and flow section. Charles McKenzie provided guidance on interpretation of reviewed literature and critically revised the manuscript. Any paragraphs which are adapted from this published works are taken from the sections written by Stephanie Giza and are identified in Chapter 1.

The work in Chapter 2 titled “Measuring fetal adipose tissue using 3D water-fat magnetic resonance imaging: a feasibility study” is published in the Journal of Maternal-Fetal & Neonatal Medicine and is co-authored by Craig Olmstead, Daniel A. McCooeye, Michael R. Miller, Deborah A. Penava, Genevieve D. Eastabrook, Charles A. McKenzie and Barbra de Vrijer. Stephanie Giza was responsible for assisting with acquiring the MRI images, segmenting all images, assisting with data analysis, and writing the manuscript. Craig Olmstead assisted with acquiring the MRI images. Daniel McCooeye provided a second segmentation to assess inter-rater reliability. Michael Miller provided statistical expertise and assisted with data analysis. Deborah Penava and Genevieve Eastabrook recruited participants and critically revised the manuscript. Charles McKenzie provided guidance on the MRI acquisitions, study design and data analysis and critically revised the manuscript. Barbra de Vrijer provided guidance on study design and interpretation of results, recruited participants, and critically revised the manuscript.

The work in Chapter 3 titled “Comparison of modified two-point Dixon and chemical shift encoded MRI water-fat separation methods for fetal fat quantification” is published in the Journal of Magnetic Resonance Imaging and is co-authored by Michael R. Miller, Prasiddha Parthasarathy, Barbra de Vrijer and Charles A. McKenzie. Stephanie Giza contributed to the study design, assisted with acquiring the MRI images, segmented all images, assisted with data analysis, and wrote the manuscript. Michael Miller provided statistical expertise and assisted with data analysis. Prasiddha Parthasarathy provided a second segmentation to assess inter-rater reliability. Barbra de Vrijer recruited participants and critically revised the manuscript. Charles McKenzie provided guidance on study design, MRI techniques and acquisitions, data analysis and critically revised the manuscript.

The work in Chapter 4 titled “Water-fat magnetic resonance imaging of adipose tissue compartments in the normal third trimester fetus” is published in Pediatric Radiology and is co-authored by Tianna L. Koreman, Simran Sethi, Michael R. Miller, Debbie A. Penava, Genevieve D. Eastabrook, Charles A. McKenzie, Barbra de Vrijer. Stephanie Giza contributed to the study design, assisted with acquiring the MRI images, segmented all images, assisted with data analysis, and wrote the manuscript. Tianna Koreman provided a second segmentation to assess inter-rater reliability, and Simran Sethi assisted with some segmentations. Michael Miller provided statistical expertise and assisted with data analysis. Debbie Penava and Genevieve Eastabrook recruited participants and critically revised the manuscript. Charles McKenzie provided guidance on the MRI acquisitions, study design and data analysis and critically revised the manuscript. Barbra de Vrijer provided guidance on study design and interpretation of results, recruited participants, and critically revised the manuscript.

Dedicated to Marshall and Lorelei.

Acknowledgments

For anyone who has stuck with me since the beginning of my time at grad school, can you believe I am finishing? It has been a long road, and I have grown professionally and personally during this experience. I will carry the lessons I have learned from the people I have worked with for the rest of my life.

I must start by acknowledging my supervisors, Dr. Charles McKenzie and Dr. Barbra de Vrijer. I don't think I will ever be able to fully express my gratitude to you both for working with me for the last eight years. Without you, I would not be the scientist or person I am today.

Charlie, thank you for responding to the nervous undergraduate student that emailed you looking to come to grad school all those years ago. I could not have asked for a better mentor or project. Your encouragement has never failed me; you have believed in me when I have not believed in myself. I will never forget the opportunities you provided to help me grow as a scientist and communicator. Your support of my family and career choices and gently pushing me outside of my comfort zone have helped me during grad school, and I believe it will continue to benefit me in my future pursuits. Thank you for making my Ph.D. studies educational, inspiring, and fun.

Barb, you encouraged me in ways that I didn't know I needed, and I believe I have become a more confident person as a result. Thank you for your patience as I asked many physiology and clinical questions. Thank you for pushing me to improve both my written and oral communications. Thank you for offering your insight into results interpretation and your excitement when designing new research questions with me. I sincerely appreciate the time and energy you put into mentoring me.

Thank you to my advisory committee members, Dr. Tamie Poepping and Dr. Terry Thompson. Your guidance before and throughout my Ph.D. was impactful and appreciated.

I want to thank all the people I have worked with in the McKenzie lab and the Pregnancy Research Group for their support, collaboration, and collegiality. Dr. Lanette Friesen-Waldner, Dr. Trevor Wade, Kevin Sinclair, Dr. Amanda MacCannell, Dr. Lauren Smith,

Daniel McCooeye, Dr. Conrad Rockel, Dr. Alireza Akbari, Dr. Takashi Hashimoto, Dr. Simran Sethi, Mary-Ellen Empey, Lindsay Morris, Dr. Genevieve Eastabrook, Dr. Deborah Penava, Jennifer Ryder, Laura McMurphy, Samantha Bedell, and Dr. Tianna Koreman. Thank you for contributing to my fond memories of my time in grad school.

To my family, thank you for supporting me through this long journey, encouraging me in my moments of doubt, and celebrating my moments of triumph. Mom and Dad, thank you for listening to me talk about my research, reading my papers and thesis introduction, and loving me through it all. My entire life, you both set me up for this success, and now you can finally stop telling people your daughter is still in school!

Gord, I'm not sure what words could convey my appreciation for your support all these years. You have picked me up more than anyone else, kept our house running when I have been too busy, reminded me not to undersell my accomplishments, and never doubted my ability to complete this degree. Together we made it to the end.

To Marshall and Lorelei, thank you for being the reason I thoughtfully considered what I want to do with my life, and thank you for being the reason I was motivated to complete my Ph.D. You have both brought such joy to my life, and I am delighted to dedicate this thesis to you.

Table of Contents

Abstract.....	ii
Summary for Lay Audience.....	iv
Co-Authorship Statement.....	v
Acknowledgments.....	viii
Table of Contents.....	x
List of Tables	xiii
List of Figures.....	xiv
List of Appendices	xviii
List of Symbols, Acronyms and Abbreviations.....	xix
Chapter 1.....	1
1 Introduction.....	1
1.1 Metabolic Health and Programming.....	1
1.2 Fetal Adipose Tissue.....	3
1.2.1 White Adipose Tissue.....	3
1.2.2 Brown Adipose Tissue.....	5
1.3 Adipose Tissue Assessment.....	8
1.3.1 Ultrasound.....	8
1.3.2 Magnetic Resonance Imaging.....	9
1.4 MRI Physics.....	10
1.4.1 MRI Signal Generation and Contrasts	10
1.4.2 Water-fat MRI.....	12
1.4.2.1 Two-point Dixon	12
1.4.2.2 Three-Point Dixon.....	15
1.4.2.3 Modified Two-Point Dixon	15

1.4.2.4	Correction of T1 Bias	16
1.4.2.5	Chemical-Shift Encoded MRI	17
1.5	Fetal Adipose Tissue Imaging	20
1.5.1	Ultrasound Assessment of Fetal Adipose Tissue.....	20
1.5.2	MRI Assessment of Fetal Adipose Tissue	20
1.5.3	Water-Fat MRI for Fetal Adipose Tissue Assessment	23
1.6	Thesis Outline	24
1.7	References.....	25
Chapter 2	33
2	Feasibility of measuring fetal adipose tissue with 3D water-fat separated magnetic resonance imaging.....	33
2.1	Introduction.....	33
2.2	Materials and Methods.....	34
2.3	Results.....	36
2.4	Discussion.....	40
2.5	Conclusions.....	42
2.6	References.....	43
Chapter 3	47
3	Comparison of modified two-point Dixon and chemical shift encoded magnetic resonance imaging water-fat separation methods for fetal fat quantification	47
3.1	Introduction.....	47
3.2	Materials and methods	49
3.3	Results.....	52
3.4	Discussion.....	59
3.5	Conclusions.....	63
3.6	References.....	63
Chapter 4	68

4	Water-fat magnetic resonance imaging of adipose tissue compartments in the third trimester fetus.....	68
4.1	Introduction.....	68
4.2	Materials and Methods.....	70
4.3	Results.....	73
4.4	Discussion.....	79
4.5	Conclusions.....	83
4.6	References.....	83
Chapter 5	86
5	Conclusions.....	86
5.1	Chapter Summaries.....	86
5.2	Thesis Conclusions.....	87
5.3	Thesis Limitations.....	88
5.4	Future Directions.....	91
5.4.1	Increase the signal-to-noise ratio of water-fat MRI for fetal adipose tissue assessment.....	91
5.4.2	Assess the entire gestational period of lipid accumulation in fetal adipose tissue.....	93
5.4.3	Investigate differences between different clinical populations.....	94
5.4.4	Measure the fatty acid composition of fetal adipose tissue.....	95
5.5	Significance and Impact.....	96
5.6	References.....	97
Appendices	100
Curriculum Vitae	113

List of Tables

Table 3.1 Participant demographics. Data listed as n (%). Total N = 21. BMI = body mass index.....	50
Table 3.2. Imaging parameters for modified two-point Dixon and CSE-MRI acquisitions...	51
Table 4.1. Participant Demographics. N = 22.....	74
Table 4.2. Size of Compartment Segmentation. Values given as mean \pm standard deviation.	74
Table 4.3. Results of Pearson Correlations and ANCOVA of PDFF with GA for All Compartments. R^2 gives the goodness of fit. The rate of PDFF change with GA (slope \pm standard error) is given to describe the line, and the p-value testing if the rate of PDFF change with GA (slope) is different from zero is listed.....	75
Table 4.4. Results of Pearson Correlations and ANCOVA of $R2^*$ with GA for All Compartments. R^2 gives the goodness of fit. The rate of $R2^*$ change with GA (slope \pm standard error) and $R2^*$ at 30 weeks + 2 days gestation (Y-intercept \pm standard error) are given to describe the line, and the p-value testing if the rate of $R2^*$ change with GA (slope) is different from zero is also listed.	77

List of Figures

Figure 1.1 Schematic of the development of white and brown adipocytes. 5

Figure 1.2 Electron micrograph of developing adipocytes from a newborn rabbit. The developing brown adipocyte is on the left and contains many more mitochondria adjacent to the multiple lipid vacuoles compared to the developing white adipocyte on the right, with some small lipid vacuoles and one large lipid vacuole. This figure was reproduced from Hull, D., The structure and function of brown adipose tissue, British Medical Bulletin, 1966, 22(1), pages 92 - 96 [26] by permission of Oxford University Press. See Appendix C for permission. 7

Figure 1.3 Water (blue) and lipid (red) magnetization are shown in the transverse plane. The magnetizations are pointing in the same direction during In Phase and opposite directions in the Opposed Phase. 13

Figure 1.4 Schematic of triglyceride structure and chemical shifts. The peaks are labelled to identify which hydrogen proton on the triglyceride molecule corresponds to which peak. This figure was reproduced from Berglund, J., Ahlström, H., Kullberg, J., Model-based mapping of fat unsaturation and chain length by chemical-shift imaging – phantom validation and in vivo feasibility, Magnetic Resonance in Medicine, 2012, 69(6), pages 1815 - 1827 by permission of John Wiley and Sons. See Appendix D for permission. 18

Figure 2.1. (A) 3D rendering of total fetal adipose tissue, (B) 3D rendering of fTSAT segmentation on total fetal adipose tissue, (C) 2D fTSAT segmentation on fetus with 10 ml lipid volume, and (D) 2D fTSAT segmentation on fetus with 80 ml lipid volume. 3D rendering in panel A shows the distribution of adipose tissue above a 10% FSF threshold. The rendering in B shows a different orientation so that the limbs do not obscure the upper and lower boundaries of the fTSAT segmentation demonstrated in green. Three orthogonal planes of Fast Imaging Employing Steady-state Acquisition (FIESTA) images are shown to reference maternal anatomy, and an axes marker is included to indicate maternal orientation. The 2D images in panels C and D show fetuses that had similar ultrasound EFW percentiles (C = 98%, D = 96%) but different lipid volumes, in part due to differences in the mean FSF (C = 12%, D = 30%). This can be seen as a brighter segmented region in panel D and panel

C. It is also important to note that these fetuses have different GA at MRI (C = 30 weeks and D = 34 + 1 weeks). 2D images are displayed axial to the fetal abdomen to show a comparison of slices through the umbilicus. 37

Figure 2.2. (A) GA versus lipid volume, (B) GA versus mean FSF, (C) custom MRI EFW percentile versus lipid volume, and (D) custom MRI EFW percentile versus mean FSF. A positive correlation was found between GA and lipid volume ($p = 0.007$), between GA and mean FSF ($p=0.005$), and between custom MRI EFW percentile and lipid volume ($p=0.012$). Lipid volume error bars represent a 5% estimated error in lipid volume measurement; some error bars are too small to be visualized. FSF measurement error bars represent the standard deviation of values across slices measured. 39

Figure 3.1. Total fetal fat (A) segmentation on modified two-point Dixon, (B) segmentation on CSE-MRI, (C) 3D rendering from modified two-point Dixon, (D) 3D render from CSE-MRI. Images A and B are displayed axial to the fetal abdomen through the fetal umbilicus. 3D renders C and D are created from the segmentations in A and B. The hands and feet have limited lipid and, therefore, appear incomplete and patchy in the 3D renders. 54

Figure 3.2. Bland-Altman plots of fetal (A) fat volume and (B) PDFF/FSF from modified two-point Dixon and CSE-MRI. The solid black line indicates the mean difference between the techniques (A: -180 mL, B: 3.0%), while the two dashed lines indicate the 95% confidence intervals (A: -380, 20 mL, B: -3.6, 9.5%). This demonstrates that modified two-point Dixon underestimates fetal fat volume while overestimating fetal PDFF/FSF compared with CSE-MRI. 55

Figure 3.3. Comparison of pseudo-fat free and pseudo-fat fetuses. (A) Modified two-point Dixon lipid image without pseudo-fat in the liver, (B) Modified two-point Dixon lipid image showing pseudo-fat in the liver, (C) CSE-MRI PDFF image from the same participant and slice as A, (D) CSE-MRI PDFF image from the same participant and slice as B, (E) CSE-MRI R2* map from the same participant and slice as A, and (F) CSE-MRI R2* map from the same participant and slice as B. Images are displayed axial to the fetal abdomen, with the spherical liver ROI outlined in red. Lipid images have been windowed and levelled to display the signal in the fetal livers. The fat fraction measured in image C (pseudo-fat free) was

6.9%, and in image D (pseudo-fat) was 3.7%. The $R2^*$ measured in image E (pseudo-fat free) was 31 s^{-1} , and in image F (pseudo-fat) was 45 s^{-1} 56

Figure 3.4. Box and whisker plots of fetal liver (A) $R2^*$ values and (B) PDFF measured from CSE-MRI, and (C) GA at MRI for the pseudo-fat and pseudo-fat free groups. Mann-Whitney U-test indicates a significant difference between the groups $R2^*$ values ($p < 0.001$), where the pseudo-fat group has a higher fetal liver $R2^*$ than the pseudo-fat free group. No significant differences were found in the PDFF or GA between the groups ($p = 0.881$, $p = 0.654$). Outliers are shown as circles outside of the box and whisker plots. 57

Figure 3.5. Bland-Altman plot of fetal (A) fat volume and (B) PDFF from CSE-MRI test-retest. The solid black line indicates the mean difference between the acquisitions (A: -50 mL, B: 0.9%), while the two dashed lines indicate the 95% confidence intervals (A: -340, 230 mL, B: -2.4, 4.2%). This demonstrates that there is no proportional bias in the fetal fat volume between the acquisitions, and a small bias (<1%) for higher PDFF measurements in the first CSE-MRI acquisition relative to the second acquisition..... 58

Figure 3.6. Bland-Altman plot of fetal (A) fat volume and (B) PDFF measured by two readers. The solid black line indicates the mean difference between the two readers' measurements (A: 20 mL, B: -0.4%), while the two dashed lines indicate the 95% confidence intervals (A: -480, 520 mL, B: -7.2, 6.4%). This demonstrates that there is no proportional bias between the readers' measurements of fetal fat volume or PDFF..... 59

Figure 4.1. Segmentation of fetal adipose tissue. A. Surface rendering of a female fetus at 32 w 5 d of gestation. B. total fetal adipose tissue. C. Fetal adipose tissue compartment segmentation. The cheeks are shown in *red*, thorax in *blue*, upper arms in *dark green*, forearms in *light green*, abdomen in *orange*, thighs in *dark purple* and lower legs in *light purple*. D. Perirenal adipose tissue compartment segmentation. The perirenal compartment, in *yellow*, is shown within the fetus and identified by *white arrows*..... 72

Figure 4.2. PDFF versus GA. The lines of best fit and individual data points are shown for (A) cheeks, (B) thorax, (C) upper arms, (D) forearms, (E) abdomen, (F) perirenal, (G) thighs, (H) lower legs, and (I) the adipose tissue from the whole body. All compartments except perirenal have PDFFs significantly increasing with GA ($p < 0.001$). The rate of PDFF change

with GA, PDFF at 30 weeks + 2 days of gestation and R^2 for each are given in Table 4.3. The rates of PDFF change with GA are not significantly different between the white adipose tissue compartments ($p = 0.97$), but the PDFFs at 30 weeks + 2 days of gestation are significantly different ($p < 0.0001$), with the cheeks having a much higher PDFF over the GA range studied. The perirenal brown adipose tissue compartment does not have a significantly different rate of PDFF change over GA ($p = 0.21$) compared to the upper arm white adipose tissue compartment, but does have a significantly lower PDFF at 30 weeks + 2 days of gestation ($p < 0.0001$). 76

Figure 4.3. $R2^*$ versus GA. The lines of best fit and individual data points are shown for (A) cheeks, (B) thorax, (C) upper arms, (D) forearms, (E) abdomen, (F) perirenal, (G) thighs, (H) lower legs, and (I) the adipose tissue from the whole body. The thorax, abdomen, lower legs and whole body have rates of $R2^*$ change with GA significantly different from zero ($p < 0.05$). The rate of $R2^*$ change with GA, $R2^*$ at 30 weeks + 2 days of gestation and R^2 for each are given in Table 4.4. The rates of $R2^*$ change with GA are not significantly different between the white adipose tissue compartments ($p = 0.96$), and the $R2^*$ at 30 weeks + 2 days of gestation are significantly different ($p = 0.0002$). The perirenal brown adipose tissue compartment did not have a significantly different rate of $R2^*$ change with GA ($p = 0.08$) or $R2^*$ at 30 weeks + 2 days of gestation ($p = 0.16$) compared to the upper arm white adipose tissue compartment. 78

List of Appendices

Appendix A: Ethics approval notice. Signatures and addresses have been redacted.	100
Appendix B: Waived Permission Request to reproduce paragraphs of content from the Journal of Developmental Origins of Health and Disease.....	101
Appendix C Permission to reprint figure from the British Medical Bulletin in Chapter 1, Figure 1.2. Addresses have been redacted.	101
Appendix D: Permission to reprint figure from the Magnetic Resonance in Medicine in Chapter 1, Figure 1.4. Addresses have been redacted.	103
Appendix E: Permission to reprint article from the Journal of Maternal-Fetal and Neonatal Medicine in Chapter 2. Email addresses, addresses, and phone numbers have been redacted.	106
Appendix F: Permission to reprint article from the Journal of Magnetic Resonance Imaging in Chapter 3. Addresses have been redacted.....	109
Appendix G: Permission to reprint article from Pediatric Radiology in Chapter 4. Addresses have been redacted.....	111

List of Symbols, Acronyms and Abbreviations

ANCOVA	Analysis of covariance
ARC	Autocalibrating reconstruction for cartesian imaging
ATP	Adenosine triphosphate
B_0	Main magnetic field
BMI	Body mass index
CL	Chain length
CSE	Chemical-shift encoded
DOHaD	Developmental origins of health and disease
EFW	Estimated fetal weight
F	Magnitude of lipid magnetization
FIESTA	Fast imaging employing steady-state acquisition
FSF	fat signal fraction
fTSA	fetal trunk subcutaneous adipose tissue
GA	Gestational age
ICC	Intraclass correlation coefficient
IDEAL	Iterative decomposition of water and fat with echo asymmetry and least squares estimation
IOM	Institute of Medicine
LAVA	Liver acceleration volume acquisition
M_F	Proton density of lipid
M_W	Proton density of water
MR	Magnetic resonance
MRI	Magnetic resonance imaging
MRS	Magnetic resonance spectroscopy
ndb	number of double bonds
nmidb	number of methylene interrupted double bonds
PDFF	Proton density fat fraction
ppm	Parts per million
ROI	Region of Interest
S	Signal
SGA	Small for gestational age

SNR	Signal to noise ratio
SOGC	Society of Obstetricians and Gyneacologists of Canada
SSFSE	Single Shot Fast Spin Echo
T	Tesla
TE	Echo time
TR	Repetition time
UCP	Uncoupling protein
W	Magnitude of water magnetization
α	Flip angle
ϕ	Phase errors due to magnetic field inhomogeneities
γ	Gyromagnetic ratio
ΔB_0	Magnetic field inhomogeneity
θ	Phase angle of lipid relative to water
ρ_p	Relative amplitude of the p^{th} lipid peak
σ	Chemical shift between water and lipid
σ_p	Chemical shift of the p^{th} lipid peak

Chapter 1

1 Introduction

Developmental programming of metabolic diseases is the concept that the environment a fetus experiences *in utero* can impact their metabolism for their entire life. Excess adipose tissue is linked to metabolic disorders such as diabetes and obesity. Examining fetal adipose tissue development may provide insight into the prenatal programming of such disorders at a time when interventions can have life-long impact. This thesis provides the building block necessary for the non-invasive measurement of fetal adipose tissue lipid content simultaneously with volume and distribution measurements through water-fat MRI.

This introductory chapter provides information necessary to understand the following thesis chapters. A description of fetal adipose tissue development is given to aid in interpreting the results presented in Chapters 2 and 4. A description of the development of water-fat MRI provides the background necessary to understand the advantages and limitations of the imaging techniques used in this thesis. An overview of ultrasound and magnetic resonance imaging (MRI) studies examining fetal adipose tissue is provided to highlight the knowledge gap this thesis aims to fill.

1.1 Metabolic Health and Programming

Obesity is a major global health problem, with over a third of the World's adult population suffering from overweight or obesity [1]. This number is higher in developed countries and increasing in developing countries [2]. In 2018, 36.3% and 26.8% of Canadian adults were overweight and obese, respectively [3]. Defined by the ratio between an individual's weight and height (body mass index, BMI) exceeding 30 kg/m^2 , obesity is usually associated with increased adipose tissue [1]. Many chronic health conditions are associated with obesity, including type 2 diabetes and cardiovascular disease [1].

With such high rates of obesity and associated metabolic dysfunction in adult populations, we see similarly high rates of obesity and metabolic dysfunction in women

of reproductive age. Poor metabolic health in pregnancy carries risks for both the mother and offspring; however, in this thesis, I will focus on the impact on the offspring.

Maternal obesity and diabetes (both before or during pregnancy) are independently related to birth weight and high infant percent body fat, with an even greater risk when both obesity and diabetes are present [4]. This does not just pose a risk during fetal life and infancy, as offspring of mothers with obesity have an elevated risk of increased adipose tissue through to adulthood [5]. Increased adiposity is related to metabolic dysfunction as early as infancy [6,7], indicating that the adverse metabolic environment a fetus experiences during their gestation affects their metabolic health throughout their lives.

This metabolic programming is often described as part of the developmental origins of health and disease (DOHaD) hypothesis, which suggests that the environment a fetus experiences *in utero* can impact that individual's lifelong health [8]. Alterations in the maternal metabolic environment will alter the metabolic, inflammatory, and epigenetic signals and products passing through the placenta to the fetus, affecting the fetal metabolic environment. For example, the supply of triglyceride precursors, such as free fatty acids and glucose, passed to the fetus will affect the amount of triglyceride a fetus can create and store within their adipose tissue [7]. Thus, maternal conditions such as obesity and diabetes can also affect the development of the fetus and result in alterations in adipose tissue development [7]. A better understanding of the early life development of adipose tissue may help reduce the burden of metabolic health concerns for future generations by aiding in developing strategies to mitigate negative fetal programming. This thesis describes a non-invasive method to study fetal adipose tissue development that can be used for studies aiming to improve metabolic health.*

* Adapted from Giza, S.A., Sethi, S., Smith, L.M., Empey, M.E.T., Morris, L.E., McKenzie, C.A., The application of in utero magnetic resonance imaging in the study of the metabolic and cardiovascular consequences or the developmental origins of health and disease, *Journal of Developmental Origins of Health and Disease*, 2021, 12(2), pages 193-202 by permission of Cambridge University Press. See Appendix B for permission.

1.2 Fetal Adipose Tissue

Fetal adipose tissue is of interest for investigating the effects of developmental programming because it reflects the fetus's energy balance through pregnancy [9]. For instance, fetuses of mothers with diabetes have an increased risk of being born with macrosomia, defined as growth over the 90th percentile for gestational age (GA) or birthweight above 4000g, which has been attributed to an increase in adipose tissue [10]. Changes in adipose tissue may be an early indicator of an altered fetal metabolism that could result in the development of metabolic syndrome later in life.*

Two main types of adipose tissue must be considered, white adipose tissue and brown adipose tissue. Each type comprises connective tissues, blood vessels and adipose cells called adipocytes, but they have different appearances and functions.

1.2.1 White Adipose Tissue

The largest white adipose tissue depot is in subcutaneous adipose tissue, with smaller depots within the body, including visceral adipose tissue in adults. White adipocytes, the primary cell type within white adipose tissue, are large cells that, when fully developed, are dominated by a single large lipid vacuole which occupies nearly 90% of the cell volume [11].

White adipose tissue stores potential energy as triglycerides in these large lipid vacuoles [12]. In times of starvation, white adipose tissue breaks down these triglycerides into glycerol and free fatty acids. The glycerol then travels to the liver, where it is used to make glucose through gluconeogenesis [12]. The free fatty acids are used by skeletal muscle and the heart for oxidative metabolism or sent to the liver to produce ketone bodies which are used for energy in organs including the brain [12].

* Adapted from Giza, S.A., Sethi, S., Smith, L.M., Empey, M.E.T., Morris, L.E., McKenzie, C.A., The application of in utero magnetic resonance imaging in the study of the metabolic and cardiovascular consequences or the developmental origins of health and disease, *Journal of Developmental Origins of Health and Disease*, 2021, 12(2), pages 193-202 by permission of Cambridge University Press. See Appendix B for permission.

White adipose tissue also has an important role as an endocrine organ; it releases factors involved in fat mass regulation and development, blood flow, lipid and cholesterol metabolism and immune system function [13].

While adipose tissue has a bad reputation, it is a vital organ, especially early in life. Humans are the fattest species at birth [12], with 15% of a newborn's body weight contributed by adipose tissue [14]. Human infants have much more white adipose tissue at birth than other species but similar levels of brown adipose tissue [12]. The role of white adipose tissue as an energy storage organ may help explain why humans have evolved to have such a large amount of adipose tissue at birth, as humans have also developed to have a brain with very high energy demands at birth [12]. It has been hypothesized that these two traits are linked and that the large energy reserve in an infant's white adipose tissue can support the significant energy demands of their brain in times of nutritional disruption, such as birth and weaning [12,15]. For infants to have a sizeable adipose tissue reserve ready at birth, adipose tissue development must begin prenatally.

Development begins with the structural subunit of white adipose tissue, the fat lobule, a group of adipocytes with a vascular network surrounded by a membrane [16]. Before 14 weeks gestation, connective tissue is present where this fat lobule will develop, containing multipotent mesenchymal stem cells [16,17]. The earliest signs of fat lobule development occur after 14 weeks in the buccal fat pad when the mesenchymal cells begin to cluster and early blood vessels begin to form [16]. As the capillary network develops, the mesenchymal cells differentiate into unipotent adipoblasts and then preadipocytes, which do not contain lipids at this stage of their development [16,17]. Lipid storage begins around gestational week 16, and multiple small lipid vacuoles are present in the cytoplasm of the preadipocytes [18,16]. At this GA, definitive fat lobules can be seen with light microscopy as the surrounding mesenchyme thickens to form the septa that separate neighbouring fat lobules [16]. As the preadipocytes develop into adipocytes, the lipid vacuoles combine to create a single vacuole that will grow to occupy nearly 90% of the cell volume at maturity [11]. Figure 1.1 shows the cellular development of adipocytes.

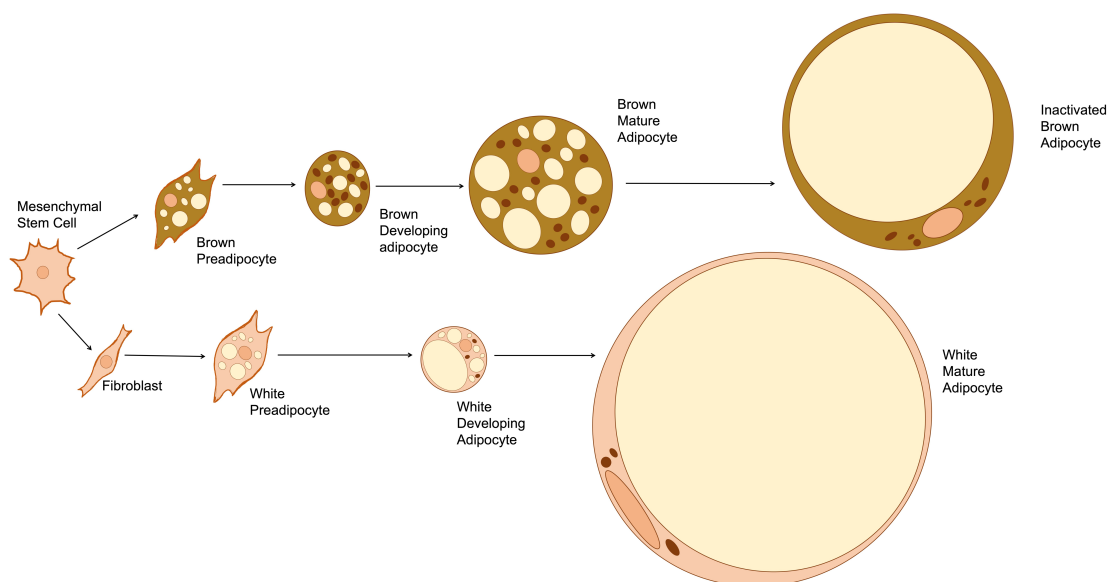


Figure 1.1 Schematic of the development of white and brown adipocytes.

This process begins at different time points in different white adipose tissue regions or compartments [19]. The white adipose tissue begins developing first in the head and neck around 14 weeks gestation, then in different trunk regions from 14.5 – 16 weeks gestation, and finally in the upper and lower limbs from 15 – 16.5 weeks’ gestation [19]. This temporal development is described as “cranial to caudal and proximal to distal” [19,17].

1.2.2 Brown Adipose Tissue

Adults have small deposits of brown adipose tissue located in the axillary, cervical, supraclavicular, and paravertebral regions [20-22], while infants have much more brown adipose tissue located in the axillary, cervical, perirenal and periadrenal regions [23,24]. The primary cell within brown adipose tissue is the brown adipocyte, which contains multiple small lipid vacuoles when activated [25,26]. Brown adipocytes contain many mitochondria, which contribute to the brown colour of the tissue [25,26]. Brown adipose tissue has more blood vessels than white adipose tissue, which also causes the tissue to look brown [26]. This additional blood supply aids in distributing heat via warmed blood,

as the primary role of brown adipose tissue is to produce heat through non-shivering thermogenesis [26]. Brown adipose tissue is especially critical for infants whose primary source of thermoregulation is via non-shivering thermogenesis [27].

Brown adipocytes are activated to create heat using the unique uncoupling protein, UCP-1, which functions within the mitochondria [28]. Typically, an electrochemical gradient is created across the mitochondrial matrix, which is used to generate adenosine triphosphate (ATP). UCP-1 disrupts this electrochemical gradient and dissipates that energy as heat [28]. In addition to containing more blood vessels, brown adipose tissue has more nerves than white adipose tissue because the sympathetic nervous system activates it in response to cold exposure [29].

Developing brown adipocytes look like mature brown adipocytes in that they have multiple small lipid vacuoles surrounded by many mitochondria. While both have multiple small lipid vacuoles, a developing brown adipocyte can be distinguished from a developing white adipocyte because the white adipocyte has fewer mitochondria than the brown adipocyte, and the mitochondria do not lie adjacent to the lipid vacuoles (Figure 1.2) [24-26]. The lipid vacuoles begin combining during white adipocyte development, while the brown adipocyte maintains multiple lipid vacuoles to maturity [25,26]. As early as infancy, MRI has distinguished brown adipose tissue from white adipose tissue because MRI is sensitive to the lower lipid content of brown adipocytes [30-32]. It should be noted that if the mature brown adipose tissue is not activated over long periods, it is also possible for the lipid content of brown adipocytes to increase and the vacuoles to incorporate into a single large vacuole (Figure 1.1) [24-26]. This process is called the whitening of brown adipose tissue and results in the tissue appearing very similar to white adipose tissue [26].

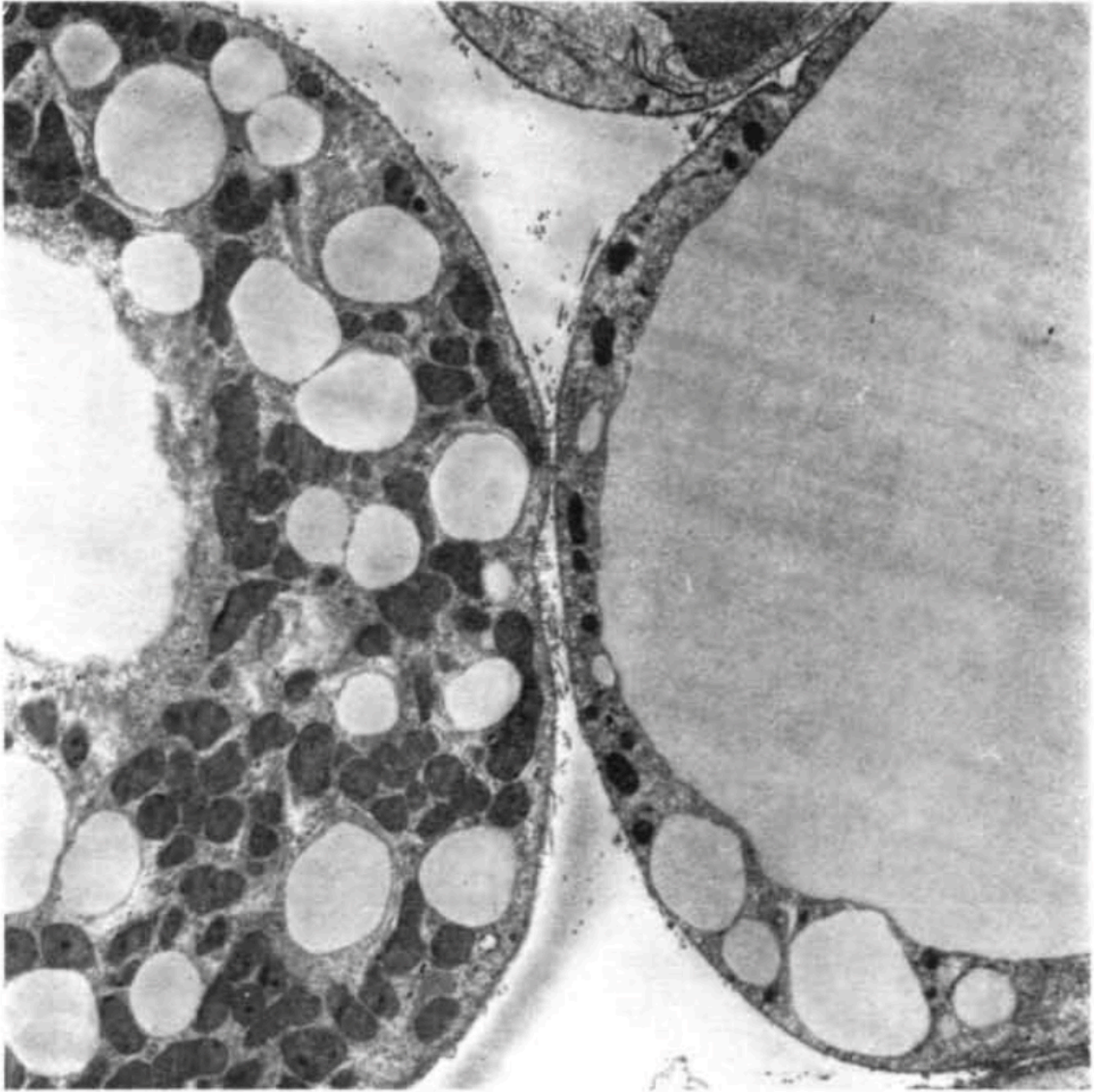


Figure 1.2 Electron micrograph of developing adipocytes from a newborn rabbit. The developing brown adipocyte is on the left and contains many more mitochondria adjacent to the multiple lipid vacuoles compared to the developing white adipocyte on the right, with some small lipid vacuoles and one large lipid vacuole. This figure was reproduced from Hull, D., The structure and function of brown adipose tissue, British Medical Bulletin, 1966, 22(1), pages 92 - 96 [26] by permission of Oxford University Press. See Appendix C for permission.

1.3 Adipose Tissue Assessment

Body composition measurements separate the body into fat mass and fat-free mass compartments. Many techniques can measure fat mass, including anthropometrics such as BMI or skinfold thickness, hydrostatic weighing, air displacement plethysmography, bioelectric impedance analysis, and dual-energy x-ray absorptiometry [33,34]. There are challenges in applying these techniques to pregnant individuals, and while adjustments can be made for pregnancy for many of these techniques, their main limitation is that they do not allow separate assessments of fetal and maternal fat mass [35].

Imaging can assess adipose tissue volume and distribution, with ultrasound and MRI suitable for fetal adipose tissue assessment *in utero* [36]. Other imaging modalities, such as X-ray and computed tomography, are not commonly used in pregnancy due to the risks associated with ionizing radiation [37].

1.3.1 Ultrasound

Ultrasound is frequently used in pregnancy to assess structure, blood flow and limited functional parameters [38]. Its relatively small field of view and typical 2D image acquisition and presentation makes visualization of the entire fetus difficult late in gestation [39]. Despite these limitations, ultrasound is the most common imaging method used to assess fetal development, and it has been applied to assess fetal adipose tissue. The subcutaneous adipose tissue layer is visible on ultrasound, and the tissue's thickness, area and volume can be measured.

Quantitative ultrasound methods to assess the lipid content in the adult liver have been developed, including backscatter and attenuation value [40-43] and hepato-renal attenuation ratio [44,42,43]. These techniques correlate reasonably well to proton density fat fraction (PDFF) [45], a quantitative magnetic resonance measurement, which is considered the noninvasive reference standard for quantifying hepatic lipid [46] and will be discussed further in section 1.4.2.5. Quantitative ultrasound techniques have shown utility in quantifying lipids in the adult liver, but they have not been applied to measuring lipids within adipose tissue or specifically for fetal adipose tissue. Typically, methods used to quantify lipids within a tissue include biopsy, which is far too invasive and risky

to perform in the fetus for research purposes and suffers from sampling error, and MRI, which will be discussed in the following sections.

1.3.2 Magnetic Resonance Imaging

MRI was developed in the 1970s and is used to visualize the internal anatomy and function of the human body [47]. In the 1980s, the technique was applied to visualize the pregnant anatomy and offered a new modality to visualize the fetus and placenta [48]. Safety concerns, including concerns about potential mutagenicity [48], limited the use of MRI in pregnancy for many years. The current use of *in utero* MRI follows guidelines such as those by the American College of Radiology [49]. Recent safety studies have not found an increase in adverse outcomes during pregnancy and early childhood after *in-utero* exposure to MRI if contrast agents are not used [50-52].*

The use of *in utero* MRI is increasing in research and clinical practice, as MRI offers many advantages over other imaging modalities [53]. MRI does not use ionizing radiation and is noninvasive, both of which are crucial in studying fetuses [51]. It is a modality with a large field of view, allowing visualization of the entire pregnant uterus and its content in an image volume [54]. MRI provides excellent soft-tissue contrast and is multi-parametric, allowing the flexibility of providing many sources of contrast in a single examination [55].*

MRI does have limitations such as accessibility [56], cost [57], and barriers to health centers without access to advanced MRI techniques [56], as well as the expertise to use them *in utero*. Furthermore, MRI is a relatively slow imaging technique and is therefore sensitive to maternal and fetal motion, the latter of which is random and unpredictable [58]. When investigating the small anatomy of a developing fetus, partial volumes and spatial resolution can also be limiting. Additionally, the MRI system can limit the

* Adapted from Giza, S.A., Sethi, S., Smith, L.M., Empey, M.E.T., Morris, L.E., McKenzie, C.A., The application of in utero magnetic resonance imaging in the study of the metabolic and cardiovascular consequences or the developmental origins of health and disease, *Journal of Developmental Origins of Health and Disease*, 2021, 12(2), pages 193-202 by permission of Cambridge University Press. See Appendix B for permission.

patient's size that can be imaged, particularly in the late second and third trimesters. The increasing availability of larger bore MRI systems (≥ 70 cm bore) alleviates this issue. Despite these limitations, *in-utero* MRI can provide a wealth of knowledge about fetal growth, development, and programming not previously available.*

1.4 MRI Physics

The following sections review the MRI physics concepts necessary to understand the advantages and disadvantages of the techniques used in this thesis. To that end, a detailed description of water-fat MRI techniques is the focus.

1.4.1 MRI Signal Generation and Contrasts

The most abundant MR visible nuclei in the body are that of hydrogen, also referred to as protons. These hydrogen nuclei have magnetic moments, and when many align with each other, they generate enough of a magnetic field to detect through MRI. These magnetic moments precess around a large magnetic field, such as that of an MRI machine. In aggregate, they align with the main magnetic field of the MRI, generating a net magnetization. To generate an MRI signal, a radiofrequency pulse rotates the magnetization by pushing it out of alignment with the main magnetic field, such that a portion of the net magnetization is in a plane perpendicular to the main magnetic field, called the transverse plane. The transverse magnetization then precesses around the main field, generating a varying electromagnetic field that can be detected with a radiofrequency coil, turning the rotation of the magnetization into an electric signal. The MRI signal is detected during an echo, with the duration of the data collection centered around the echo time (TE). The signal has an amplitude related to the amount of transverse magnetization, and a frequency equal to the precession rate of the magnetization. The properties of this signal are used to generate different contrasts that

* Adapted from Giza, S.A., Sethi, S., Smith, L.M., Empey, M.E.T., Morris, L.E., McKenzie, C.A., The application of in utero magnetic resonance imaging in the study of the metabolic and cardiovascular consequences or the developmental origins of health and disease, *Journal of Developmental Origins of Health and Disease*, 2021, 12(2), pages 193-202 by permission of Cambridge University Press. See Appendix B for permission.

allowing the assessment of structure and function of the body. Before discussing adipose tissue assessment by MRI, three primary sources of contrast in MRI are worth noting: proton density, T1 and T2.

Proton density is the MRI contrast source present in all conventional MR images (excluding MR of other visible nuclei). Proton density is proportional to how many hydrogen atoms the MRI signal comes from in a particular location. The more hydrogen atoms in a given tissue volume, the more signal will be generated from that tissue.

T1 is an MR tissue property. It measures how quickly the hydrogen nuclei return to an unexcited state after a radiofrequency pulse excites them. The signal is generated by exciting hydrogen nuclei with a radiofrequency pulse, then measuring the signal during the time the hydrogen nuclei are returning to a relaxed state. Therefore, when measuring the signal at some time after the radiofrequency pulse, the tissues will have a different amount of signal depending on how quickly they experience T1 relaxation. Tissues with a fast T1 relaxation will have more signal relative to tissue with slower T1 relaxation, and images that use this to generate contrast are referred to as T1-weighted images.

T2 is another MR tissue property. It is related to signal decay stemming from the precession of magnetizations not being exactly the same. A hydrogen nucleus will experience a magnetic field that is the combination of the applied (main) magnetic field and the magnetic fields generated by nearby nuclei. Therefore, as molecules (and therefore nuclei) move around, the local magnetic field experienced by the nuclei will change with time. The precession rate of hydrogen nuclei will briefly change in response to this changing local magnetic field, resulting in the accumulation of phase relative to other nuclei. Phase refers to a magnetic moment's direction in the transverse plane. When nuclei accumulate different phase (since they are all experiencing different local magnetic fields), they become misaligned with each other within the transverse plane resulting in a decrease in the net transverse magnetization. The process of misalignment of the magnetic moments is called dephasing. Techniques using additional radiofrequency pulses or gradients can reverse some dephasing and temporarily increase

the signal. This signal increase is called an echo and occurs at the echo time. Therefore, we collect our data centred on the echo time to avoid some of these dephasing effects.

The main magnetic field also contains spatial inhomogeneities that increase the rate at which the magnetic moments dephase. These inhomogeneities cause an “effective T2” decay, which we call T2* decay. T2 or T2* decay happens more quickly than T1 relaxation. Images that take advantage of T2 or T2* decay are referred to as T2 or T2* weighted images.

1.4.2 Water-fat MRI

Neither ultrasound nor conventional MRI techniques can quantify the lipid within the adipose tissue, but water-fat MRI is a technique that separates the signal in MRI into its parts from water and lipid, allowing lipid quantification.

The bulk of hydrogen MRI signal is from the hydrogens in water and lipids, which are highly abundant in the human body [59]. Due to the different chemical structures of water and lipid and thus different electromagnetic shielding, the hydrogens on the different molecules experience different local magnetic fields, resulting in different precession frequencies [60]. There is a difference of 3.35 parts per million (ppm) between the frequencies of water and lipid [60], called the water-lipid chemical shift.

1.4.2.1 Two-point Dixon

In 1984, Dixon realized that this frequency difference could be used to separate the composite MR signal into water-only and lipid-only parts [59]. After a radiofrequency pulse, the hydrogen magnetizations from water and lipid are in phase, which is to say they are pointing in the same direction (Figure 1.3)[59]. After the radiofrequency pulse, the hydrogen magnetizations can begin precessing around the main magnetic field. Since water and lipid magnetizations precess with different frequencies, they will move from pointing in the same direction to pointing in different directions, eventually pointing in opposite directions, then returning to point back in the same direction, and this will repeat with a period inversely proportional to their chemical shift [59]. When the magnetizations

from water and lipid point in opposite directions, we call this the opposed phase (Figure 1.3) [59].

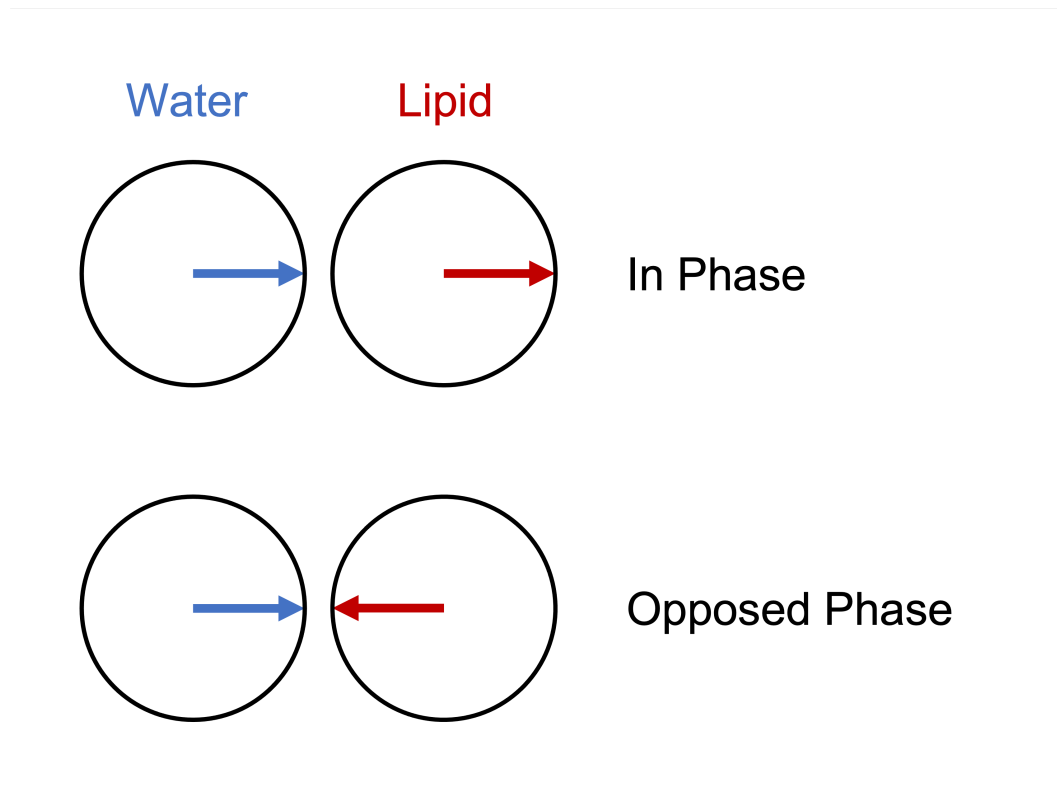


Figure 1.3 Water (blue) and lipid (red) magnetization are shown in the transverse plane. The magnetizations are pointing in the same direction during In Phase and opposite directions in the Opposed Phase.

The signal we detect in MRI is the total magnetization or the vector sum of the water and lipid magnetizations, Eq. 1.1.

$$S = W + F * e^{i\theta} \quad \text{Eq. 1.1}$$

Here S is the acquired signal, W and F and the magnitudes of the magnetizations of water and lipid, and θ is the phase angle of lipid relative to water due to their chemical shift. As the water and lipid magnetizations move from being in-phase ($\theta=0^\circ$) to opposed phase ($\theta=180^\circ$) and repeat, the signal moves through periods of maximum and minimums, again with a period inversely proportional to the chemical shift between water and lipid [59]. If we use images taken at a maximum and minimum of the signal, we have an

image with water and lipid in phase and one with water and lipid in the opposed phase [59]. The in-phase image represents water plus lipid, Eq. 1.2, and the opposed-phase image represents water minus lipid, Eq. 1.3 [59].

$$S_{in\ phase} = (W + F) \quad \text{Eq. 1.2}$$

$$S_{opposed\ phase} = (W - F) \quad \text{Eq. 1.3}$$

We can then add these images to obtain a water-only image, Eq. 1.4, and subtract them to obtain a lipid-only image, Eq. 1.5 [59].

$$S_{in\ phase} + S_{opposed\ phase} = (W + F) + (W - F) = 2 * W \quad \text{Eq. 1.4}$$

$$S_{in\ phase} - S_{opposed\ phase} = (W + F) - (W - F) = 2 * F \quad \text{Eq. 1.5}$$

Once the lipid and water signals have been separated, a fat fraction can be calculated in Eq 1.6 to describe the proportion of the signal that comes from lipids.

$$fat\ fraction = \frac{F}{F+W} \quad \text{Eq. 1.6}$$

The major limitation of this technique is due to magnetic field inhomogeneities [59]. These field inhomogeneities change the phase of the magnetizations, which introduces errors in our water and lipid images when using a simple addition and subtraction method [59]. When included in the signal equation, we have Eq. 1.7:

$$S = (W + F * e^{i\theta}) * e^{i\phi} \quad \text{Eq. 1.7}$$

Here ϕ represents phase errors due to magnetic field inhomogeneities. We can expand the θ and ϕ terms, which have a dependency on the time the echo data is collected, TE:

$$\theta = \gamma * B_0 * \sigma * TE \quad \text{Eq. 1.8}$$

$$\phi = \gamma * \Delta B_0 * TE \quad \text{Eq. 1.9}$$

Here γ is the gyromagnetic ratio of hydrogen, B_0 is the main magnetic field, σ is the chemical shift between water and lipid, and ΔB_0 is the magnetic field inhomogeneity.

Putting these into Eq. 1.7 we get:

$$S = (W + F * e^{i*\gamma*B_0*\sigma*TE}) * e^{i*\gamma*\Delta B_0*TE} \quad \text{Eq. 1.10}$$

This means that when ΔB_0 is not equal to zero, the addition/subtraction of in-phase and opposed-phase images will not provide a clean separation of water and lipid signals. For example:

$$S_{in\ phase} + S_{opposed\ phase} = (W + F) * e^{i*\gamma*\Delta B_0*TE_{in\ phase}} + (W - F) * e^{i*\gamma*\Delta B_0*TE_{opposed\ phase}}$$

Eq. 1.11

1.4.2.2 Three-Point Dixon

A solution to the errors introduced by magnetic field inhomogeneities was presented with three-point Dixon techniques. If another image is collected, solving for ϕ is possible [61-63]. An additional in-phase image is collected with a different TE than the first, then the two in-phase images can be used to calculate phase differences due to magnetic field inhomogeneities [61-63]. That extra phase can be removed from the data, and a simple addition/subtraction can be used as in the original two-point Dixon technique.

Another method accounts for the magnetic field inhomogeneities by estimating the water and lipid signals simultaneously as the magnetic field inhomogeneities [64]. In this technique, the images are collected with three different phase angles between water and lipid; however, the phase angles are not required to be in phase and opposed phase but are flexible [64]. This method calculates W , F , and ϕ using least-squares fitting and an initial ϕ guess, and then calculates the difference between the calculated ϕ and the ϕ guess [64]. The process is repeated with the newly calculated ϕ as the new ϕ guess until the difference in ϕ is below a selected threshold [64]. The most well-known implementation of this technique is termed iterative decomposition of water and fat with echo asymmetry and least squares estimation (IDEAL) [64,65].

1.4.2.3 Modified Two-Point Dixon

Another method to overcome the errors introduced by magnetic field inhomogeneities is modified two-point Dixon [66]. This technique estimates the phase by placing constraints on the amount of phase variation allowed between neighbouring pixels [66]. After

correcting for the phase variation across the image, water and fat are separated by adding or subtracting the in-phase and opposed-phase images [66].

While the three-point Dixon and modified two-point Dixon techniques address the major limitation of the original two-point Dixon, there are still limitations that need to be discussed. The first limitation is that they only use a single lipid frequency, but lipid produces a spectrum of frequencies corresponding to hydrogens at different locations on a triglyceride molecule. Some MRI properties will also bias the fat fraction, including T1 and T2*. The above techniques minimize T1 bias by using a small flip angle and will be discussed next, while the lipid spectrum and T2* limitations will be addressed in Section 1.4.2.5.

1.4.2.4 Correction of T1 Bias

The W and F terms in Eq. 1.10 represent the signal from water and lipid, respectively, which is the proton density of the water and lipid (M_w and M_f , respectively) modulated by a T1-weighting term:

$$W = \frac{M_w (1 - e^{-TR/T1_w}) \sin \alpha}{(1 - e^{-TR/T1_w} \cos \alpha)} \quad \text{Eq. 1.12}$$

$$F = \frac{M_f (1 - e^{-TR/T1_f}) \sin \alpha}{(1 - e^{-TR/T1_f} \cos \alpha)} \quad \text{Eq. 1.13}$$

Here we can see a dependency on T1, TR (repetition time, the time the nuclei are allowed to relax before the next excitation), and flip angle α [67,68]. When using small flip angles, $\cos \alpha$ approaches 1 and $\sin \alpha \cong \alpha$, and we can remove the T1 dependency [69]:

$$W = \frac{M_w (1 - e^{-TR/T1_w}) \alpha}{(1 - e^{-TR/T1_w})} = M_w \quad \text{Eq. 1.14}$$

$$F = \frac{M_f (1 - e^{-TR/T1_f}) \alpha}{(1 - e^{-TR/T1_f})} = M_f \quad \text{Eq. 1.15}$$

Of course, with a small α we are reducing our signal in the process. We find a balance between lowering T1 dependency and receiving a sufficient signal to overcome the noise by using a flip angle of 7° . So far, three-point Dixon and modified two-point Dixon techniques have addressed biases from magnetic field inhomogeneities and T1 relaxation. The lipid spectrum and T2* effects are still biasing the measurement of water and lipid signals.

1.4.2.5 Chemical-Shift Encoded MRI

An expansion of the IDEAL technique described above is generally called chemical-shift encoded (CSE) MRI. This technique collects data during multiple gradient echoes and performs nonlinear curve-fitting through an iterative process to separate the water and lipid signals [70]. It also addresses the biases mentioned above, the multipeak lipid spectrum and T2* decay.

The model uses a multipeak lipid frequency spectrum, which is crucial for correctly identifying the signal from lipids rather than water (Figure 1.4) [71,72]. When using only a single peak, part of the lipid signal is incorrectly assigned as the water signal, as some of the lipid frequency peaks occur nearer to the water frequency than the single lipid frequency used in the Dixon techniques from sections 1.4.2.1 to 1.4.2.3 [72].

Eq. 1.7 can be altered to include the multipeak lipid spectrum:

$$S = (W + F \sum_{p=1}^P \rho_p * e^{i*\gamma*B_0*\sigma_p*TE}) * e^{i*\gamma*\Delta B_0*TE} \quad \text{Eq. 1.16}$$

Here ρ_p is the relative amplitude of the p^{th} lipid peak, and σ_p is the chemical shift of the p^{th} lipid peak[72]. Both the relative amplitudes and the chemical shifts are known *a priori*. The lipid frequency spectrum of the adult liver is used in this model, with six peaks included in the spectrum [72,73].

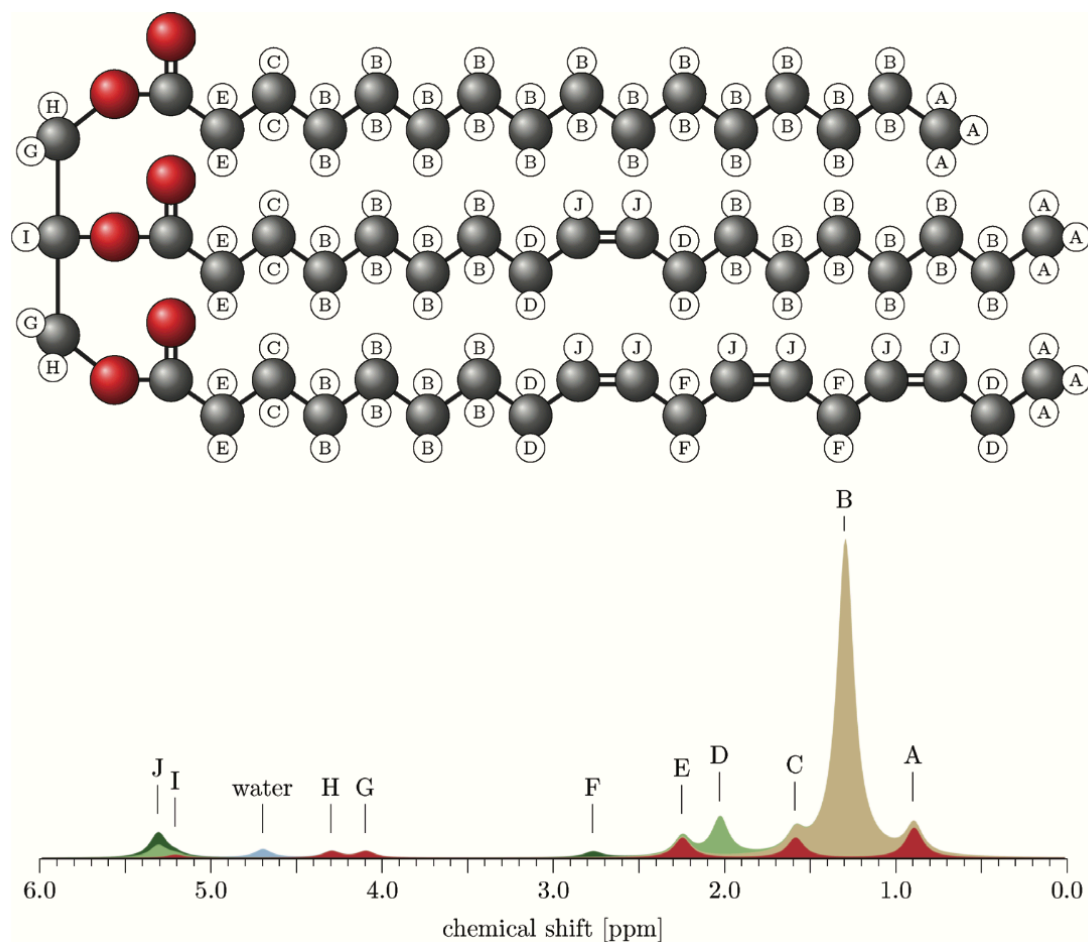


Figure 1.4 Schematic of triglyceride structure and chemical shifts. The peaks are labelled to identify which hydrogen proton on the triglyceride molecule corresponds to which peak. This figure was reproduced from Berglund, J., Ahlström, H., Kullberg, J., Model-based mapping of fat unsaturation and chain length by chemical-shift imaging – phantom validation and in vivo feasibility, *Magnetic Resonance in Medicine*, 2012, 69(6), pages 1815 - 1827 by permission of John Wiley and Sons. See Appendix D for permission.

The other source of bias that CSE-MRI addresses compared to the previous Dixon techniques is that from T_2^* decay. It takes some time to collect multiple gradient echoes; during this time, the magnetization is undergoing T_2^* decay. It is possible to fit this decay simultaneously with the fitting of W , F and ΔB_0 (magnetic field inhomogeneities).

A single $T2^*$ value is fit for the voxel, and it is combined with the ΔB_0 term as shown in Eq. 1.17:

$$S = \left(W + F \sum_{p=1}^P \rho_p * e^{i*\gamma*B_0*\sigma_p*TE} \right) * e^{i*\gamma*\Delta B_0*TE} * e^{-TE/T2^*} \quad \text{Eq. 1.17}$$

$$S = \left(W + F \sum_{p=1}^P \rho_p * e^{i*\gamma*B_0*\sigma_p*TE} \right) * e^{i(\gamma*\Delta B_0 + 1/T2^*)TE} \quad \text{Eq. 1.18}$$

The inverse of $T2^*$ is $R2^*$, giving Eq. 1.19:

$$S = \left(W + F \sum_{p=1}^P \rho_p * e^{i*\gamma*B_0*\sigma_p*TE} \right) * e^{i(\gamma*\Delta B_0 + iR2^*)TE} \quad \text{Eq. 1.19}$$

Now the $\Delta B_0/R2^*$ term is fit to the data yielding a complex field map, which is then decomposed into its magnitude ($R2^*$) and phase (ΔB_0) components. Ultimately, CSE-MRI provides four images: water, lipid, ΔB_0 , and $R2^*$.

When all these sources of bias are addressed, the fat fraction measured by CSE-MRI is equivalent to that measured with spectroscopy, which is considered the non-invasive reference standard [74].

Using Eq. 1.6, 1.14, and 1.15, the fat fraction then becomes:

$$\text{fat fraction} = \frac{F}{F+W} = \frac{M_f \alpha}{M_f \alpha + M_w \alpha} = \frac{M_f}{M_f + M_w} = \text{PDFF} \quad \text{Eq. 1.20}$$

In this case, with these sources of bias addressed, the measured fat fraction is equal to the PDFF [75]. PDFF is defined as the “ratio of the density of mobile protons from triglycerides and the total density of protons from mobile triglycerides and mobile water” [75]. PDFF is considered the standardized MR-based biomarker of tissue lipid concentration as it is accurate, precise, robust and reproducible [75]. It is a validated measure of the MR visible lipid within tissues and ranges from 0 to 100%.

The acquisition used in this thesis acquires six spoiled gradient echoes with a spacing that has been determined to maximize the signal-to-noise ratio (SNR) [71]. These echoes are acquired in 2 shots of 3 echoes [71] with parallel imaging acceleration to allow 3D acquisition of the entire uterus within a single breath hold. Parallel imaging reduces the amount of data necessary to reconstruct an image, therefore reducing the imaging time [76]. As seen in Eq 1.20, PDFF does not depend on imaging parameters such as TR, TE,

and slice thickness; therefore, these parameters can be adjusted to allow coverage of the entire uterus in a breath hold manageable for most participants.

1.5 Fetal Adipose Tissue Imaging

In this section, I will describe some of the literature that used ultrasound or MRI to assess fetal adipose tissue.

1.5.1 Ultrasound Assessment of Fetal Adipose Tissue

Ultrasound has been used to measure fetal adipose tissue's thickness, area and volume on the thighs, arms and abdomen (reviewed in [77]). Bernstein *et al.* examined lean and adipose tissues from 19 to 40 weeks gestation and found that in the extremities, both lean and adipose tissue areas had accelerating growth, with adipose tissue area undergoing a 10-fold increase over the investigated period [78].

Ultrasound measures of fetal adipose tissue have been used to study adipose tissue in fetal growth restriction and macrosomia, as well as in maternal conditions such as diabetes and obesity. While these studies have provided information on the amount of tissue through measures of thickness, area, or volume, they do not quantify the lipid content of the tissue.

1.5.2 MRI Assessment of Fetal Adipose Tissue

In the 1980s, the earliest reports of MR images in pregnancy include a description of visible fetal adipose tissue [48,79]. Today, the ability to image adipose tissue, including that of the fetus, has far surpassed these early descriptions. MRI is considered a gold-standard technique for simultaneously measuring the content and distribution of adipose tissue [80]. The assessment of fetal adipose tissue with MRI is described in the following studies.

In 1985, fetal adipose tissue was well visualized on T1 weighted and inversion recovery images, and the thickness could be measured after 32 weeks gestation [81]. A group of fetuses was ranked based on the amount of observed subcutaneous adipose tissue, from most to least adipose tissue. Macrosomic fetuses had the most adipose tissue, while the

two fetuses with the least or no discernible subcutaneous adipose tissue suffered from fetal growth restriction [82]. The most promising result from this study showed a potential for MRI assessment of fetal adipose tissue to differentiate between fetal growth restriction and small for gestational age (SGA). SGA describes a constitutionally small fetus, defined as below the 10th percentile, while fetal growth restriction represents undergrowth relative to the genetic potential of a fetus due to placental dysfunction and/or reduced oxygen and nutrient supply during pregnancy. The two fetuses with SGA appeared to have normal amounts of adipose tissue, falling within the rankings of control fetuses, compared to much lower observable adipose tissue in two fetuses with fetal growth restriction [82].

Fetal adipose tissue quantification was the next step, and in 1989, T1 images were used to measure the fetal adipose tissue volume [83]. The average adipose tissue volume/fetal volume for a group of control fetuses was 17.2% (11.8 - 25%), while in a group of fetuses with diabetic mothers, it was elevated to 27.4% (15.6 – 33.6%), and in a single growth restricted fetus it was reduced to 3.6% [83]. There is some overlap between the control and diabetic groups; however, it still provides evidence that fetal adipose tissue quantification by MRI can detect differences between two metabolically different groups. Later in 1993, T1 weighted images were also used to assess macrosomia, and increased fetal subcutaneous adipose tissue correlated with an increased risk of macrosomia in a group of mothers with diabetes [84].

It was not until 2011 that the next study was published; T1 weighted images were also used to measure the smallest thickness of fetal subcutaneous adipose tissue on the trunk and extremities [85]. The trunk subcutaneous adipose tissue thickness ranged from 2 mm at 29 weeks to 4.5 mm at the end of gestation, while extremities had 2 mm subcutaneous adipose tissue at 29 weeks, which expanded to 6 mm at the end of gestation [85]. They also compared the measurements of this control group to those of a group with mothers who had well-controlled diabetes and found that most of the diabetic group's measurements fell within the values of the control group [85]. Those in the diabetic group that did not fall within the control group had subcutaneous adipose tissue thickness smaller than the control group [85]. These results show that if diabetes is well controlled,

the fetus does not have increased adipose tissue thickness, suggesting that negative fetal programming is reduced.

In 2013, semi-automated segmentation was combined with T1-weighted, water-suppressed images to measure the fetal adipose tissue volume [86]. A pixel-intensity histogram had a bimodal distribution, and the peak not associated with background noise was selected to quantify the fetal adipose tissue [86]. This technique was applied to control fetuses and those with diabetic mothers and found a strong correlation between fetal adipose tissue volume and birthweight centile, with increased amounts of fetal adipose tissue in the diabetic group [86]. They also manually evaluated the presence of intra-abdominal adipose tissue and found that it was identified more frequently in the diabetic group than in controls [86]. Finally, they showed it was possible to combine adipose tissue measurements and fetal volumes with the density of lipid and water to calculate estimated fetal weight (EFW), although they did not report on the accuracy of this EFW calculation [86].

In a 2018 study comparing MRI to histology, T1-weighted images provided information on fetal adipose tissue development. The adipose tissue to muscle T1-weighted signal intensity ratios were measured and increased with GA, with adipose tissue being hypointense relative to adjacent muscle until 29 weeks and hyperintense after that [87]. This finding corresponded to a change in adipose tissue from mostly multivacuolated cells before 29 weeks to mostly univacuolated cells after 29 weeks, as found by histology in a group of control fetuses at autopsy [87]. The adipose tissue to muscle intensity ratio was assessed in multiple locations, including the chin, buttocks, thighs, trunk and scalp, and they all had similar slopes with GA but different intercepts [87]. This result indicates that all the tissues develop at a similar rate (conversion of cells from multivacuolated to univacuolated) but may start this process at different GA, in agreement with previous histology studies [19].

These MRI studies used weighted images to differentiate adipose tissue from surrounding tissues and allow volume measurement. However, the pixel intensity values are not quantitative on their own. Ratios between tissues can be applied, as done in one study,

but interpreting these intensity ratios is complicated. Changes in either tissue can cause the ratio to change; for example, a change in the T1 of muscle or adipose tissue could be responsible for changes in adipose to muscle intensity ratio. Additionally, changes in the T1 of adipose tissue could be due to development other than lipid accumulation since other microenvironment changes could co-occur.

It is clear from both the ultrasound and MRI literature that noninvasive assessment of fetal adipose tissue provides information that could be used clinically or to investigate DOHaD. However, none of the techniques discussed above are directly sensitive to the lipid within the adipose tissue, and this thesis aims to address this gap. Using water-fat MRI to measure the amount of lipid within the tissue rather than the amount of tissue alone may provide additional information that helps us better understand fetal adipose tissue development and how it can be altered.

1.5.3 Water-Fat MRI for Fetal Adipose Tissue Assessment

In this thesis, I aim to use this water-fat MRI to assess human fetal adipose tissue. Additional challenges arise when applying an MRI technique to pregnancy compared to infants, children or adults, including the comfort of our volunteers and motion.

The work included in this thesis investigates fetal adipose tissue during the third trimester (27+ weeks gestation), as it is well known that this is the time when fetal adipose tissue is developing rapidly. Of course, during the third trimester, a pregnant woman's abdomen is larger than in earlier trimesters, making undergoing an MRI more challenging. To increase the comfort of our participants, we used a large bore (70 cm diameter) MRI and worked with the participants to find a comfortable position, have them lay on their side or provide comfort with pillows and wedges for support.

Motion during MRI in pregnancy is a two-part problem, as there are two subjects that can be moving during the image acquisition [58]. Since we are imaging the mother's abdomen, her respiratory motion is a major concern. We addressed maternal respiratory motion by imaging during maternal breath hold and monitored the mother's breathing and breath hold capabilities using a monitor placed around the mother's abdomen. After

imaging 18 participants, we determined that 16 seconds was an acceptable breath-hold time for 95% of our participants and used this as our initial imaging time. The length of breath hold could then be lowered as necessary. Fetal motion is the other major source of motion that must be considered. Fetal motion is unpredictable, but some techniques can be used to reduce its effects. We scheduled our MRI study visits during the afternoon, as this is a time of fetal sleep after lunch. Additionally, we performed 2D acquisitions earlier in the MRI exam as these acquisitions are less motion sensitive, giving the fetus time to become accustomed to the noise and vibration of the MRI and settle down before the more motion-sensitive 3D water-fat MRI acquisition. Finally, our main defense against fetal (and maternal) motion is to image quickly. We used image acceleration techniques to acquire a 3D image covering the entire fetal volume within our 16 second breath hold. All images were viewed during the MRI exam, and any determined to be too degraded by motion were repeated.

1.6 Thesis Outline

Throughout this thesis, I will use water-fat MRI to assess the lipid content of fetal adipose tissue. At the onset of this work, I found no other studies that provided a non-invasive method to measure the lipid content of adipose tissue during the fetal period, and I believe such a method will prove useful for the investigations into fetal metabolic health and programming.

In Chapter 2, I examine the feasibility of using water-fat separated MRI to measure fetal adipose tissue. I used modified two-point Dixon imaging to measure fetal trunk adipose tissue's fat signal fraction (FSF) during the third trimester. This work contains the first description of a change in the fat fraction of fetal adipose tissue with increasing gestation, as previous methods did not use water-fat separated techniques.

In Chapter 3, I examine whether there are differences in the fat fraction measured using modified two-point Dixon or with CSE-MRI. I demonstrate that the fat fraction measured in fetal subcutaneous adipose tissue is comparable between the methods during the third trimester. A false lipid signal from the fetal liver was seen when using a modified two-point Dixon that was corrected by using CSE-MRI.

In Chapter 4, I demonstrate that CSE-MRI is sensitive to the regional variation in adipose tissue development. The PDFF was assessed in different body compartments during the third trimester, with higher values measured in regions that develop earlier in gestation. This work has promising implications for the identification of brown and white adipose tissue in the fetus using MRI.

In Chapter 5, I summarize the work presented in this thesis and propose future directions.

1.7 References

1. Hruba A, Hu FB (2015) The Epidemiology of Obesity: A Big Picture. *Pharmacoeconomics* 33 (7):673-689. doi:10.1007/s40273-014-0243-x
2. Inoue Y, Qin B, Poti J, Sokol R, Gordon-Larsen P (2018) Epidemiology of Obesity in Adults: Latest Trends. *Curr Obes Rep* 7 (4):276-288. doi:10.1007/s13679-018-0317-8
3. Canada S (2019) Overweight and obese adults, 2018. Health Fact Sheets.
4. Catalano PM, McIntyre HD, Cruickshank JK, McCance DR, Dyer AR, Metzger BE, Lowe LP, Trimble ER, Coustan DR, Hadden DR, Persson B, Hod M, Oats JJ (2012) The hyperglycemia and adverse pregnancy outcome study: associations of GDM and obesity with pregnancy outcomes. *Diabetes Care* 35 (4):780-786. doi:10.2337/dc11-1790
5. Catalano PM, Shankar K (2017) Obesity and pregnancy: mechanisms of short term and long term adverse consequences for mother and child. *BMJ* 356:j1. doi:10.1136/bmj.j1
6. Boney CM, Verma A, Tucker R, Vohr BR (2005) Metabolic syndrome in childhood: association with birth weight, maternal obesity, and gestational diabetes mellitus. *Pediatrics* 115 (3):e290-296. doi:10.1542/peds.2004-1808
7. Catalano PM, Hauguel-De Mouzon S (2011) Is it time to revisit the Pedersen hypothesis in the face of the obesity epidemic? *Am J Obstet Gynecol* 204 (6):479-487. doi:10.1016/j.ajog.2010.11.039
8. Barker DJ (1990) The fetal and infant origins of adult disease. *BMJ* 301 (6761):1111. doi:10.1136/bmj.301.6761.1111
9. Ornoy A (2011) Prenatal origin of obesity and their complications: Gestational diabetes, maternal overweight and the paradoxical effects of fetal growth restriction and macrosomia. *Reprod Toxicol* 32 (2):205-212. doi:10.1016/j.reprotox.2011.05.002
10. Catalano PM, Thomas A, Huston-Presley L, Amini SB (2003) Increased fetal adiposity: a very sensitive marker of abnormal in utero development. *Am J Obstet Gynecol* 189 (6):1698-1704. doi:10.1016/s0002-9378(03)00828-7

11. Abe T, Thiebaud RS, Loenneke JP (2021) The Fat Fraction Percentage of White Adipose Tissue at various Ages in Humans: An Updated Review. *J Clin Densitom* 24 (3):369-373. doi:10.1016/j.jocd.2021.01.011
12. Kuzawa CW (1998) Adipose tissue in human infancy and childhood: an evolutionary perspective. *Am J Phys Anthropol Suppl* 27:177-209. doi:10.1002/(sici)1096-8644(1998)107:27+<177::aid-ajpa7>3.0.co;2-b
13. Poulos SP, Hausman DB, Hausman GJ (2010) The development and endocrine functions of adipose tissue. *Mol Cell Endocrinol* 323 (1):20-34. doi:10.1016/j.mce.2009.12.011
14. Widdowson EM (1950) Chemical composition of newly born mammals. *Nature* 166 (4224):626-628. doi:10.1038/166626a0
15. Kuzawa CW, Blair C (2019) A hypothesis linking the energy demand of the brain to obesity risk. *Proc Natl Acad Sci U S A* 116 (27):13266-13275. doi:10.1073/pnas.1816908116
16. Poissonnet CM, Burdi AR, Bookstein FL (1983) Growth and development of human adipose tissue during early gestation. *Early Hum Dev* 8 (1):1-11. doi:10.1016/0378-3782(83)90028-2
17. Desoye G, Herrera E (2021) Adipose tissue development and lipid metabolism in the human fetus: The 2020 perspective focusing on maternal diabetes and obesity. *Prog Lipid Res* 81:101082. doi:10.1016/j.plipres.2020.101082
18. Dunlop M, Court JM (1978) Lipogenesis in developing human adipose tissue. *Early Hum Dev* 2 (2):123-130. doi:10.1016/0378-3782(78)90004-x
19. Poissonnet CM, Burdi AR, Garn SM (1984) The chronology of adipose tissue appearance and distribution in the human fetus. *Early Hum Dev* 10 (1-2):1-11. doi:10.1016/0378-3782(84)90106-3
20. Hany TF, Gharehpapagh E, Kamel EM, Buck A, Himms-Hagen J, von Schulthess GK (2002) Brown adipose tissue: a factor to consider in symmetrical tracer uptake in the neck and upper chest region. *Eur J Nucl Med Mol Imaging* 29 (10):1393-1398. doi:10.1007/s00259-002-0902-6
21. Yeung HW, Grewal RK, Gonen M, Schöder H, Larson SM (2003) Patterns of (18)F-FDG uptake in adipose tissue and muscle: a potential source of false-positives for PET. *J Nucl Med* 44 (11):1789-1796
22. Nedergaard J, Bengtsson T, Cannon B (2007) Unexpected evidence for active brown adipose tissue in adult humans. *Am J Physiol Endocrinol Metab* 293 (2):E444-452. doi:10.1152/ajpendo.00691.2006

23. Merklin RJ (1974) Growth and distribution of human fetal brown fat. *Anat Rec* 178 (3):637-645. doi:10.1002/ar.1091780311
24. Aherne W, Hull D (1966) Brown adipose tissue and heat production in the newborn infant. *J Pathol Bacteriol* 91 (1):223-234. doi:10.1002/path.1700910126
25. Hull D, Segall MM (1966) Distinction of brown from white adipose tissue. *Nature* 212 (5061):469-472. doi:10.1038/212469a0
26. Hull D (1966) The structure and function of brown adipose tissue. *Br Med Bull* 22 (1):92-96. doi:10.1093/oxfordjournals.bmb.a070447
27. Dawkins MJ, Scopes JW (1965) Non-shivering thermogenesis and brown adipose tissue in the human new-born infant. *Nature* 206 (980):201-202. doi:10.1038/206201b0
28. Harms M, Seale P (2013) Brown and beige fat: development, function and therapeutic potential. *Nat Med* 19 (10):1252-1263. doi:10.1038/nm.3361
29. Hsieh AC, Carlson LD, Gray G (1957) Role of the sympathetic nervous system in the control of chemical regulation of heat production. *Am J Physiol* 190 (2):247-251. doi:10.1152/ajplegacy.1957.190.2.247
30. Hu HH, Perkins TG, Chia JM, Gilsanz V (2013) Characterization of human brown adipose tissue by chemical-shift water-fat MRI. *Am J Roentgenol* 200 (1):177-183. doi:10.2214/ajr.12.8996
31. Hu HH, Yin L, Aggabao PC, Perkins TG, Chia JM, Gilsanz V (2013) Comparison of brown and white adipose tissues in infants and children with chemical-shift-encoded water-fat MRI. *J Magn Reson Imaging* 38 (4):885-896. doi:10.1002/jmri.24053
32. Rasmussen JM, Entringer S, Nguyen A, van Erp TG, Burns J, Guijarro A, Oveisi F, Swanson JM, Piomelli D, Wadhwa PD, Buss C, Potkin SG (2013) Brown adipose tissue quantification in human neonates using water-fat separated MRI. *PLoS One* 8 (10):e77907. doi:10.1371/journal.pone.0077907
33. Borga M, West J, Bell JD, Harvey NC, Romu T, Heymsfield SB, Dahlqvist Leinhard O (2018) Advanced body composition assessment: from body mass index to body composition profiling. *J Investig Med* 66 (5):1-9. doi:10.1136/jim-2018-000722
34. Lemos T, Gallagher D (2017) Current body composition measurement techniques. *Curr Opin Endocrinol Diabetes Obes* 24 (5):310-314. doi:10.1097/med.0000000000000360
35. Most J, Marlatt KL, Altazan AD, Redman LM (2018) Advances in assessing body composition during pregnancy. *Eur J Clin Nutr* 72 (5):645-656. doi:10.1038/s41430-018-0152-8

36. Toro-Ramos T, Paley C, Pi-Sunyer FX, Gallagher D (2015) Body composition during fetal development and infancy through the age of 5 years. *Eur J Clin Nutr* 69 (12):1279-1289. doi:10.1038/ejcn.2015.117
37. Sreetharan S, Thome C, Tharmalingam S, Jones DE, Kulesza AV, Khaper N, Lees SJ, Wilson JY, Boreham DR, Tai TC (2017) Ionizing Radiation Exposure During Pregnancy: Effects on Postnatal Development and Life. *Radiat Res* 187 (6):647-658. doi:10.1667/rr14657.1
38. ACOG Practice Bulletin No. 101: Ultrasonography in pregnancy (2009). *Obstet Gynecol* 113 (2 Pt 1):451-461. doi:10.1097/AOG.0b013e31819930b0
39. Elliott ST (2006) A User Guide to Extended Field of View in Ultrasonography. *Ultrasound* 14 (1):55-28. doi: 10.1179/174313405X83597
40. Lin SC, Heba E, Wolfson T, Ang B, Gamst A, Han A, Erdman JW, Jr., O'Brien WD, Jr., Andre MP, Sirlin CB, Loomba R (2015) Noninvasive Diagnosis of Nonalcoholic Fatty Liver Disease and Quantification of Liver Fat Using a New Quantitative Ultrasound Technique. *Clin Gastroenterol Hepatol* 13 (7):1337-1345.e1336. doi:10.1016/j.cgh.2014.11.027
41. Lu ZF, Zagzebski JA, Lee FT (1999) Ultrasound backscatter and attenuation in human liver with diffuse disease. *Ultrasound Med Biol* 25 (7):1047-1054. doi:10.1016/s0301-5629(99)00055-1
42. Xia MF, Yan HM, He WY, Li XM, Li CL, Yao XZ, Li RK, Zeng MS, Gao X (2012) Standardized ultrasound hepatic/renal ratio and hepatic attenuation rate to quantify liver fat content: an improvement method. *Obesity (Silver Spring)* 20 (2):444-452. doi:10.1038/oby.2011.302
43. Zhang B, Ding F, Chen T, Xia LH, Qian J, Lv GY (2014) Ultrasound hepatic/renal ratio and hepatic attenuation rate for quantifying liver fat content. *World J Gastroenterol* 20 (47):17985-17992. doi:10.3748/wjg.v20.i47.17985
44. Webb M, Yeshua H, Zelber-Sagi S, Santo E, Brazowski E, Halpern Z, Oren R (2009) Diagnostic value of a computerized hepatorenal index for sonographic quantification of liver steatosis. *Am J Roentgenol* 192 (4):909-914. doi:10.2214/ajr.07.4016
45. Kaliaev A, Chavez W, Soto J, Huda F, Xie H, Nguyen M, Shamdasani V, Anderson S (2022) Quantitative Ultrasound Assessment of Hepatic Steatosis. *J Clin Exp Hepatol* 12 (4):1091-1101. doi:10.1016/j.jceh.2022.01.007
46. Hu HH, Börnert P, Hernando D, Kellman P, Ma J, Reeder S, Sirlin C (2012) ISMRM workshop on fat-water separation: insights, applications and progress in MRI. *Magn Reson Med* 68 (2):378-388. doi:10.1002/mrm.24369
47. Mansfield P, Maudsley AA (1977) Medical imaging by NMR. *Br J Radiol* 50 (591):188-194. doi:10.1259/0007-1285-50-591-188

48. Smith FW, Adam AH, Phillips WD (1983) NMR Imaging in Pregnancy. *The Lancet* Jan 1 (1):61-62
49. Radiology ACo (2015) ACR-SPR Practice Parameter for the Safe and Optimal Performance of Fetal Magnetic Resonance Imaging (MRI).
50. Ray JG, Vermeulen MJ, Bharatha A, Montanera WJ, Park AL (2016) Association Between MRI Exposure During Pregnancy and Fetal and Childhood Outcomes. *JAMA* 316 (9):952-961. doi:10.1001/jama.2016.12126
51. Stecco A, Saponaro A, Carriero A (2007) Patient safety issues in magnetic resonance imaging: state of the art. *Radiol Med* 112 (4):491-508. doi:10.1007/s11547-007-0154-4
52. Bulas D, Egloff A (2013) Benefits and risks of MRI in pregnancy. *Semin Perinatol* 37 (5):301-304. doi:10.1053/j.semperi.2013.06.005
53. Glenn OA (2010) MR imaging of the fetal brain. *Pediatr Radiol* 40 (1):68-81. doi:10.1007/s00247-009-1459-3
54. Levine D (2001) Ultrasound versus magnetic resonance imaging in fetal evaluation. *Top Magn Reson Imaging* 12 (1):25-38. doi:10.1097/00002142-200102000-00004
55. Frates MC, Kumar AJ, Benson CB, Ward VL, Tempany CM (2004) Fetal anomalies: comparison of MR imaging and US for diagnosis. *Radiology* 232 (2):398-404. doi:10.1148/radiol.2322030504
56. Iron K, Przybysz R, Laupacis A (2003) Access to MRI in Ontario: Addressing the Information Gap. Institute for Clinical Evaluative Sciences,
57. Sarraçanie M, LaPierre CD, Salameh N, Waddington DEJ, Witzel T, Rosen MS (2015) Low-Cost High-Performance MRI. *Sci Rep* 5:15177. doi:10.1038/srep15177
58. Quinn TM, Hubbard AM, Adzick NS (1998) Prenatal magnetic resonance imaging enhances fetal diagnosis. *J Pediatr Surg* 33 (4):553-558. doi:10.1016/s0022-3468(98)90315-3
59. Dixon WT (1984) Simple proton spectroscopic imaging. *Radiology* 153 (1):189-194. doi:10.1148/radiology.153.1.6089263
60. Haacke EM, Brown RW, Thompson MR, Venkatesan R (1999) *Magnetic Resonance Imaging, Physical Principles and Sequence Design*. John Wiley & Sons. doi:10.1002/9781118633953
61. Glover GH (1991) Multipoint Dixon technique for water and fat proton and susceptibility imaging. *J Magn Reson Imaging* 1 (5):521-530. doi:10.1002/jmri.1880010504

62. Glover GH, Schneider E (1991) Three-point Dixon technique for true water/fat decomposition with B₀ inhomogeneity correction. *Magn Reson Med* 18 (2):371-383. doi:10.1002/mrm.1910180211
63. Yeung HN, Kormos DW (1986) Separation of true fat and water images by correcting magnetic field inhomogeneity in situ. *Radiology* 159 (3):783-786. doi:10.1148/radiology.159.3.3704157
64. Reeder SB, Wen Z, Yu H, Pineda AR, Gold GE, Markl M, Pelc NJ (2004) Multicoil Dixon chemical species separation with an iterative least-squares estimation method. *Magn Reson Med* 51 (1):35-45. doi:10.1002/mrm.10675
65. Reeder SB, Pineda AR, Wen Z, Shimakawa A, Yu H, Brittain JH, Gold GE, Beaulieu CH, Pelc NJ (2005) Iterative decomposition of water and fat with echo asymmetry and least-squares estimation (IDEAL): application with fast spin-echo imaging. *Magn Reson Med* 54 (3):636-644. doi:10.1002/mrm.20624
66. Ma J (2004) Breath-hold water and fat imaging using a dual-echo two-point Dixon technique with an efficient and robust phase-correction algorithm. *Magn Reson Med* 52 (2):415-419. doi:10.1002/mrm.20146
67. Wang X, Colgan TJ, Hinshaw LA, Roberts NT, Bancroft LCH, Hamilton G, Hernando D, Reeder SB (2020) T(1)-corrected quantitative chemical shift-encoded MRI. *Magn Reson Med* 83 (6):2051-2063. doi:10.1002/mrm.28062
68. Yang IY, Cui Y, Wiens CN, Wade TP, Friesen-Waldner LJ, McKenzie CA (2014) Fat fraction bias correction using T1 estimates and flip angle mapping. *J Magn Reson Imaging* 39 (1):217-223. doi:10.1002/jmri.24126
69. Liu CY, McKenzie CA, Yu H, Brittain JH, Reeder SB (2007) Fat quantification with IDEAL gradient echo imaging: correction of bias from T(1) and noise. *Magn Reson Med* 58 (2):354-364. doi:10.1002/mrm.21301
70. Reeder SB, McKenzie CA, Pineda AR, Yu H, Shimakawa A, Brau AC, Hargreaves BA, Gold GE, Brittain JH (2007) Water-fat separation with IDEAL gradient-echo imaging. *J Magn Reson Imaging* 25 (3):644-652. doi:10.1002/jmri.20831
71. Yu H, McKenzie CA, Shimakawa A, Vu AT, Brau AC, Beatty PJ, Pineda AR, Brittain JH, Reeder SB (2007) Multiecho reconstruction for simultaneous water-fat decomposition and T2* estimation. *J Magn Reson Imaging* 26 (4):1153-1161. doi:10.1002/jmri.21090
72. Yu H, Shimakawa A, McKenzie CA, Brodsky E, Brittain JH, Reeder SB (2008) Multiecho water-fat separation and simultaneous R2* estimation with multifrequency fat spectrum modeling. *Magn Reson Med* 60 (5):1122-1134. doi:10.1002/mrm.21737

73. Hamilton G, Yokoo T, Bydder M, Cruite I, Schroeder ME, Sirlin CB, Middleton MS (2011) In vivo characterization of the liver fat ¹H MR spectrum. *NMR Biomed* 24 (7):784-790. doi:10.1002/nbm.1622
74. Meisamy S, Hines CD, Hamilton G, Sirlin CB, McKenzie CA, Yu H, Brittain JH, Reeder SB (2011) Quantification of hepatic steatosis with T1-independent, T2-corrected MR imaging with spectral modeling of fat: blinded comparison with MR spectroscopy. *Radiology* 258 (3):767-775. doi:10.1148/radiol.10100708
75. Reeder SB, Hu HH, Sirlin CB (2012) Proton density fat-fraction: a standardized MR-based biomarker of tissue fat concentration. *J Magn Reson Imaging* 36 (5):1011-1014. doi:10.1002/jmri.23741
76. Griswold MA, Jakob PM, Heidemann RM, Nittka M, Jellus V, Wang J, Kiefer B, Haase A (2002) Generalized autocalibrating partially parallel acquisitions (GRAPPA). *Magn Reson Med* 47 (6):1202-1210. doi:10.1002/mrm.10171
77. Ikenoue S, Kasuga Y, Endo T, Tanaka M, Ochiai D (2021) Newer Insights Into Fetal Growth and Body Composition. *Front Endocrinol (Lausanne)* 12:708767. doi:10.3389/fendo.2021.708767
78. Bernstein IM, Goran MI, Amini SB, Catalano PM (1997) Differential growth of fetal tissues during the second half of pregnancy. *Am J Obstet Gynecol* 176 (1 Pt 1):28-32. doi:10.1016/s0002-9378(97)80006-3
79. Smith FW, MacLennan F, Abramovich DR, MacGilivray I, Hutchison JMS (1984) NMR Imaging in Human Pregnancy: A Preliminary Study. *Magn Reson Med* 2:57-64
80. Thomas EL, Fitzpatrick JA, Malik SJ, Taylor-Robinson SD, Bell JD (2013) Whole body fat: content and distribution. *Prog Nucl Magn Reson Spectrosc* 73:56-80. doi:10.1016/j.pnmrs.2013.04.001
81. Smith FW (1985) The potential use of nuclear magnetic resonance imaging in pregnancy. *J Perinat Med* 13 (6):265-276
82. Stark DD, McCarthy SM, Filly RA, Callen PW, Hricak H, Parer JT (1985) Intrauterine growth retardation: evaluation by magnetic resonance. Work in progress. *Radiology* 155 (2):425-427. doi:10.1148/radiology.155.2.3885309
83. Deans HE, Smith FW, Lloyd DJ, Law AN, Sutherland HW (1989) Fetal fat measurement by magnetic resonance imaging. *Br J Radiol* 62:603-607
84. Jovanovic-Peterson L, Crues J, Durak E, Peterson CM (1993) Magnetic resonance imaging in pregnancies complicated by gestational diabetes predicts infant birthweight ratio and neonatal morbidity. *Am J Perinatol* 10 (6):432-437. doi:10.1055/s-2007-994624
85. Berger-Kulemann V, Brugger PC, Reissegger M, Klein K, Hachemian N, Koelblinger C, Weber M, Prayer D (2011) Quantification of the subcutaneous fat layer with MRI in

fetuses of healthy mothers with no underlying metabolic disease vs. fetuses of diabetic and obese mothers. *J Perinat Med* 40 (2):179-184. doi:10.1515/JPM.2011.122

86. Anblagan D, Deshpande R, Jones NW, Costigan C, Bugg G, Raine-Fenning N, Gowland PA, Mansell P (2013) Measurement of fetal fat in utero in normal and diabetic pregnancies using magnetic resonance imaging. *Ultrasound Obstet Gynecol* 42 (3):335-340. doi:10.1002/uog.12382

87. Blondiaux E, Chougar L, Gelot A, Valence S, Audureau E, Ducou le Pointe H, Jouannic JM, Dhombres F, Garel C (2018) Developmental patterns of fetal fat and corresponding signal on T1-weighted magnetic resonance imaging. *Pediatr Radiol* 48 (3):317-324. doi:10.1007/s00247-017-4038-z

Chapter 2

2 Feasibility of measuring fetal adipose tissue with 3D water-fat separated magnetic resonance imaging

The contents of this chapter were previously published in the Journal of Maternal-Fetal and Neonatal Medicine: Giza, S.A., Olmstead, C., McCooeye, D.A., Miller, M.R., Penava, D.A., Eastabrook, G.D., McKenzie, C.A., de Vrijer, B. (2020) Measuring fetal adipose tissue using 3D water-fat magnetic resonance imaging: a feasibility study. Journal of Maternal-Fetal & Neonatal Medicine 33 (5):831-837. © 2018 International Society for Magnetic Resonance in Medicine. Reproduced with permission from John Wiley and Sons. See Appendix E for permission.

2.1 Introduction

It has been suggested that the trigger for abnormal adipose tissue deposition and metabolism is set *in utero* [1], as both limited and excessive fetal growth are associated with increased risks for obesity and metabolic syndrome later in life [2-4]. Differences in adipose tissue in neonates, normally 14% of weight at birth, explain 46% of the variation seen in birth weight [5]. Also, neonates of obese mothers with gestational diabetes have been found to have abnormal adipose tissue distribution when measured 1-3 weeks after birth [6]. Ultrasound and magnetic resonance imaging (MRI) have found that fetal adipose tissue thickness and/or volume is altered with diabetic pregnancies, growth restriction and macrosomia [7-15]. This suggests that assessment of fetal adipose tissue development *in utero* has the potential to provide additional insights into fetal health and nutritional status, especially in circumstances where altered metabolism may put the fetus at risk for adverse pregnancy outcomes [16,17].

As fetal adipocytes develop, the amount of lipid they contain increases, a process for which 3D water-fat MRI is sensitive. Previous MRI studies have differentiated adipose tissue (lipid) from lean tissue (water) based on different T1 values, an intrinsic MRI tissue property [10,12,11]. However, these methods have been restricted to assessing the volume of subcutaneous tissue as they cannot measure the relative amounts of lipid and water within tissues. Water-fat MRI can separate the water signal from the lipid signal,

allowing water-fat MRI to provide a quantitative ratio of signal from lipid and water in a tissue. Measuring the lipid content of the fetal adipose tissue may give more insight into the expansion of adipose tissue in fetal development, adding to the tools used to assess fetal health in late pregnancy.

This study aims to assess whether fetal adipose tissue volume can be measured reliably using 3D water-fat MRI. We hypothesize that water-fat MRI will be sensitive to increases in the adipose tissue lipid volume and lipid content as a function of gestational age (GA), mirroring the increased lipid deposition as the fetus grows. This study aims to provide an initial demonstration of the ability of MRI to measure fetal adipose tissue development during the third trimester of pregnancy. If successful, these measurements would be useful for assessing abnormal fetal growth and metabolic health.

2.2 Materials and Methods

This study was approved by the Western University Research Ethics Board (HSREB# 103845, see Appendix A). Between January 2014 and October 2015, pregnant women over the age of 18 with singleton pregnancies between 29 and 35w GA were recruited from Obstetrics clinics at London Health Sciences Centre for the sole indication of participation in the MRI study. Patients with medical contraindications or body habitus preventing them from safely undergoing a non-contrast MRI were excluded. Consenting participants underwent a fetal MRI in a wide-bore (70 cm diameter) 1.5 Tesla (T) MRI (General Electric Optima 450w, Milwaukee, WI, USA) with a 32-coil abdominal phased array. Women were positioned supine or rolled towards a left lateral decubitus position with a cushion under either their back or right side for comfort. Scout images (T2 weighted Single Shot Fast Spin Echo (SSFSE)) were acquired to locate the fetus and determine its orientation. Water-only and fat-only images were produced during a maternal breath hold with a modified 3D two-point Dixon (Liver Acceleration Volume Acquisition (LAVA) Flex) acquisition in a plane axial to the fetal abdomen (TR 6.0-6.4 ms, flip angle 5°, Field of View 48 cm, 160×160 pixels, slice thickness 4 mm, 38-82 slices, 2× parallel MRI acceleration with Autocalibrating Reconstruction for Cartesian imaging (ARC), acquisition time 10-24 s).

Total fetal volume was manually segmented from 2D SSFSE images using OsiriX (v5.6)[18] by tracing the boundary of the lower signal intensity of the fetus relative to the high signal intensity of the amniotic fluid. MRI estimated fetal weight (EFW) was calculated from total fetal volume using a fetal density formula ($\text{MRI EFW} = 0.12 + 1.031 \times \text{fetal volume}$) [19].

Clinical data on maternal and fetal characteristics were collected prospectively from mothers and infants after delivery. Gestational age was estimated with ultrasound in the first trimester as described by the Society of Obstetricians and Gynaecologists of Canada (SOGC) Clinical Practice Guideline [20], with an error of ± 2 days [21]. Sonographic estimates of fetal weight were taken from the closest ultrasound studies prior to the date of the MRI (range 0-35 days) using the Hadlock 2 formula [22]. MRI EFW percentiles have previously been shown to be more accurate than ultrasound EFW percentiles when measured within 3 hours of caesarean delivery [23]. The EFW calculated from both MRI and ultrasound were then used with custom weight standards from Gardosi and Francis (2015) to calculate the fetal weight percentiles [24]. Birthweights were recorded from infant charts, and birthweight percentiles were calculated using the standards from Kramer et al. [25].

Fat signal fraction (FSF) image volumes were calculated voxel-by-voxel from the lipid and water signal intensities ($\text{FSF} = \text{Lipid}/(\text{Water}+\text{Lipid})$) for the entire MRI volume collected, which always included the fetal abdomen. Using OsiriX v5.6 (Pixmeo, Bernex, Switzerland), 3D FSF volumes were reformatted to axial to the fetal abdomen when the original images were not oriented optimally, usually due to fetal movement after scout images. The fetal trunk subcutaneous adipose tissue (fTSAT) was manually segmented from the FSF images by manually tracing the boundary of high FSF of the adipose tissue relative to the approximately zero FSF of the surrounding tissues (amniotic fluid and internal fetal tissues). This segmentation was performed in all slices (25 -51 slices) between the axillary and hip skin folds. The trunk subcutaneous adipose tissue was chosen as it contributes to abdominal circumference measures frequently performed with ultrasound to assess fetal growth.

The lipid volume within the fTSAT region was calculated by correcting the manually segmented fTSAT volume by the mean FSF of that volume in each slice. Through this method, we could correct for partial volumes and determine the quantitative amount of lipid in the fTSAT. Measured variables included the amount of lipid in the fTSAT (lipid volume), lipid volume normalized to fetal volume (lipid volume/fetal volume) and the mean FSF in the fTSAT.

To assess inter-rater reliability, three independent readers (SG, CO and DM) each manually segmented 10 FSF sets and the segmented volumes were compared using intraclass correlation coefficient (ICC). Intra-rater reliability was assessed by one reader (SG) with 10 FSF manually segmented twice two months apart with the segmented volumes compared using ICC.

Pearson correlations and linear regression analyses were used to examine bivariate relations between fetal adipose tissue measurements (lipid volume, lipid volume/fetal volume, and FSF) and GA at MRI and MRI EFW percentile. All statistical analyses were conducted in SPSS v.24 (IBM Corporation, Armonk, NY, USA), and p-values <0.05 were considered statistically significant.

2.3 Results

Eighteen women were recruited for the study. One participant with a high body mass index (BMI) (61 kg/m^2) was successfully positioned in the MRI bore but was unable to commence imaging due to claustrophobia. The remaining 17 participants provided images of adequate quality for segmentation of the fTSAT; intra-abdominal adipose tissue content was insufficient for segmentation.

The median number of previous pregnancies was 1 (range 0-2), and the mean maternal age at delivery was 32 years (range 23-41 years). The mean pre-pregnancy BMI of participants was 34.6 kg/m^2 (range $19.2\text{-}52.5 \text{ kg/m}^2$). Most participants were recruited from our specialized clinic for elevated BMI and pregnancy, resulting in a high percentage of participants with a pre-pregnancy BMI in the obese categories (76%). Seventeen percent of the participants had a BMI in the normal range, while 6% were

overweight. Seventy percent of the participants were non-diabetic, 6% had pre-existing type 1 diabetes, 12% had pre-existing type 2 diabetes, and 12% had gestational diabetes. The mean GA at MRI was 32 weeks (range 29-34), and 53% of the fetuses examined were female. The mean birthweight percentile was 58.1 (range 0.5-96.6), with 12% of the fetuses below the 10th and 23% above the 90th percentile.

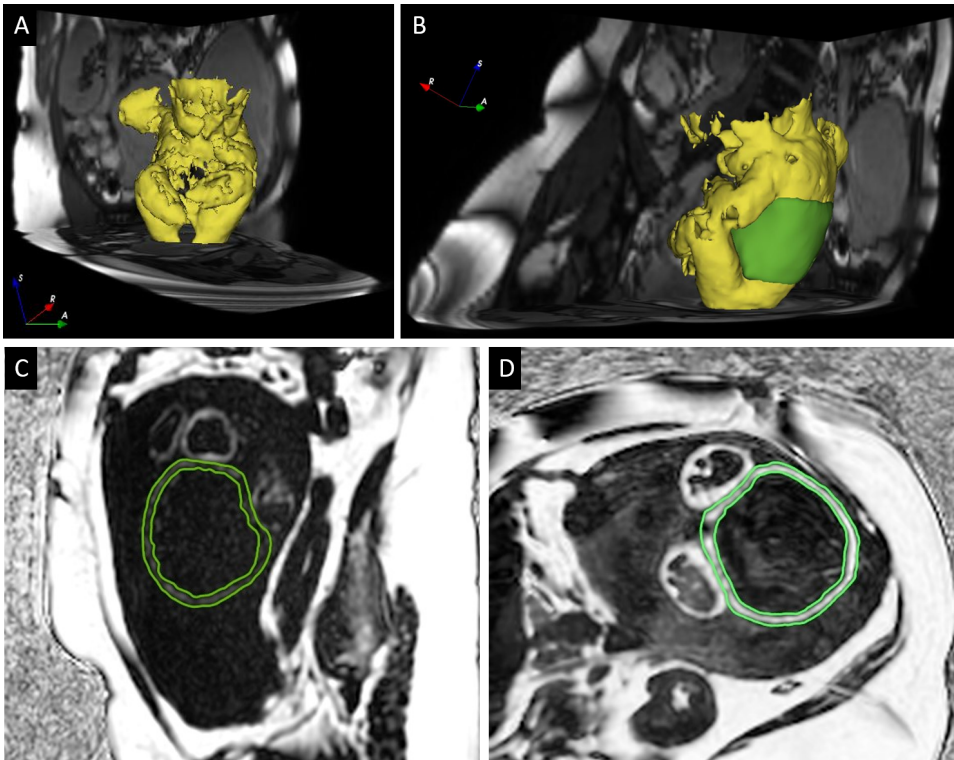


Figure 2.1. (A) 3D rendering of total fetal adipose tissue, (B) 3D rendering of fTSAT segmentation on total fetal adipose tissue, (C) 2D fTSAT segmentation on fetus with 10 ml lipid volume, and (D) 2D fTSAT segmentation on fetus with 80 ml lipid volume. 3D rendering in panel A shows the distribution of adipose tissue above a 10% FSF threshold. The rendering in B shows a different orientation so that the limbs do not obscure the upper and lower boundaries of the fTSAT segmentation demonstrated in green. Three orthogonal planes of Fast Imaging Employing Steady-state Acquisition (FIESTA) images are shown to reference maternal anatomy, and an axes marker is included to indicate maternal orientation. The 2D images in panels C and D show fetuses that had similar ultrasound EFW percentiles (C = 98%, D = 96%) but different lipid volumes, in part due to differences in the mean

FSF (C = 12%, D = 30%). This can be seen as a brighter segmented region in panel D and panel C. It is also important to note that these fetuses have different GA at MRI (C = 30 weeks and D = 34 + 1 weeks). 2D images are displayed axial to the fetal abdomen to show a comparison of slices through the umbilicus.

Total fetal volume and fTSAT volume were segmented for all 17 participants. Figure 2.1 shows a visualization of the fetal adipose tissue with the fTSAT segmentation highlighted in green, created using 3D Slicer (v4.5.0)[26,27]. The ICC for the inter-rater reliability was 0.936 ($p < 0.001$), and the ICC for the intra-rater reliability was 0.992 ($p < 0.001$).

Figure 2.1 also shows the fTSAT segmentation for two different participants. The fetuses have different GA at MRI (C; 30 weeks and D; 34+1 weeks) and very different FSF (C = 12% and D = 30%) with different lipid volumes (C = 10 mL and D = 80 mL), illustrated with different greyscale values within the segmented regions. It is important to note that both fetuses have similar ultrasound EFW percentiles (C = 98% and D = 96%), suggesting that FSF and lipid volume are affected by GA.

Over the GA period studied, fetal lipid volume showed a rapid increase from 4 mL at 30 weeks to 48 mL at 34 weeks gestation (Figure 2.2A), or 0.3% to 1.8% lipid volume/fetal volume. This is paralleled by an increase in FSF from 10% to 24% from 30 to 34 weeks (Figure 2.2B). These increases demonstrate the positive correlations between GA at MRI and lipid volume ($r = 0.63$, $p = 0.007$), GA at MRI and lipid volume/fetal volume ($r = 0.65$, $p = 0.005$), and GA at MRI and FSF ($r = 0.65$, $p = 0.005$) (Figure 2.2A & B).

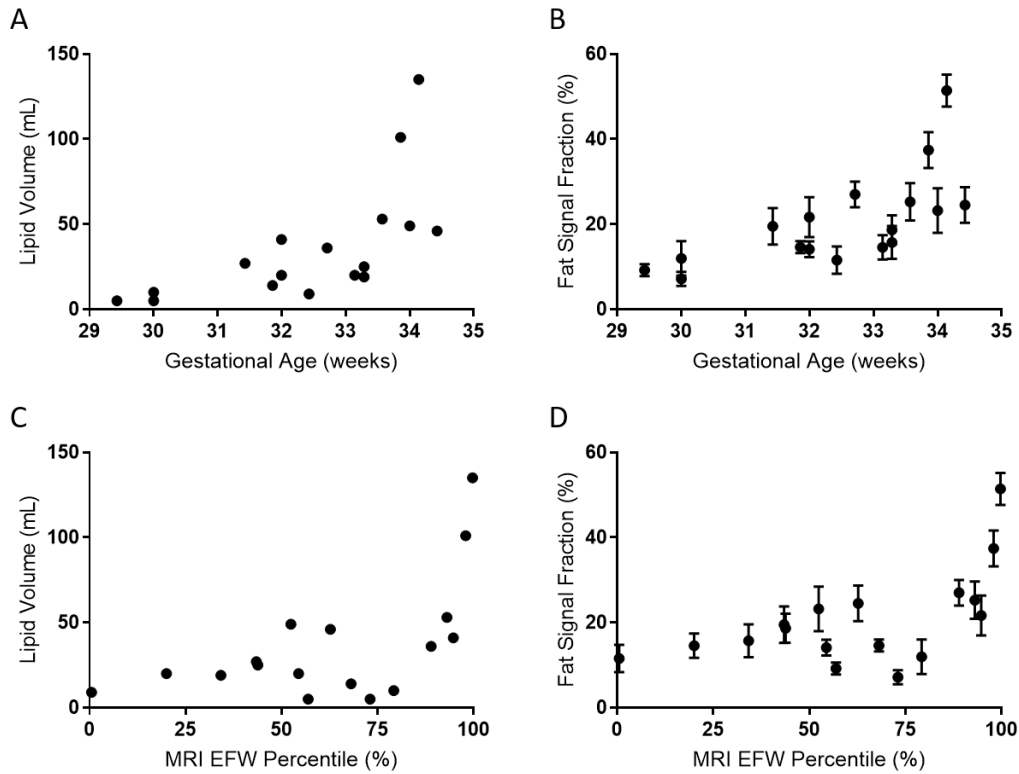


Figure 2.2. (A) GA versus lipid volume, (B) GA versus mean FSF, (C) custom MRI EFW percentile versus lipid volume, and (D) custom MRI EFW percentile versus mean FSF. A positive correlation was found between GA and lipid volume ($p = 0.007$), between GA and mean FSF ($p=0.005$), and between custom MRI EFW percentile and lipid volume ($p=0.012$). Lipid volume error bars represent a 5% estimated error in lipid volume measurement; some error bars are too small to be visualized. FSF measurement error bars represent the standard deviation of values across slices measured.

The relationships between adipose tissue measures and fetal weight indices were also examined. Custom EFW percentiles calculated from MRI volumes were positively correlated with lipid volume ($r = 0.62$, $p = 0.009$), lipid volume/fetal volume ($r = 0.55$, $p = 0.022$) and FSF ($r = 0.60$, $p = 0.012$) (Figure 2.2C & D). Due to the small sample size and heterogeneous population, we did not analyze for differences in the FSF or lipid volume of the fTSAT with BMI less than or greater than 30 kg/m^2 ($n = 4$; BMI $< 30 \text{ kg/m}^2$, and $n = 13$; BMI $\geq 30 \text{ kg/m}^2$), maternal diabetes ($n = 12$; non-diabetic, and $n = 5$;

diabetes), fetal growth restriction or macrosomia (n = 11; 10th percentile < BW < 90th percentile, n = 2; BW < 10th percentile, and n = 4; BW > 90th percentile).

2.4 Discussion

We describe a method for measuring fetal abdominal subcutaneous adipose tissue with 3D water-fat MRI, for the first time allowing monitoring of fetal adipose tissue development by assessing the lipid content of adipose tissue rather than tissue volume alone. Measurements were made by defining a region of interest in the fetal trunk based on soft tissue landmarks that were easily and consistently recognizable regardless of the fetal position, size or GA. This methodology resulted in a segmentation technique with excellent inter- and intra-rater reliabilities.

We observed a rapid lipid accumulation between 29 and 34w GA, with an increase from 10 to 24% in FSF and from 4 to 48 mL in trunk subcutaneous tissue volume. Previous studies describe a rapid increase in fetal subcutaneous tissue thickness in the fetal leg and abdomen between 29 and 40 weeks with MRI [11], or 19 and 40 weeks with ultrasound [28,29]. These findings highlight the importance of this GA window for fetal subcutaneous adipose tissue development.

The increase in FSF during this time is of interest since the measurement of FSF is a much more direct indicator of adipocyte lipid content than adipose tissue volume. Indeed, the FSF measured in the fetuses at all GA studied was below that of mature adult adipose tissue. Even at birth, neonatal adipose tissue is not fully developed as neonatal fat fractions have been reported to be 67.7% [30] and 77.9% [31], compared to a fat fraction of approximately 90% in adults [31]. The linear regression indicates a fetal fat fraction of 24% at 34w, suggesting that a further rapid increase in fat fraction and lipid volume can be expected between 34 and 40w GA.

In our study, we elected to measure fetal abdominal adipose tissue development because abdominal subcutaneous tissue thickness measured by ultrasound is correlated to neonatal body composition while allowing for assessment of intraabdominal adipose tissue. However, none of the fetuses had any measurable amounts of intraabdominal adipose

tissue, possibly because very little intraabdominal adipose tissue develops at this GA [12] or there is not enough lipid accumulation to be visualized with MRI. The lowest measurable FSF in our study was 4%, based on the noise signal in amniotic fluid (data not shown), and therefore intra-abdominal or intrahepatic fat fractions below this percentage should not be reported.

Water-fat MRI is an MRI technique that provides separate water and lipid images. In this study, these images were acquired using a modified two-point Dixon technique; this technique has a faster image acquisition, making it less likely to be affected by fetal motion. Additionally, it has better signal-to-noise efficiency than other water-fat MRI, which will allow it to measure relatively lower fat fractions [32,33]. While this sequence has recognized limitations of sensitivity to T2* effects (caused by, e.g. iron) and incomplete lipid spectrum modelling (MRI lipid signal at multiple frequencies due to the complex chemical structure of triglyceride)[34], the work in Chapter 3 demonstrates that these effects do not cause bias in estimates of fat fraction with modified two-point Dixon in fTSAT [35]. However, it should be noted that in Chapter 3, we did demonstrate biases in estimates of fat fraction with modified two-point Dixon in other tissues, including the liver [35].

Our study was limited by the small sample size, its cross-sectional nature and a selection bias from recruiting from the elevated BMI pregnancy clinic resulting in the high percentage of patients with elevated BMI. In our institution, 44% of women are overweight or obese, with 20% of the total maternal population having a BMI greater than 30 kg/m² (unpublished data). This pilot study demonstrated the feasibility of MRI in the early third trimester in a large-bore MRI, even in patients with significant obesity (BMI>40; n=5). Due to the small sample size and heterogeneous population, we were unable to comment on normal values for GA or ‘normal’ and ‘abnormal’ adipose tissue development. While FSF is strongly affected by GA, other factors, including maternal BMI, maternal diabetes, fetal sex and natural variation in fetal growth and development, could also be contributing to the FSF differences seen in our study data.

Future studies with comparisons between normal pregnancies and those affected by high maternal BMI, maternal diabetes, and fetal growth extremes (fetal growth restriction and macrosomia) are needed to establish the utility of fetal lipid measurements in clinical practice or research.

We also acknowledge some limitations of our manual segmentation method. First, a fetal position with a curved rather than straight spine resulted in an inability to extend the segment to the axillary or hip skinfold on both the right and left sides of the fetus, in which case the measurement leading to the smallest trunk volume was chosen. This resulted in an underestimation of fetal adipose tissue volume, which can be overcome by performing segmentations in a program that allows editing in 3D, so that the start/end points can be drawn between the left and right sides. Second, partial volume effects would lower the mean FSF and lead to a universal and likely consistent underestimation of fetal lipid accumulation. More accurate estimates of FSF may be obtained using a segmentation program that allows for the segmentation to be eroded to exclude such partial volume pixels.

We note that there is a fetus with a very low MRI EFW percentile (0.5%) and one fetus with a very high MRI EFW percentile (99.7%). While these fetuses were identified as small or large with conventional ultrasound EFW percentile and birthweight percentile, these extreme values raise questions about the custom EFW percentile calculation. Future research should include measuring fat fractions in pregnancies in women of normal BMI with gestational weight gain within the recommended Institute of Medicine (IOM) limits (11.5-16 kg [36]), and at both earlier and later GA, to determine the MRI growth and development trajectories of fetal adipose tissue. Limitations in the lowest threshold for fetal fat fraction measurement (4%) will limit the earliest gestation that changes in subcutaneous lipid content can be adequately measured.

2.5 Conclusions

In conclusion, we have shown that fetal adipose tissue volumes can be reliably measured while correcting for the lipid content of the adipose tissue using 3D water-fat MRI. We have also confirmed our hypothesis that fetal adipose tissue lipid volume and lipid

content increase with GA. Further investigation with a larger sample size and MRI quantitative PDFF measurement should be pursued to further investigate the potential utility of these adipose tissue measurements.

2.6 References

1. Tomar AS, Tallapragada DS, Nongmaithem SS, Shrestha S, Yajnik CS, Chandak GR (2015) Intrauterine Programming of Diabetes and Adiposity. *Current obesity reports* 4 (4):418-428. doi:10.1007/s13679-015-0175-6
2. Barker DJP, Hales CN, Fall CHD, Osmond C, Phipps K, Clark PMS (1993) Type 2 (non-insulin-dependent) diabetes mellitus, hypertension and hyperlipidaemia (syndrome X): relation to reduced fetal growth. *Diabetologia* 36:62-67
3. Hales CN, Barker DJP (2001) The thrifty phenotype hypothesis. *Br Med Bull* 60:5-20
4. Harder T, Rodekamp E, Schellong K, Dudenhausen JW, Plagemann A (2007) Birth weight and subsequent risk of type 2 diabetes: a meta-analysis. *Am J Epidemiol* 165 (8):849-857. doi:10.1093/aje/kwk071
5. Bernstein IM, Catalano PM (1992) Influence of fetal fat on the ultrasound estimation of fetal weight in diabetic mothers. *Obstet Gynecol* 79 (4):561-563
6. Brumbaugh DE, Tarse P, Cree-Green M, Fenton LZ, Brown M, Scherzinger A, Reynolds R, Alston M, Hoffman C, Pan Z, Friedman JE, Barbour LA (2013) Intrahepatic fat is increased in the neonatal offspring of obese women with gestational diabetes. *J Pediatr* 162 (5):930-936 e931. doi:10.1016/j.jpeds.2012.11.017
7. Larciprete G, Valensise H, Vasapollo B, Novelli GP, Parretti E, Altomare F, Di Pierro G, Menghini S, Barbati G, Mello G, Arduini D (2003) Fetal subcutaneous tissue thickness (SCTT) in healthy and gestational diabetic pregnancies. *Ultrasound Obstet Gynecol* 22 (6):591-597. doi:10.1002/uog.926
8. Tantanasis T, Daniilidis A, Giannoulis C, Tzafettas M, Dinas K, Loufopoulos A, Papathanasiou K (2010) Sonographic assessment of fetal subcutaneous fat tissue thickness as an indicator of gestational diabetes. *Eur J Obstet Gynecol Reprod Biol* 152 (2):157-162. doi:10.1016/j.ejogrb.2010.05.035
9. Rigano S, Ferrazzi E, Radaelli T, Taricco E, Cetin I, Pardi G (2000) Sonographic Measurements of Subcutaneous Fetal Fat in Pregnancies Complication by Gestational Diabetes and in Normal Pregnancies. *Croat Med J* 41:240-244
10. Deans HE, Smith FW, Lloyd DJ, Law AN, Sutherland HW (1989) Fetal fat measurement by magnetic resonance imaging. *Br J Radiol* 62:603-607

11. Berger-Kulemann V, Brugger PC, Reisseger M, Klein K, Hachemian N, Koelblinger C, Weber M, Prayer D (2011) Quantification of the subcutaneous fat layer with MRI in fetuses of healthy mothers with no underlying metabolic disease vs. fetuses of diabetic and obese mothers. *J Perinat Med* 40 (2):179-184. doi:10.1515/JPM.2011.122
12. Anblagan D, Deshpande R, Jones NW, Costigan C, Bugg G, Raine-Fenning N, Gowland PA, Mansell P (2013) Measurement of fetal fat in utero in normal and diabetic pregnancies using magnetic resonance imaging. *Ultrasound Obstet Gynecol* 42 (3):335-340. doi:10.1002/uog.12382
13. Skinner J, O'Donoghue K, Gardeil F, Greene R, Turner MJ (2001) Is fetal abdominal subcutaneous fat comparable with established indices of growth restriction? *J Obstet Gynaecol* 21 (5):439-442. doi:10.1080/01443610120071947
14. Gardeil F, Greene R, Stuart B, Turner MJ (1999) Subcutaneous fat in the fetal abdomen as a predictor of growth restriction. *Obstet Gynecol* 94 (2):209-212. doi:10.1016/s0029-7844(99)00270-7
15. Jovanovic-Peterson L, Crues J, Durak E, Peterson CM (1993) Magnetic resonance imaging in pregnancies complicated by gestational diabetes predicts infant birthweight ratio and neonatal morbidity. *Am J Perinatol* 10 (6):432-437. doi:10.1055/s-2007-994624
16. Segovia SA, Vickers MH, Gray C, Reynolds CM (2014) Maternal obesity, inflammation, and developmental programming. *BioMed research international* 2014:418975. doi:10.1155/2014/418975
17. Schmatz M, Madan J, Marino T, Davis J (2010) Maternal obesity: the interplay between inflammation, mother and fetus. *Journal of perinatology : official journal of the California Perinatal Association* 30 (7):441-446. doi:10.1038/jp.2009.182
18. Rosset A, Spadola L, Ratib O (2004) OsiriX: an open-source software for navigating in multidimensional DICOM images. *Journal of digital imaging* 17 (3):205-216. doi:10.1007/s10278-004-1014-6
19. Baker PN, Johnson IR, Gowland PA, Hykin J, Harvey PR, Freeman A, Adams V, Worthington BS, Mansfield P (1994) Fetal Weight estimation by echo-planar magnetic resonance imaging. *The Lancet* 343:644-645
20. Butt K, Lim KI (2019) Guideline No. 388-Determination of Gestational Age by Ultrasound. *J Obstet Gynaecol Can* 41 (10):1497-1507. doi:10.1016/j.jogc.2019.04.010
21. Sladkevicius P, Saltvedt S, Almstrom H, Kublickas M, Grunewald C, Valentin L (2005) Ultrasound dating at 12-14 weeks of gestation. A prospective cross-validation of established dating formulae in in-vitro fertilized pregnancies. *Ultrasound Obstet Gynecol* 26 (5):504-511. doi:10.1002/uog.1993

22. Hadlock FP, Harrist RB, Martinez-Poyer J (1991) In utero analysis of fetal growth: a sonographic weight standard. *Radiology* 181 (1):129-133. doi:10.1148/radiology.181.1.1887021
23. Hassibi S, Farhataziz N, Zaretsky M, McIntire D, Twickler DM (2004) Optimization of fetal weight estimates using MRI: comparison of acquisitions. *Am J Roentgenol* 183 (2):487-492. doi:10.2214/ajr.183.2.1830487
24. Gardosi J, Francis A (2015) Customised Weight Centile Calculator. GROW v6.7.7.1(UK). Gestation Network,
25. Kramer MS, Platt RW, Wen SW, Joseph KS, Allen A, Abrahamowicz M, Blondel B, Bréart G (2001) A new and improved population-based Canadian reference for birth weight for gestational age. *Pediatrics* 108 (2):E35. doi:10.1542/peds.108.2.e35
26. Fedorov A, Beichel R, Kalpathy-Cramer J, Finet J, Fillion-Robin JC, Pujol S, Bauer C, Jennings D, Fennessy F, Sonka M, Buatti J, Aylward S, Miller JV, Pieper S, Kikinis R (2012) 3D Slicer as an image computing platform for the Quantitative Imaging Network. *Magnetic resonance imaging* 30 (9):1323-1341. doi:10.1016/j.mri.2012.05.001
27. Kikinis R, Pieper SD, Vosburgh K (2014) 3D Slicer: a platform for subject-specific image analysis, visualization, and clinical support. In: Jolesz FA (ed) *Intraoperative Imaging Image-Guided Therapy*. Springer, New York,
28. Bernstein IM, Goran MI, Amini SB, Catalano PM (1997) Differential growth of fetal tissues during the second half of pregnancy. *Am J Obstet Gynecol* 176 (1 Pt 1):28-32. doi:10.1016/s0002-9378(97)80006-3
29. Hure AJ, Collins CE, Giles WB, Paul JW, Smith R (2012) Greater Maternal Weight Gain During Pregnancy Predicts a Large but Lean Fetal Phenotype: A Prospective Cohort Study. *Matern Child Health J* 16 (7):1374-1384. doi:10.1007/s10995-011-0904-8
30. Rasmussen JM, Entringer S, Nguyen A, van Erp TG, Burns J, Guijarro A, Oveisi F, Swanson JM, Piomelli D, Wadhwa PD, Buss C, Potkin SG (2013) Brown adipose tissue quantification in human neonates using water-fat separated MRI. *PLoS One* 8 (10):e77907. doi:10.1371/journal.pone.0077907
31. Hu HH, Yin L, Aggabao PC, Perkins TG, Chia JM, Gilsanz V (2013) Comparison of brown and white adipose tissues in infants and children with chemical-shift-encoded water-fat MRI. *J Magn Reson Imaging* 38 (4):885-896. doi:10.1002/jmri.24053
32. Yu H, McKenzie CA, Shimakawa A, Vu AT, Brau AC, Beatty PJ, Pineda AR, Brittain JH, Reeder SB (2007) Multiecho reconstruction for simultaneous water-fat decomposition and T2* estimation. *J Magn Reson Imaging* 26 (4):1153-1161. doi:10.1002/jmri.21090

33. Ma J (2004) Breath-hold water and fat imaging using a dual-echo two-point Dixon technique with an efficient and robust phase-correction algorithm. *Magn Reson Med* 52 (2):415-419. doi:10.1002/mrm.20146
34. Meisamy S, Hines CD, Hamilton G, Sirlin CB, McKenzie CA, Yu H, Brittain JH, Reeder SB (2011) Quantification of hepatic steatosis with T1-independent, T2-corrected MR imaging with spectral modeling of fat: blinded comparison with MR spectroscopy. *Radiology* 258 (3):767-775. doi:10.1148/radiol.10100708
35. Giza SA, Miller MR, Parthasarathy P, de Vrijer B, McKenzie CA (2018) Comparison of modified two-point Dixon and chemical shift encoded MRI water-fat separation methods for fetal fat quantification. *J Magn Reson Imaging* 48 (1):274-282. doi:10.1002/jmri.25929
36. Medicine Io, National Research Council Committee to Reexamine IOMPWG (2009) The National Academies Collection: Reports funded by National Institutes of Health. In: Rasmussen KM, Yaktine AL (eds) *Weight Gain During Pregnancy: Reexamining the Guidelines*. National Academies Press (US)

Copyright © 2009, National Academy of Sciences., Washington (DC).
doi:10.17226/12584

Chapter 3

3 Comparison of modified two-point Dixon and chemical shift encoded magnetic resonance imaging water-fat separation methods for fetal fat quantification

The contents of this chapter were previously published in the Journal of Magnetic Resonance Imaging: Giza, S.A., Miller, M.R., Parthasarathy, P., de Vrijer, B., McKenzie, C.A. (2018) Comparison of modified two-point Dixon and chemical shift encoded magnetic resonance imaging water-fat separation methods for fetal fat quantification. *J Magn Reson Imaging* 48 (1):274-282. Reproduced with permission from John Wiley and Sons. See Appendix F for permission.

3.1 Introduction

The assessment of abnormalities in fetal adipose tissue development may provide insight into fetal metabolic health because it is reflective of the energy balance within the fetus [1]. This energy balance may be disrupted in the case of placental insufficiency or when there are disruptions in maternal metabolism (obesity, diabetes) [2]. Previous imaging studies have found increased amounts of adipose tissue in macrosomic fetuses [3-5] and fetuses of diabetic mothers [6-8], and decreased adipose tissue in fetal growth restriction fetuses [8-10]. However, there are limited imaging studies that have examined the lipid content of the fetal adipose tissue, which changes through gestation as adipocytes are maturing.

Water-fat magnetic resonance imaging (MRI) is a reasonable technique to assess fetal adipose tissue development as it is sensitive to the amount of lipid within a tissue [11,12]. Two-point Dixon and chemical-shift encoded (CSE)-MRI are water-fat MRI methods that can be used to assess the lipid content of fetal adipose tissue. Each of these techniques have different strengths and weaknesses.

The modified two-point Dixon technique uses an opposed-phase gradient recalled echo combined with two-point Dixon water-fat separation [13]. Using two echoes, two-point Dixon produces in-phase and opposed-phase images, which are added or subtracted to

give lipid-only and water-only images. These can then be used to produce a fat signal fraction (FSF: lipid/(water + lipid)) image. Like two-point Dixon, CSE-MRI is a gradient recalled echo sequence, but instead of two echoes, it acquires six echoes that are used for water-fat separation [14-16]. The addition of multiple echoes allows for the modelling of more variables than that of modified two-point Dixon. In CSE-MRI, the fat fraction values calculated are equal to proton density fat fraction (PDFF) because of the additional variables [14-16].

Both techniques correct for B_0 field inhomogeneities; in modified two-point Dixon this is done through post-processing using a region-growing phase-correction algorithm developed by Ma [13]. In CSE-MRI, the B_0 field inhomogeneities are accounted for in the model used to fit the data [16]. Both modified two-point Dixon and CSE-MRI can use small flip angles to reduce the effects of T1 relaxation and therefore minimize T1 bias [17].

CSE-MRI differs from modified two-point Dixon in the modelling of both $R2^*$ relaxation and a six-peak lipid spectrum to the acquired data [13-16]. Meisamy et al. showed through comparison to magnetic resonance spectroscopy (MRS) that failing to correct for $R2^*$ relaxation and a multi-peak lipid spectrum introduces a bias in the fat fraction measured in the adult liver [15]. Additional corrections for eddy currents and noise bias are also included in the reconstruction [17,18]. Since these biases are not corrected in modified two-point Dixon, the FSF measured may not be as accurate as the PDFF obtained through CSE-MRI.

The strength of modified two-point Dixon lies in its availability and speed. Modified two-point Dixon is a more widely available sequence than CSE-MRI, which increases the use of this technique in multiple institutions. CSE-MRI requires the acquisition of images at more echo times (TEs) than modified two-point Dixon (at least 6 echoes vs. 2), resulting in inherently longer acquisitions for the same resolution and anatomic coverage. Additionally, the signal-to-noise ratio (SNR) of CSE-MRI is reduced due to the modelling of additional factors ($R2^*$) not included in the modified two-point Dixon signal model. For this reason, modified two-point Dixon may allow the acquisition of

images with both better SNR and/or shorter scan time, which is key in fetal imaging where motion is a major concern.

The purpose of this study was to compare modified two-point Dixon and CSE-MRI techniques for the quantification of fetal fat volume and PDFF/FSF.

3.2 Materials and methods

This study was approved by our institution's Human Studies Research Ethics Board (REB# 103845, see Appendix A). Informed consent was obtained when women were recruited from low-risk and specialized high-body mass index (BMI) obstetric clinics at our institution. Inclusion criteria consisted of the following: pregnant women over the age of 18 between 29 and 38 weeks gestational age (GA). Patients with any medical contraindication to safely undergoing a non-contrast MRI, weight/body habitus that would prevent a successful MRI study, or multiple pregnancy were excluded. One participant was excluded due to medical contraindication to safely undergoing a non-contrast MRI. Clinical data were collected from the participant's charts, including GA at the time of MRI, pre-pregnancy BMI, and diagnoses of fetal growth restriction or maternal diabetes (Table 3.1). Ultrasound was used to determine gestational age as described by the Society of Obstetricians and Gynaecologists of Canada (SOGC) Clinical Practice Guideline [19], with an error of ± 2 days [20].

Consenting participants underwent a fetal MRI in a wide-bore (70 cm diameter) 1.5 T MRI (General Electric Optima 450w, Milwaukee, WI, USA) with a 32-coil abdominal phased array. Women were positioned left decubitus or rolled towards a left lateral decubitus position with a cushion under either their back or their right side for comfort. Scout images (T2 weighted single shot fast spin echo (SSFSE)) were acquired to locate the fetus and determine its orientation.

Table 3.1 Participant demographics. Data listed as n (%). Total N = 21. BMI = body mass index

Characteristic	n (%)
Maternal BMI (kg/m ²)	
Underweight: < 18.5	2 (9.5%)
Normal: 18.5 – 24.9	10 (47.6%)
Overweight: 25 – 29.9	1 (4.8%)
Class I Obesity: 30 – 34.9	1 (4.8%)
Class II Obesity: 35 – 39.9	3 (14.3%)
Class III Obesity: ≥ 40	3 (14.3%)
Diabetic Status	
Pre-existing Type-1 Diabetes	1 (4.8%)
Pre-existing Type-2 Diabetes	1 (4.8%)
Gestational Diabetes	2 (9.5%)
Non-diabetic	17 (81.0%)
Growth Restriction	58.1 (0.5 – 96.6)
Growth Restricted	3 (14.3%)
Appropriate Growth	18 (85.7%)

Both 3D CSE-MRI (specific implementation iterative decomposition of water and fat with echo asymmetry and least squares estimation (IDEAL)-IQ) and modified 3D two-point Dixon (specific implementation Liver Acceleration Volume Acquisition (LAVA)-Flex) volumes were acquired in a plane axial to the fetal abdomen during a maternal breath hold (imaging parameters in Table 3.2). The two-point Dixon and CSE-MRI volumes were prescribed to match the anatomic coverage as closely as possible. Phase field of view and resolution, and slice thickness were altered as necessary to allow acquisition in the maternal breath hold, approximately 16 seconds. A second 3D CSE-MRI volume with anatomic coverage matched to the first acquisition was acquired at the end of each MRI exam.

Water-only, lipid-only, PDFF and R2* maps were reconstructed from the 3D CSE-MRI data using the method of Yu et al. [16,21,22]. Water-only and lipid-only images were reconstructed from the 3D Dixon data using the method of Ma et al. [13]. FSF image volumes were calculated voxel-by-voxel from the two-point Dixon lipid and water signal intensities ($FSF = \text{Lipid}/(\text{Water}+\text{Lipid})$).

Table 3.2. Imaging parameters for modified two-point Dixon and CSE-MRI acquisitions.

Parameter	Modified two-point Dixon	CSE-MRI
Repetition Time	6.0 – 6.6 ms	9.7 – 12.7 ms
Flip Angle	5°	6-7°
Field of View	50 cm	50 cm
Frequency Encodes	160	128 – 160
Phase Encodes	160	128 – 160
Slice Thickness	4 – 6.5 mm	4 – 6.5 mm
Number of Slices	42 – 64	42 – 78
ARC Acceleration Phase	2x	2x
ARC Acceleration Slice	2x	2.5x
ARC Acceleration Calibration Lines	32x32	32x32

Total fetal fat from the entire fetal volume was manually segmented (SG, 2 years experience) from all the PDFFF/FSF images using 3D Slicer (4.7.0 nightly build 2016-12-06) [21,22] by tracing along the border of high signal intensity corresponding to fetal fat. This included subcutaneous adipose tissue, perirenal adipose tissue, orbital adipose tissue, paravertebral adipose tissue and bone marrow when visible. Measured variables included the total segmented volume and the mean PDFFF/FSF within the segmented volume.

To investigate the failure to correct for R2* decay resulting in the appearance of artefactual “pseudo-fat” in Dixon acquisitions, all modified two-point Dixon volumes were evaluated for the appearance of fetal liver lipid through observation by two trained readers (SG 2 years experience, CM 25 years experience). The image volumes were sorted into either a pseudo-fat group when lipid appeared in the fetal liver, or a pseudo-fat-free group, when no lipid appeared in the fetal liver. The occurrence of elevated R2* in the fetal liver was evaluated by placing a 15mm spherical region of interest (ROI) within the fetal liver. R2* and PDFFF values were measured from these liver ROIs on CSE-MRI images.

Statistical analysis

The reliability of fat volume and PDFF/FSF measurements made with modified two-point Dixon and CSE-MRI were tested to assess the consistency of ordering between participants between the modified two-point Dixon and CSE-MRI. The inter-rater reliability of fat volume and PDFF were tested to assess the consistency of ordering between participants between two trained independent readers (SG 2 years experience, PP no previous experience), who each manually segmented 10 CSE-MRI PDFF sets. The inter-rater reliability of modified two-point Dixon segmentation was previously found to be very high in Chapter 2. Test-retest reliability of CSE-MRI derived fat volume and PDFF measurements were assessed by comparing measurements from the two 3D CSE-MRI acquisitions to assess the consistency of ordering between participants for each test. Intraclass correlation was used to test all three reliability assessments.

To assess the level of agreement (i.e., identical results) between modified two-point Dixon and CSE-MRI measurement of fat volume and PDFF/FSF, a one-sample t-test was performed on the fat measurements difference values (modified two-point Dixon minus CSE-MRI). These difference scores were tested against a value of 0, which would indicate that the measurements were identical. The average modified two-point Dixon/CSE-MRI measurement was plotted against the difference between the methods in Bland-Altman plots. The level of agreement for inter-rater and test-retest was examined in the same manner, with Bland-Altman plots using log values when appropriate. Mann-Whitney U tests were applied to detect differences between the pseudo-fat and pseudo-fat free groups' R2*, PDFF, and GA. All statistical analyses were conducted in SPSS v.24 (IBM Corporation, Armonk, NY, USA), and p-values < 0.05 were considered statistically significant.

3.3 Results

Twenty-nine women participated in the study. One participant was unable to complete the MRI, 3 were excluded from analysis related to fetal motion, and 2 were excluded from analysis for severe artefact. Two fetuses had no segmentable fat. Of the remaining 21 fetuses, one had severe motion artifacts in modified two-point Dixon, leaving 20 fetuses for the comparison of modified two-point Dixon and CSE-MRI. 3D renderings and segmentations of total fetal fat from modified two-point Dixon and CSE-MRI are

shown in Figure 3.1. The intraclass correlation coefficient (ICC) between modified two-point Dixon and CSE-MRI for fetal fat volume was 0.928 ($p < 0.001$) and for fetal PDFF/FSF was 0.898 ($p < 0.001$), indicating strong reliability for both measurements. The t-test for fetal fat volume difference (modified two-point Dixon – CSE-MRI) against 0 was significant ($p < 0.001$), indicating that the two methods were not statistically identical. The mean and standard deviation for fetal fat volume measured by modified two-point Dixon was 980 ± 360 mL, and by CSE-MRI was 1180 ± 390 mL. The mean difference (modified two-point Dixon – CSE-MRI) for fetal fat volume was -180 mL. The Bland-Altman plot for fetal fat volume is shown in Figure 3.2A. The t-test for fetal PDFF/FSF difference (modified two-point Dixon – CSE-MRI) against 0 was also significant ($p = 0.001$), again indicating that the two methods were not statistically identical. The mean difference (modified two-point Dixon – CSE-MRI) for PDFF/FSF was 3.0%. The Bland-Altman plot for fetal PDFF/FSF is shown in Figure 3.2B.

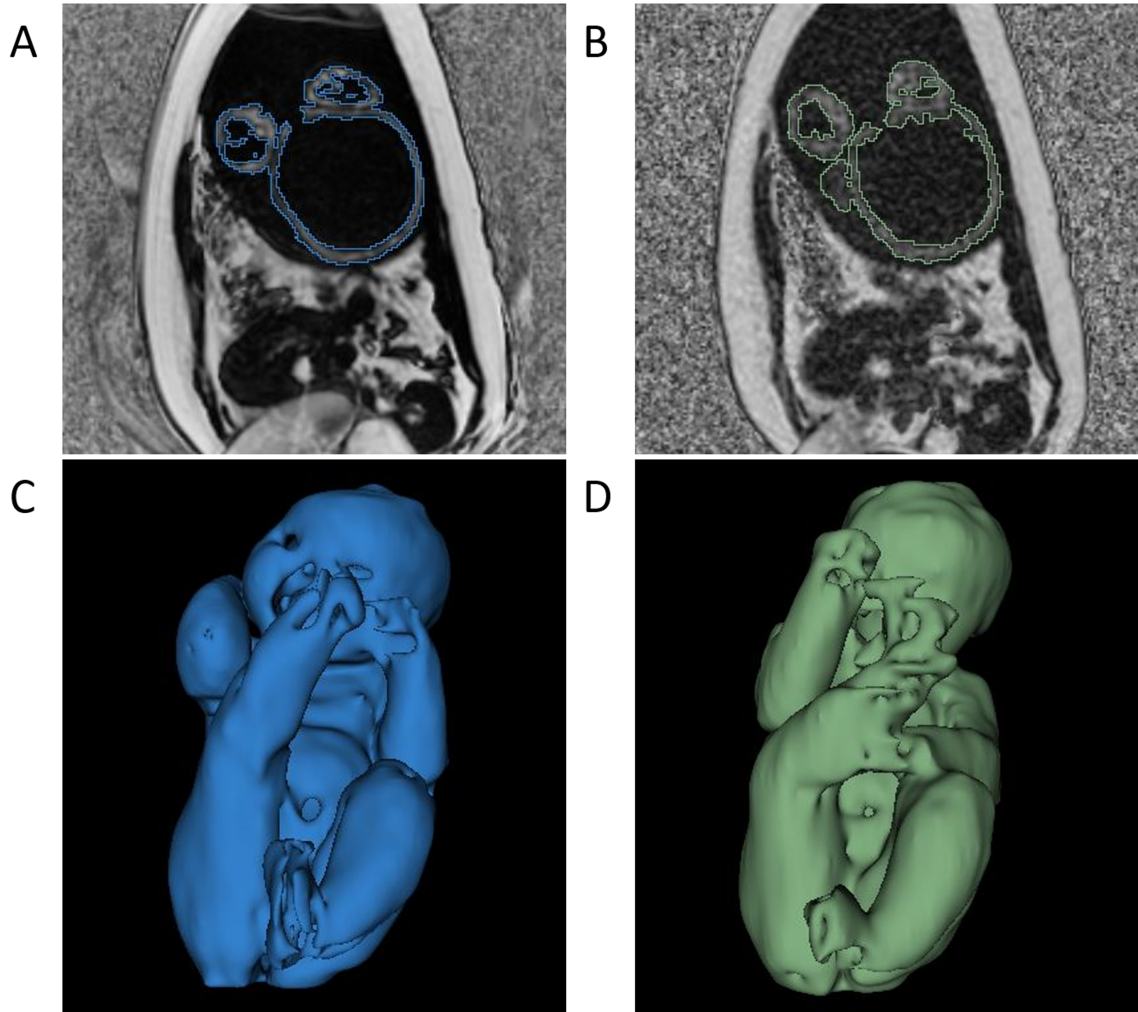


Figure 3.1. Total fetal fat (A) segmentation on modified two-point Dixon, (B) segmentation on CSE-MRI, (C) 3D rendering from modified two-point Dixon, (D) 3D render from CSE-MRI. Images A and B are displayed axial to the fetal abdomen through the fetal umbilicus. 3D renders C and D are created from the segmentations in A and B. The hands and feet have limited lipid and, therefore, appear incomplete and patchy in the 3D renders.

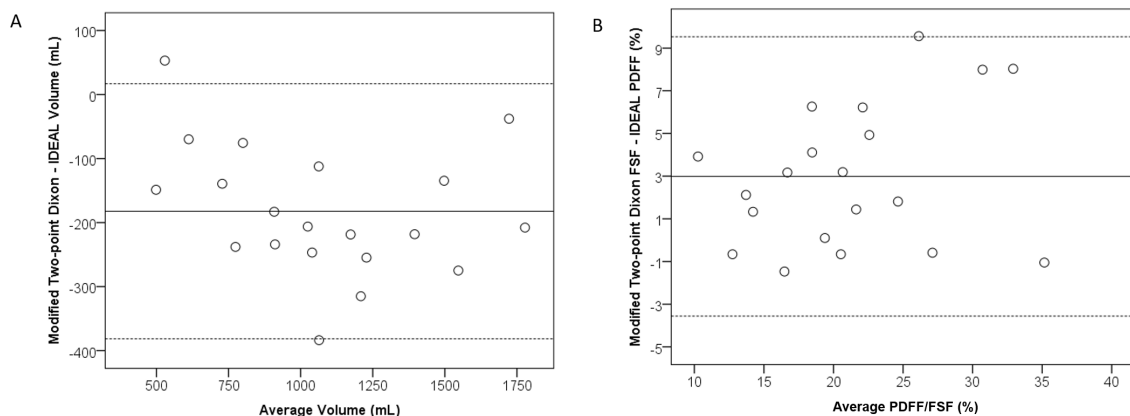


Figure 3.2. Bland-Altman plots of fetal (A) fat volume and (B) PDFF/FSF from modified two-point Dixon and CSE-MRI. The solid black line indicates the mean difference between the techniques (A: -180 mL, B: 3.0%), while the two dashed lines indicate the 95% confidence intervals (A: -380, 20 mL, B: -3.6, 9.5%). This demonstrates that modified two-point Dixon underestimates fetal fat volume while overestimating fetal PDFF/FSF compared with CSE-MRI.

Of the 21 fetuses examined, 7 had pseudo-fat appear in their livers with modified two-point Dixon, while no fetuses had detectable liver lipid with CSE-MRI. Sample images, including modified two-point Dixon lipid images, CSE-MRI PDFF images, and CSE-MRI R2* maps for pseudo-fat and pseudo-fat free groups, are shown in Figure 3.3.

Mann-Whitney U tests indicated that there was a significant difference in the fetal liver R2* between the pseudo-fat and pseudo-fat free groups ($p < 0.001$) (Figure 3.4A), but not in their liver PDFF measured by CSE-MRI ($p = 0.332$) (Figure 3.4B) or their GA at MRI ($p = 0.654$) (Figure 3.4C). All the fetuses with pseudo-fat had liver R2* values ≥ 45 s⁻¹, whereas all the fetuses without pseudo-fat had liver R2* values ≤ 35 s⁻¹.

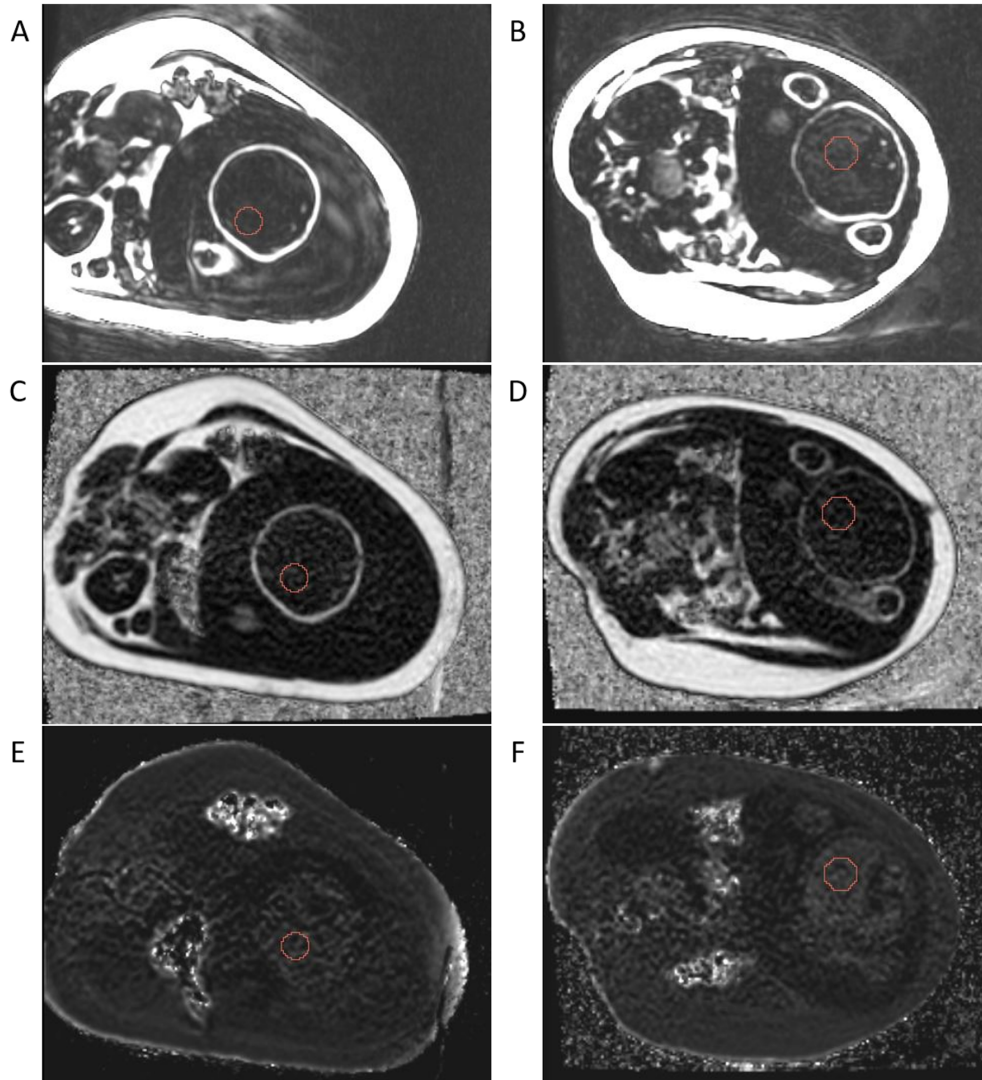


Figure 3.3. Comparison of pseudo-fat free and pseudo-fat fetuses. (A) Modified two-point Dixon lipid image without pseudo-fat in the liver, (B) Modified two-point Dixon lipid image showing pseudo-fat in the liver, (C) CSE-MRI PDFF image from the same participant and slice as A, (D) CSE-MRI PDFF image from the same participant and slice as B, (E) CSE-MRI $R2^*$ map from the same participant and slice as A, and (F) CSE-MRI $R2^*$ map from the same participant and slice as B. Images are displayed axial to the fetal abdomen, with the spherical liver ROI outlined in red. Lipid images have been windowed and levelled to display the signal in the fetal livers. The fat fraction measured in image C (pseudo-fat free) was 6.9%,

and in image D (pseudo-fat) was 3.7%. The $R2^*$ measured in image E (pseudo-fat free) was 31 s^{-1} , and in image F (pseudo-fat) was 45 s^{-1} .

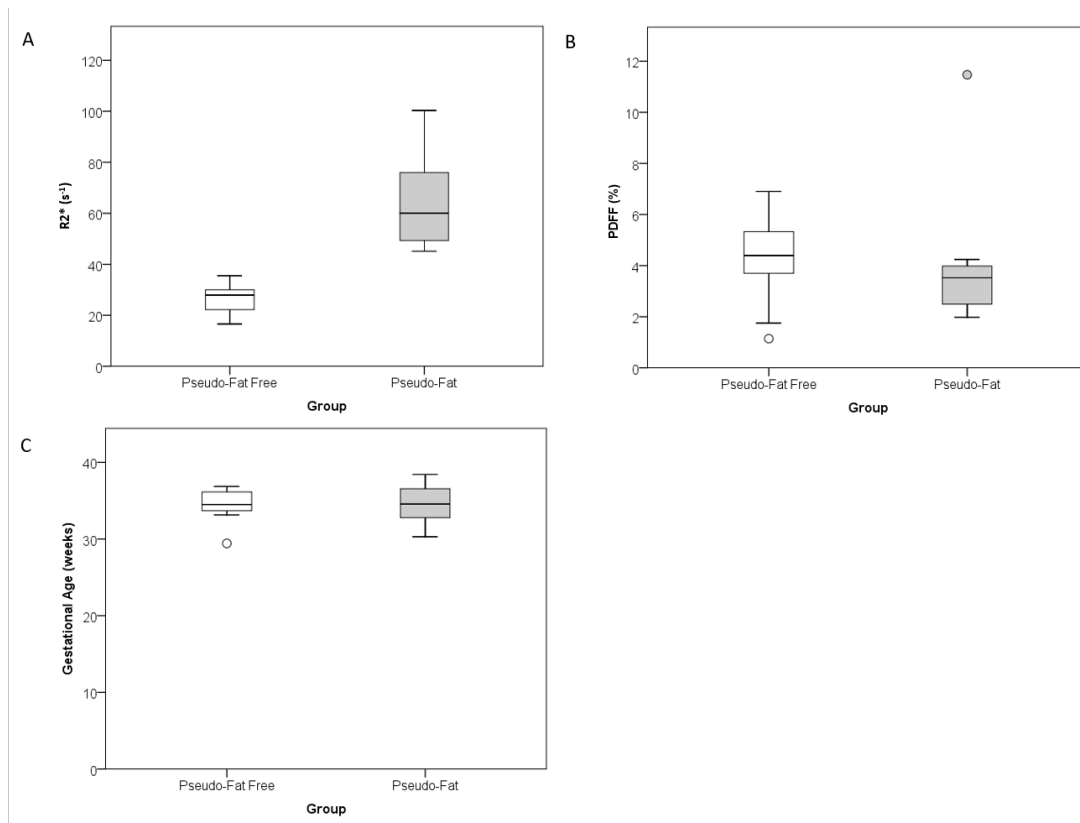


Figure 3.4. Box and whisker plots of fetal liver (A) $R2^*$ values and (B) PDFF measured from CSE-MRI, and (C) GA at MRI for the pseudo-fat and pseudo-fat free groups. Mann-Whitney U-test indicates a significant difference between the groups $R2^*$ values ($p < 0.001$), where the pseudo-fat group has a higher fetal liver $R2^*$ than the pseudo-fat free group. No significant differences were found in the PDFF or GA between the groups ($p = 0.881$, $p = 0.654$). Outliers are shown as circles outside of the box and whisker plots.

Seventeen fetuses had 2 sets of motion-free CSE-MRI images and were used for test-retest reliability. The ICC for fetal fat volume was 0.971 ($p < 0.001$) and for fetal PDFF was 0.980 ($p < 0.001$), indicating strong test-retest reliability. The t-test for difference (test-retest) against 0 for fetal fat volume was not significant ($p = 0.152$), indicating the results were statistically similar. No proportional bias was detected, as shown in the

Bland Altman plot (Figure 3.5A). The t-test for difference (test – retest) against 0 for fetal PDFF was significant ($p = 0.045$), indicating that the test-retest was not statistically identical. The magnitude of the difference gives an estimate of the bias detected, which was 0.9%. The Bland-Altman plot is shown in Figure 3.5B.

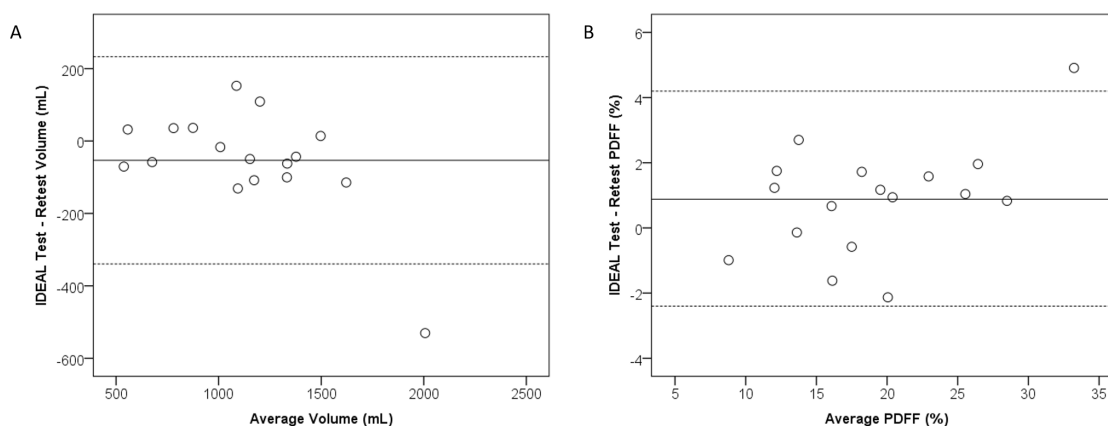


Figure 3.5. Bland-Altman plot of fetal (A) fat volume and (B) PDFF from CSE-MRI test-retest. The solid black line indicates the mean difference between the acquisitions (A: -50 mL, B: 0.9%), while the two dashed lines indicate the 95% confidence intervals (A: -340, 230 mL, B: -2.4, 4.2%). This demonstrates that there is no proportional bias in the fetal fat volume between the acquisitions, and a small bias (<1%) for higher PDFF measurements in the first CSE-MRI acquisition relative to the second acquisition.

The ICC between the two readers for fetal fat volume was 0.897 ($p = 0.002$), and for fetal PDFF was 0.946 ($p < 0.001$). This shows strong inter-rater reliability. The t-tests for difference (reader 1 – reader 2) against 0 for fetal fat volume and PDFF were not significant ($p = 0.847$ and $p = 0.706$), indicating the results were statistically similar. No proportional bias was detected, as shown in the Bland-Altman plots (Figure 3.6).

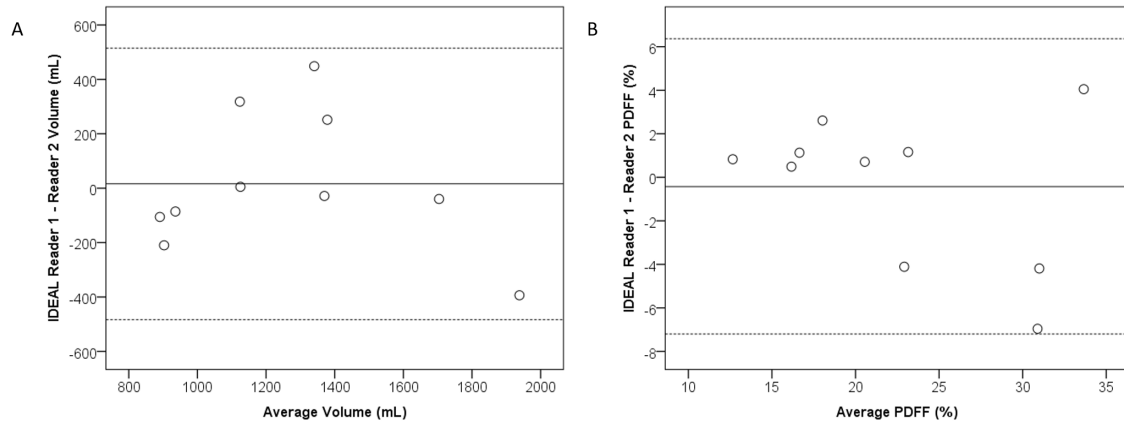


Figure 3.6. Bland-Altman plot of fetal (A) fat volume and (B) PDFF measured by two readers. The solid black line indicates the mean difference between the two readers' measurements (A: 20 mL, B: -0.4%), while the two dashed lines indicate the 95% confidence intervals (A: -480, 520 mL, B: -7.2, 6.4%). This demonstrates that there is no proportional bias between the readers' measurements of fetal fat volume or PDFF.

3.4 Discussion

Our results indicate that modified two-point Dixon and CSE-MRI measurements of fat fraction and fat volume are reliable, but not in agreement. Although both methodologies have good ICCs and can be used for comparison between participants, differences between measured total fetal fat fraction warrants questions regarding the accuracy of one or both methods.

Modified two-point Dixon has biases present in the FSF because it does not correct for $R2^*$ and does not use a multiphase lipid spectrum [13]. Meisamy et al. have shown that failing to incorporate these two factors into the modelling of signal from Dixon methods introduces a bias compared to spectroscopy results [15]. This bias can result in the appearance of pseudo-fat in tissue with elevated $R2^*$ values when no lipid actually exists in that tissue.

In our imaging of fetal fat, we observed examples of this bias in the fetal liver. When the fetal liver had elevated $R2^*$ (short $T2^*$), pseudo-fat appeared in the liver on modified

two-point Dixon lipid images. This was not seen in the CSE-MRI images, since $R2^*$ is accounted for in the modelling. This was a common occurrence, with one-third of the fetuses we imaged having the appearance of pseudo-fat in the liver on modified two-point Dixon images. It has previously been shown that the fetal liver in the third trimester has a larger $R2^*$ (50 s^{-1} at 1.5 T) compared to that in the adult liver (36 s^{-1} at 1.5 T) [23]. This occurs because the fetal liver is a major hemopoietic site during fetal development and therefore acts as a reservoir for iron in the third trimester [23]. $R2^*$ -weighted gradient recalled echo sequences have previously been used in the investigation of hemochromatosis [24], and together these results suggest that CSE-MRI could be used in the future to investigate hematopoiesis through gestation as well as prenatal detection of hemochromatosis.

We believe that CSE-MRI should be the preferred method for measuring fetal fat fraction, as the biases present in modified two-point Dixon have been corrected [16,25,26]. This has been shown in the adult liver by comparing to spectroscopy [15], and it is likely that similar factors are at play in the fetus, as demonstrated in the fetal livers from our study.

Previous studies have used PDFF to distinguish brown adipose tissue from white adipose tissue in infants, as brown adipose tissue has a lower PDFF [27-29]. Unbiased fat fraction measurements are key to this differentiation; therefore, CSE-MRI would be best suited to an investigation of brown adipose tissue in the fetus. This would be especially important for assessing brown adipose tissue across gestation, as white adipose tissue has a lower lipid content at earlier GA [30], and therefore the difference between the fat fractions of brown and white adipose tissues may be small.

Test-retest showed that CSE-MRI is a reliable method for measurement of fetal fat volumes and PDFF. The volumes measured with the CSE-MRI test-retest agreed; however, their PDFF values were not statistically identical. The mean bias between the two methods was less than 1%, which is small enough that there should be no practical difference in the values measured. The inter-rater reliability and agreement of the fetal fat

volumes and PDFF were also good, indicating that this is a robust method for assessment of fetal adipose tissue.

While test-retest of the CSE-MRI shows it is a reliable method, this does not account for the cases where one of the image sets was severely motion corrupted. One potential solution is to use a radial water-fat separation MRI technique which would be more motion robust [31,32]. These radial techniques allow the images to be collected free-breathing, which would allow collection of images with better SNR and increased resolution. Both improvements would be of great benefit to imaging the fetal adipose tissue, as these are smaller structures with lower PDFF values than seen in adults or even neonates. However, current implementations of radial water-fat separation MRI tend to have scan times measured in minutes, so they may be vulnerable to artefacts from motion of the fetus. Nevertheless, fetal adipose tissue imaging should be considered a promising future application for radial water-fat separation MRI techniques.

The high cost of MRI and the need for repeated measurements to follow fetal growth and adipose tissue development make it unlikely that fetal water-fat MRI will ever be used as a screening tool for abnormal growth in uncomplicated pregnancies. However, there is a clinical and research need for improved non-invasive assessment of fetal health and metabolic development during pregnancy, specifically in high-risk populations such as women with obesity, gestational diabetes and at risk for preeclampsia. Measurement of fetal adipose tissue development using water-fat MRI may, for instance, assist clinicians in the management of pregnancies with obesity and/or diabetes, a population with threefold increases in stillbirth rates in whom it is more difficult to determine abnormal fetal growth using conventional ultrasound [33,34]. In this population, fetal growth curves have limitations [35] and underlying deficiencies in placental function are inflammatory in nature [36], a process to which ultrasound is insensitive. This inability to assess fetal and placental health [37,38] leaves these pregnancies at risk for complications and may contribute to the increases in stillbirth, neonatal morbidity and mortality seen in this population. Since deficiencies in placental function will likely have downstream effects on fetal metabolic health, indirect assessment of fetal metabolism through fetal

adipose tissue measurement has potential utility in high-risk pregnancies (high BMI, diabetes) to help direct management of pregnancy and delivery.

Strengths of our study include using 3D techniques, the measurement of total fetal fat and inclusion of a heterogeneous group of participants. By using 3D techniques to measure total fetal fat with both sequences, we minimized the effect of fetal position. Since the fetus is liable to move between sequences, it is possible it is in a different position during modified two-point Dixon and CSE-MRI acquisitions. This positional effect is reduced by the assessment of the entire fetus with a 3D acquisition, resulting in measuring total fetal fat, regardless of fetal position. We recruited a heterogeneous population of participants, including normal and high BMI, growth-restricted fetuses, and diabetic mothers and have demonstrated that our results are applicable to most obstetric populations.

Limitations of this study include testing at one field strength only, limited GA range, and uncertainty about the fetal lipid spectrum. We performed this comparison at 1.5 T only, and although it is expected that results will remain similar at 3.0 T, future studies should be conducted for confirmation. Additionally, future studies at an earlier GA than 29-38 weeks can elucidate whether the performance of two-point Dixon and CSE-MRI are affected by the lower fat fractions expected earlier in gestation. The expectation is that at lower FSF the biases in two-point Dixon are minimized, whereas CSE-MRI will struggle at low PDFF values because of its lower signal-to-noise efficiency. Therefore, it is possible that modified two-point Dixon is preferable at lower GA.

An additional limitation is that we did not examine the lipid spectrum of fetal adipose tissue with MRS, and it is possible that the fetal lipid spectrum differs from the six-peak adult lipid spectrum employed by Quantitative CSE-MRI, potentially introducing a source of bias in the fetal PDFF measurements. If the fetal lipid spectrum differs from the adult lipid spectrum assumed in the model used to fit the CSE-MRI data, errors could be introduced during the separation of water and lipid signals. It has been shown that over the biologically possible range of multipeak lipid spectral models there is minimal difference in PDFF (<2%) when compared in the livers of patients with non-alcoholic

steatohepatitis [39]. So, while it is unlikely that any differences between the fetal and adult lipid spectrum would introduce large errors in PDFF measurement, MRS should be used to determine the fetal lipid spectrum and investigate GA changes and differences from the adult spectrum. This knowledge could be used to alter the spectral model of lipid used in CSE-MRI and allow more accurate PDFF estimation for fetal water-fat imaging.

3.5 Conclusions

In conclusion, either modified two-point Dixon or CSE-MRI can be used to compare fetal fat volumes and PDFF/FSF between participants. Caution should be used when imaging fetal liver with modified two-point Dixon, particularly in the third trimester where elevated $R2^*$ effects are common. In terms of potential biases in measuring PDFF and fat volume in the fetus, we feel that CSE-MRI is a better method of choice than modified two-point Dixon.

3.6 References

1. Toro-Ramos T, Paley C, Pi-Sunyer FX, Gallagher D (2015) Body composition during fetal development and infancy through the age of 5 years. *Eur J Clin Nutr* 69 (12):1279-1289. doi:10.1038/ejcn.2015.117
2. Ornoy A (2011) Prenatal origin of obesity and their complications: Gestational diabetes, maternal overweight and the paradoxical effects of fetal growth restriction and macrosomia. *Reprod Toxicol* 32 (2):205-212. doi:10.1016/j.reprotox.2011.05.002
3. Hill LM, Guzik D, Boyles D, Merolillo C, Ballone A, Gmitter P (1992) Subcutaneous tissue thickness cannot be used to distinguish abnormalities of fetal growth. *Obstet Gynecol* 80 (2):268-271
4. Higgins MF, Russell NM, Mulcahy CH, Coffey M, Foley ME, McAuliffe FM (2008) Fetal anterior abdominal wall thickness in diabetic pregnancy. *Eur J Obstet Gynecol Reprod Biol* 140 (1):43-47. doi:10.1016/j.ejogrb.2008.02.021
5. Chauhan SP, West DJ, Scardo JA, Boyd JM, Joiner J, Hendrix NW (2000) Antepartum detection of macrosomic fetus: clinical versus sonographic, including soft-tissue measurements. *Obstet Gynecol* 95 (5):639-642. doi:10.1016/s0029-7844(99)00606-7
6. Larciprete G, Di Pierro G, Barbati G, Deaibess T, Jarvis S, Valensise H, Romanini ME, Gioia S, Arduini D (2008) Could birthweight prediction models be improved by

- adding fetal subcutaneous tissue thickness? *J Obstet Gynaecol Res* 34 (1):18-26. doi:10.1111/j.1447-0756.2007.00741.x
7. Anblagan D, Deshpande R, Jones NW, Costigan C, Bugg G, Raine-Fenning N, Gowland PA, Mansell P (2013) Measurement of fetal fat in utero in normal and diabetic pregnancies using magnetic resonance imaging. *Ultrasound Obstet Gynecol* 42 (3):335-340. doi:10.1002/uog.12382
 8. Deans HE, Smith FW, Lloyd DJ, Law AN, Sutherland HW (1989) Fetal fat measurement by magnetic resonance imaging. *Br J Radiol* 62:603-607
 9. Stark DD, McCarthy SM, Filly RA, Callen PW, Hricak H, Parer JT (1985) Intrauterine growth retardation: evaluation by magnetic resonance. Work in progress. *Radiology* 155 (2):425-427. doi:10.1148/radiology.155.2.3885309
 10. Larciprete G, Valensise H, Di Pierro G, Vasapollo B, Casalino B, Arduini D, Jarvis S, Cirese E (2005) Intrauterine growth restriction and fetal body composition. *Ultrasound Obstet Gynecol* 26 (3):258-262. doi:10.1002/uog.1980
 11. Reeder SB, Hu HH, Sirlin CB (2012) Proton density fat-fraction: a standardized MR-based biomarker of tissue fat concentration. *J Magn Reson Imaging* 36 (5):1011-1014. doi:10.1002/jmri.23741
 12. Reeder SB, McKenzie CA, Pineda AR, Yu H, Shimakawa A, Brau AC, Hargreaves BA, Gold GE, Brittain JH (2007) Water-fat separation with IDEAL gradient-echo imaging. *J Magn Reson Imaging* 25 (3):644-652. doi:10.1002/jmri.20831
 13. Ma J (2004) Breath-hold water and fat imaging using a dual-echo two-point Dixon technique with an efficient and robust phase-correction algorithm. *Magn Reson Med* 52 (2):415-419. doi:10.1002/mrm.20146
 14. Hines CD, Frydrychowicz A, Hamilton G, Tudorascu DL, Vigen KK, Yu H, McKenzie CA, Sirlin CB, Brittain JH, Reeder SB (2011) T(1) independent, T(2) (*) corrected chemical shift based fat-water separation with multi-peak fat spectral modeling is an accurate and precise measure of hepatic steatosis. *J Magn Reson Imaging* 33 (4):873-881. doi:10.1002/jmri.22514
 15. Meisamy S, Hines CD, Hamilton G, Sirlin CB, McKenzie CA, Yu H, Brittain JH, Reeder SB (2011) Quantification of hepatic steatosis with T1-independent, T2-corrected MR imaging with spectral modeling of fat: blinded comparison with MR spectroscopy. *Radiology* 258 (3):767-775. doi:10.1148/radiol.10100708
 16. Yu H, Shimakawa A, Hines CD, McKenzie CA, Hamilton G, Sirlin CB, Brittain JH, Reeder SB (2011) Combination of complex-based and magnitude-based multiecho water-fat separation for accurate quantification of fat-fraction. *Magn Reson Med* 66 (1):199-206. doi:10.1002/mrm.22840

17. Liu CY, McKenzie CA, Yu H, Brittain JH, Reeder SB (2007) Fat quantification with IDEAL gradient echo imaging: correction of bias from T(1) and noise. *Magn Reson Med* 58 (2):354-364. doi:10.1002/mrm.21301
18. Yu H, Shimakawa A, McKenzie CA, Lu W, Reeder SB, Hinks RS, Brittain JH (2010) Phase and amplitude correction for multi-echo water-fat separation with bipolar acquisitions. *J Magn Reson Imaging* 31 (5):1264-1271. doi:10.1002/jmri.22111
19. Butt K, Lim KI (2019) Guideline No. 388-Determination of Gestational Age by Ultrasound. *J Obstet Gynaecol Can* 41 (10):1497-1507. doi:10.1016/j.jogc.2019.04.010
20. Sladkevicius P, Saltvedt S, Almstrom H, Kublickas M, Grunewald C, Valentin L (2005) Ultrasound dating at 12-14 weeks of gestation. A prospective cross-validation of established dating formulae in in-vitro fertilized pregnancies. *Ultrasound Obstet Gynecol* 26 (5):504-511. doi:10.1002/uog.1993
21. Fedorov A, Beichel R, Kalpathy-Cramer J, Finet J, Fillion-Robin JC, Pujol S, Bauer C, Jennings D, Fennessy F, Sonka M, Buatti J, Aylward S, Miller JV, Pieper S, Kikinis R (2012) 3D Slicer as an image computing platform for the Quantitative Imaging Network. *Magnetic resonance imaging* 30 (9):1323-1341. doi:10.1016/j.mri.2012.05.001
22. Kikinis R, Pieper SD, Vosburgh K (2014) 3D Slicer: a platform for subject-specific image analysis, visualization, and clinical support. In: Jolesz FA (ed) *Intraoperative Imaging Image-Guided Therapy*. Springer, New York,
23. Goitein O, Eshet Y, Hoffmann C, Raviv-Zilka L, Salem Y, Hamdan A, Goitein D, Kushnir T, Eshed I, Di-Segni E, Konen E (2013) Fetal liver T2* values: defining a standardized scale. *J Magn Reson Imaging* 38 (6):1342-1345. doi:10.1002/jmri.24132
24. Martí-Bonmatí L, Baamonde A, Poyatos CR, Monteagudo E (1994) Prenatal diagnosis of idiopathic neonatal hemochromatosis with MRI. *Abdom Imaging* 19 (1):55-56. doi:10.1007/bf02165863
25. Yu H, McKenzie CA, Shimakawa A, Vu AT, Brau AC, Beatty PJ, Pineda AR, Brittain JH, Reeder SB (2007) Multiecho reconstruction for simultaneous water-fat decomposition and T2* estimation. *J Magn Reson Imaging* 26 (4):1153-1161. doi:10.1002/jmri.21090
26. Yu H, Shimakawa A, McKenzie CA, Brodsky E, Brittain JH, Reeder SB (2008) Multiecho water-fat separation and simultaneous R2* estimation with multifrequency fat spectrum modeling. *Magn Reson Med* 60 (5):1122-1134. doi:10.1002/mrm.21737
27. Hu HH, Yin L, Aggabao PC, Perkins TG, Chia JM, Gilsanz V (2013) Comparison of brown and white adipose tissues in infants and children with chemical-shift-encoded water-fat MRI. *J Magn Reson Imaging* 38 (4):885-896. doi:10.1002/jmri.24053

28. Hu HH, Wu TW, Yin L, Kim MS, Chia JM, Perkins TG, Gilsanz V (2014) MRI detection of brown adipose tissue with low fat content in newborns with hypothermia. *Magn Reson Imaging* 32 (2):107-117. doi:10.1016/j.mri.2013.10.003
29. Hu HH, Tovar JP, Pavlova Z, Smith ML, Gilsanz V (2012) Unequivocal identification of brown adipose tissue in a human infant. *J Magn Reson Imaging* 35 (4):938-942. doi:10.1002/jmri.23531
30. Poissonnet CM, Burdi AR, Garn SM (1984) The chronology of adipose tissue appearance and distribution in the human fetus. *Early Hum Dev* 10 (1-2):1-11. doi:10.1016/0378-3782(84)90106-3
31. Moran CJ, Brodsky EK, Bancroft LH, Reeder SB, Yu H, Kijowski R, Engel D, Block WF (2014) High-resolution 3D radial bSSFP with IDEAL. *Magn Reson Med* 71 (1):95-104. doi:10.1002/mrm.24633
32. Benkert T, Feng L, Sodickson DK, Chandarana H, Block KT (2017) Free-breathing volumetric fat/water separation by combining radial sampling, compressed sensing, and parallel imaging. *Magn Reson Med* 78 (2):565-576. doi:10.1002/mrm.26392
33. Cedergren MI (2004) Maternal morbid obesity and the risk of adverse pregnancy outcome. *Obstet Gynecol* 103 (2):219-224. doi:10.1097/01.Aog.0000107291.46159.00
34. Flenady V, Koopmans L, Middleton P, Frøen JF, Smith GC, Gibbons K, Coory M, Gordon A, Ellwood D, McIntyre HD, Fretts R, Ezzati M (2011) Major risk factors for stillbirth in high-income countries: a systematic review and meta-analysis. *Lancet* 377 (9774):1331-1340. doi:10.1016/s0140-6736(10)62233-7
35. Luring JR, Gupta M, Kunselman AR, Repke JT, Pauli JM (2016) Identification of small for gestational age by population-based and customized growth charts in newborns of obese and normal-weight primiparous women. *J Matern Fetal Neonatal Med* 29 (21):3570-3574. doi:10.3109/14767058.2016.1139568
36. Pantham P, Aye IL, Powell TL (2015) Inflammation in maternal obesity and gestational diabetes mellitus. *Placenta* 36 (7):709-715. doi:10.1016/j.placenta.2015.04.006
37. Sarno L, Maruotti GM, Saccone G, Morlando M, Sirico A, Martinelli P (2015) Maternal body mass index influences umbilical artery Doppler velocimetry in physiologic pregnancies. *Prenat Diagn* 35 (2):125-128. doi:10.1002/pd.4499
38. Wong SF, Chan FY, Cincotta RB, McIntyre DH, Stone M (2003) Use of umbilical artery Doppler velocimetry in the monitoring of pregnancy in women with pre-existing diabetes. *Aust N Z J Obstet Gynaecol* 43 (4):302-306. doi:10.1046/j.0004-8666.2003.00094.x
39. Hong CW, Mamidipalli A, Hooker JC, Hamilton G, Wolfson T, Chen DH, Fazeli Dehkordy S, Middleton MS, Reeder SB, Loomba R, Sirlin CB (2018) MRI proton

density fat fraction is robust across the biologically plausible range of triglyceride spectra in adults with nonalcoholic steatohepatitis. *J Magn Reson Imaging* 47 (4):995-1002.
doi:10.1002/jmri.25845

Chapter 4

4 Water-fat magnetic resonance imaging of adipose tissue compartments in the third trimester fetus

The contents of this chapter were previously published in the journal *Pediatric Radiology* (<https://www.springer.com/journal/247>): Giza, S.A., Koreman, T.L., Sethi, S., Miller, M.R., Penava, D.A., Eastabrook, G.D., McKenzie, C.A., de Vrijer, B. (2021) Water-fat magnetic resonance imaging of adipose tissue compartments in the normal third trimester fetus. *Pediatric Radiology* 51 (7):1214-1222. Reproduced with permission from Springer Nature. See Appendix G for permission.

4.1 Introduction

Development and growth *in utero* are linked to infant and child health; adverse uterine environments increase risks for the development of later-life diseases such as obesity, diabetes, and cardiovascular disease [1]. These risks have been well described in the developmental origins of health and disease (DOHaD) literature and are postulated to be the result of changes in fetal metabolism in response to an altered nutrient supply [1]. With alterations in pregnancy conditions and provision of energy, such as with placental insufficiency or gestational diabetes, growth and development are affected, with some fetuses becoming lean, and some growing excessively. These changes can affect long-term metabolic health irreversibly, especially when met with a nutritional mismatch or continued exposure to insufficient or excess feeding as an infant or child [2]. Assessment of fetal adipose tissue, an indicator of energy deposition for the fetus, offers information about this potential programming *in utero*.

Fetal adipocyte formation starts with the development of pre-adipocytes, which transition from cells that contain very little lipid to cells with multiple lipid-containing vacuoles [3]. Water-fat magnetic resonance imaging (MRI) is a non-invasive technique that measures lipid accumulation in adipocytes by quantification of the ratio of lipid to lipid plus water content, called the proton density fat fraction (PDFF) and expressed in units of % [4], allowing for non-invasive and longitudinal assessment of fetal adipose tissue.

Additionally, there is a capacity to measure $R2^*$, the rate of signal decay in MRI, which is affected by the change in distribution, size, and number of lipid vesicles as the result of differences in the magnetic susceptibilities of lipid and water.

Safe assessment of subcutaneous fetal adipose tissue using MRI in the 3rd trimester of pregnancy has been demonstrated in Chapter 2. Fat signal fraction (FSF) in subcutaneous adipose tissue in the fetal trunk increase from 10% at 30 weeks to 24% at 34 weeks gestational age (GA), increasing to 78% (63 - 89%) in the infant shoulder by 5 months of age [5]. Full maturity of adipocytes is likely not reached until late childhood or adolescence [5], when the cells contain very little water and are dominated by a single, large lipid droplet, resulting in an adipose tissue lipid fraction near 90% [3]. Various locations throughout the body have been assessed for deposition of fetal and neonatal adipose tissue. Ultrasound has been used to measure tissue thickness or fetal subcutaneous adipose volume mainly in thighs and arms; these studies have correlated the amount of adipose tissue to adverse pregnancy outcomes such as gestational diabetes and fetal growth restriction [6-8]. Additionally, the adipose tissue in different compartments may be affected differently in different pregnancy conditions, making it vital to determine volumes and spatial differences of the adipose tissue (and the location in the body) being examined.

There are two main types of adipose tissue with different functions. Differences between them may help with understanding the role of adipose tissue and metabolic health. White adipose tissue is primarily used as an energy storage organ, whereas brown adipose tissue functions as a heat-generating organ. Brown adipose tissue contains multiple small lipid vacuoles and has a lower lipid content. As such, it also has a lower PDFF than white adipose tissue, which is dominated by a single large lipid vacuole when mature [9]; this makes water-fat MRI a useful tool to differentiate between white adipose tissue and brown adipose tissue. Additionally, $R2^*$ is higher in brown adipose tissue compared to white adipose tissue in children [5], due to brown adipose tissue having a large number of iron-rich mitochondria and a greater blood supply than white adipose tissue [9]. These results suggest that measurement of both PDFF and $R2^*$ may aid in identifying brown adipose tissue and white adipose tissue *in utero*.

Given the knowledge and development of fetal adipose tissue generated to date, along with the correlation to fetal and adult disease, the aim of this study was to evaluate water-fat MRI as a measurement tool to assess differences in the lipid content of different fetal adipose tissue compartments during a time of pregnancy with rapid lipid accumulation. We also compared perirenal adipose tissue, a known location of brown adipose tissue, with subcutaneous white adipose tissue to provide insight into any differences between brown adipose tissue and white adipose tissue during fetal development. We postulated that PDFFF measurement would detect the temporal sequence of fetal adipocyte development in different tissue compartments.

4.2 Materials and Methods

This study was approved by Western University Research Ethics Board (HSREB 103845, see Appendix A). Women older than 18 years with singleton pregnancies in the 3rd trimester were recruited from obstetric clinics and provided informed consent. Patients with medical contraindications to safely undergo a non-contrast MRI, or weight/body habitus that would prevent a successful MRI study were excluded. Women with suspicion of fetal growth restriction or diabetes (pre-existing or gestational) were removed from the analysis. Clinical data were collected from the participants' charts. The Society of Obstetricians and Gynaecologists of Canada (SOGC) Clinical Practice Guideline for determination of gestational age by ultrasound was followed [10], giving an estimated error of ± 2 days gestational age [11].

Consenting participants underwent fetal MRI in a wide-bore, 70 cm diameter 1.5 T MRI (General Electric Optima 450w, Milwaukee, WI, USA) with a 32-coil abdominal phased array. Women were positioned left decubitus or rolled towards a left lateral decubitus position. Scout images (T2 weighted single shot fast spin echo (SSFSE)) were acquired to locate the fetus and determine its orientation. 3D water-fat MRI (specific implementation iterative decomposition of water and fat with echo asymmetry and least squares estimation (IDEAL)-IQ, GE Healthcare [12-14]) volumes were acquired in a plane axial to the fetal or maternal abdomen during a maternal inspiration breath-hold (TR 9.7-12.7 ms, flip angle 6-7°, Field of View 50 cm, matrix = 160×160, slice thickness 4-6.5 mm,

42-78 slices, autocalibrating reconstruction for cartesian imaging (ARC) acceleration 2x phase 2.5x slice and 32x32 calibration lines, acquisition time 12-24 s). Slice thickness and field of view in the phase encode direction were adjusted as necessary to obtain full fetal coverage in a breath-hold manageable for the participant. Water-only, lipid-only, PDFF and R2* maps were reconstructed from the 3D water-fat MRI data as previously described [12,15,16].

Total fetal adipose tissue was manually segmented (SG, SS) from the PDFF images using 3D Slicer (4.7.0 nightly build 2016-12-06) [17,18] by tracing along the border of high signal intensity corresponding to fetal adipose tissue. The total fetal adipose tissue was then further segmented manually (SG, TK) into the following white adipose tissue compartments (Figure 4.1): cheeks (well delineated high-intensity region extending from corner of mouth to ear), upper arm (shoulders cut on an angle from axilla to outer shoulder to elbow diagonally cut from inner to outer elbow), lower arm (elbow diagonally cut from inner to outer elbow to wrist), thorax (top of shoulders to bottom of lungs), abdomen (bottom of lungs to where thigh meets body), thighs (along body orthogonal to thigh length to knee cut diagonally from inner to outer knee), lower leg (knee cut diagonally from inner to outer knee to ankle), as well as the perirenal (surrounding kidneys) brown adipose tissue compartment.

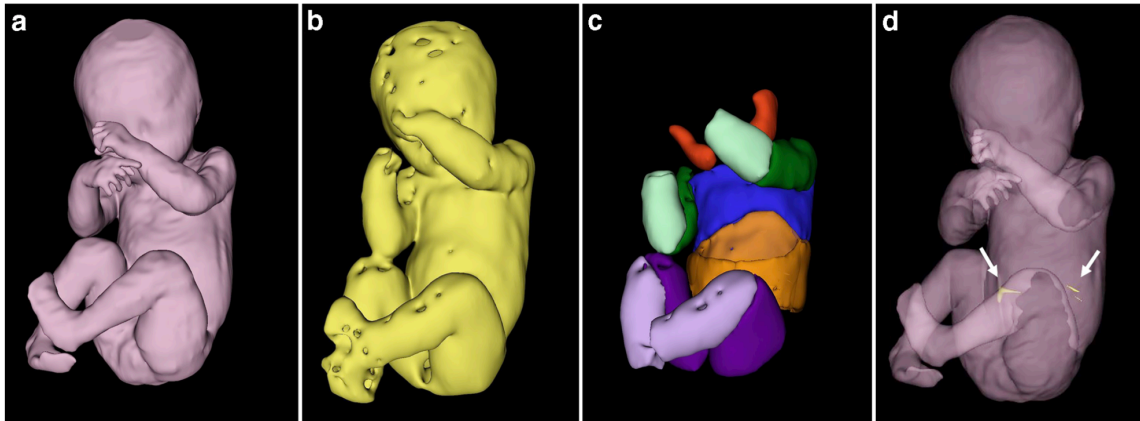


Figure 4.1. Segmentation of fetal adipose tissue. A. Surface rendering of a female fetus at 32 w 5 d of gestation. B. total fetal adipose tissue. C. Fetal adipose tissue compartment segmentation. The cheeks are shown in *red*, thorax in *blue*, upper arms in *dark green*, forearms in *light green*, abdomen in *orange*, thighs in *dark purple* and lower legs in *light purple*. D. Perirenal adipose tissue compartment segmentation. The perirenal compartment, in *yellow*, is shown within the fetus and identified by *white arrows*.

Median PDFF [19] and mean $R2^*$ values were recorded for each compartment after a 4-neighbour erosion was performed in which pixels of the segmentation are removed when having less than 4 neighbouring pixels that are also part of the segmentation. This was done to reduce partial volume effects from the border between fetal adipose tissue and surrounding organs or amniotic fluid, and 4-neighbours were chosen to balance the removal of edge pixels without removing too much of the segmented volume.

Statistical analysis

Inter-rater reliability was determined with two authors independently performing the measurements in the compartments of the first 15 fetuses; the median PDFF and mean $R2^*$ values were compared using the intraclass correlation coefficient (ICC), with 0.9 considered excellent reliability [20].

The rate of PDFF or $R2^*$ change with GA was represented by the slope, while the PDFF or $R2^*$ at 30 weeks + 2 days gestation was given by the y-intercept (for a meaningful

intercept value, GA was centred to our participants with earliest GA of 30 weeks + 2 days). Pearson correlations were performed between each compartment and GA, and an analysis of covariance (ANCOVA) was used to compare the rate of change and value at 30 weeks + 2 days gestation between the white adipose tissue compartments.

The Pearson correlations and ANCOVA were repeated to compare brown adipose tissue (perirenal) to a single white adipose tissue compartment (upper arm) with similar developmental timing [21] to reduce differences in PDFF or R2* due to developmental difference rather than differences between brown adipose tissue and white adipose tissue. All analyses were conducted using GraphPad Prism 6 Viewer (GraphPad Software, San Diego, CA) and SPSS (IBM Corporation, Armonk, NY). P-value of less than 0.05 was considered statistically significant.

4.3 Results

This study was performed as a subset of a larger study in which 92 women consented to participate. Twenty-eight participants were eligible for inclusion in this study based on the availability of CSE-MRI images and no suspicion of fetal growth restriction or maternal diabetes. Still, images from one participant were uninterpretable due to fetal motion. 5 fetuses were imaged before 30 weeks; three of these had insufficient adipose tissue to be segmented (GA = 29w 1d, 29w 5d and 29w 6d, birthweight percentiles = 28.4, 28.4% and 82.6%). As a result, participants who were < 30 weeks gestation were excluded from analyses. This resulted in our sample of 22 fetuses from low-risk pregnancies; their demographic data are summarized in Table 4.1. Inspiration breath-hold times were not recorded for 4 participants, but the remaining 18 participants tolerated breath-hold times of 19 ± 3 s. While all images were oriented at least slightly oblique to the fetal abdomen, the closest standard orientation to the fetal abdomen was axial for 15 participants, sagittal for 3 participants, and coronal for 4 participants.

Table 4.1. Participant Demographics. N = 22.

Characteristic	Mean (range) or n (%)
Number of Previous Pregnancies	1.5 (0 – 6)
Number of Previous Births	0.9 (0-3)
Maternal Age at Delivery (years)	32 (25 – 38)
Pre-pregnancy BMI	26.2 (17.8 – 41.5)
Underweight (< 18.5 kg/m ²)	2 (9.1%)
Normal (18.5 – 24.9 kg/m ²)	13 (59.1%)
Overweight (25.0 – 29.9 kg/m ²)	1 (4.5%)
Obese (> 30.0 kg/m ²)	6 (27.3%)
GA at MRI	34w 4d (30w 2d – 37w 3d)
Fetal Sex, Female	8 (36.4%)
Birthweight Percentile	47.2 (6.9 – 99.3)
Below 10 th Percentile	2 (9.1%)
Above 90 th Percentile	1 (4.5%)

The inter-rater reliability was excellent for all measurements of white adipose tissue compartments (ICC > 0.9); measurement of brown adipose tissue in the perirenal tissue compartment was 0.6, showing only moderate agreement. Since the ICC was > 0.9, results are reported from the only author who assessed compartment segmentations on all study participants. The size of the segmented compartments is given in Table 4.2.

Table 4.2. Size of Compartment Segmentation. Values given as mean ± standard deviation.

Compartment	Number of Voxels	Volume (cm³)
Checks	1007 ± 286	19.1 ± 5.6
Thorax	2876 ± 892	54.9 ± 19.0
Upper Arms	1636 ± 589	31.4 ± 13.5
Forearms	1378 ± 553	26.0 ± 10.9
Abdomen	3362 ± 1585	64.5 ± 32.0
Perirenal	55 ± 57	1.1 ± 1.2
Thighs	3263 ± 1539	62.2 ± 33.3
Lower Legs	2074 ± 870	39.3 ± 16.6
Whole Body	29483 ± 9866	560 ± 207

The rate of PDFF change with GA was significant in all white adipose tissue compartments; that is, PDFF increased with increasing GA (Table 4.3 and Figure 4.2). There were no differences in the rate of PDFF between the various white adipose tissue compartments ($p = 0.97$). However, there were significant differences in the PDFF in the white adipose tissue compartments at 30 weeks + 2 days gestation ($p < 0.0001$); the cheek compartment had the highest PDFF, followed by the upper arm, thorax, thighs, forearms, lower legs and abdomen. These results using $R2^*$ as a measure with increasing GA are shown in Table 4.4 and Figure 4.3. The rate of $R2^*$ change with GA in the thorax, abdomen, lower legs, and whole-body compartments was significant, with $R2^*$ increasing as GA increased; the other compartments did not demonstrate a significant difference in $R2^*$ with increasing GA. There was no significant difference in the rate of $R2^*$ change with GA between the white adipose tissue compartments ($p = 0.96$), but $R2^*$ at 30 weeks + 2 days gestation differed significantly ($p = 0.0002$), decreasing in order from forearms, upper arms, lower legs, thighs, thorax, abdomen, and cheek.

Table 4.3. Results of Pearson Correlations and ANCOVA of PDFF with GA for All Compartments. R^2 gives the goodness of fit. The rate of PDFF change with GA (slope \pm standard error) is given to describe the line, and the p-value testing if the rate of PDFF change with GA (slope) is different from zero is listed.

Compartment	R^2	Rate of PDFF Change with GA (PDFF/week)	p-value of rate of PDFF change	PDFF at 30 weeks + 2 days GA (PDFF)
Cheeks	0.35	2.9 ± 0.9	0.003	37 ± 4
Thorax	0.32	2.7 ± 0.9	0.006	18 ± 4
Upper Arms	0.46	3.5 ± 0.8	0.0006	20 ± 4
Forearms	0.23	2.1 ± 0.9	0.04	17 ± 4
Abdomen	0.38	2.7 ± 0.8	0.002	12 ± 4
Perirenal	0.06	1.2 ± 1.5	0.4	14 ± 8
Thighs	0.43	3.0 ± 0.8	0.0009	18 ± 3
Lower Legs	0.44	2.4 ± 0.6	0.0007	14 ± 3
Whole Body	0.36	2.4 ± 0.7	0.003	17 ± 3

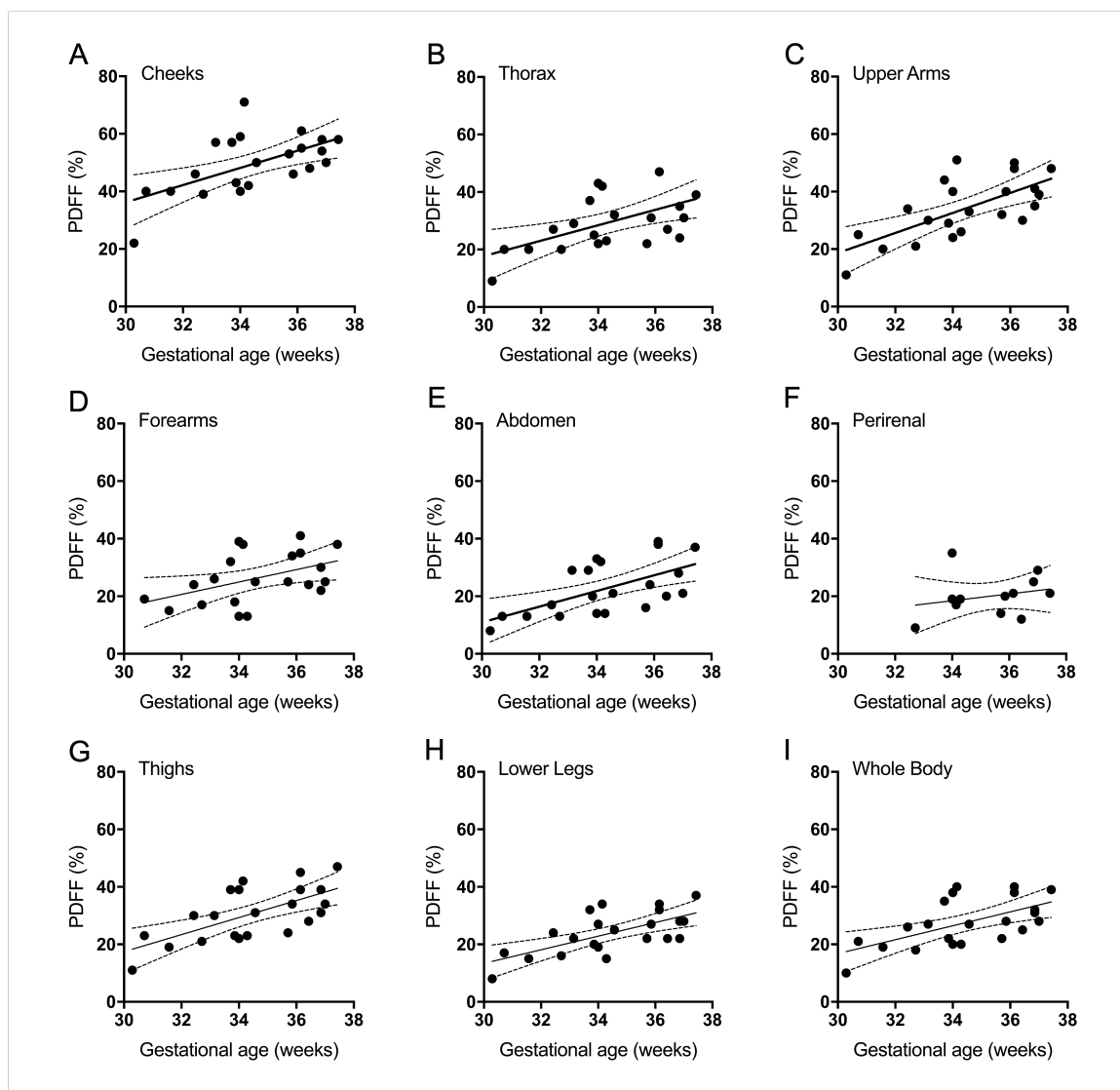


Figure 4.2. PDFF versus GA. The lines of best fit and individual data points are shown for (A) cheeks, (B) thorax, (C) upper arms, (D) forearms, (E) abdomen, (F) perirenal, (G) thighs, (H) lower legs, and (I) the adipose tissue from the whole body. All compartments except perirenal have PDFFs significantly increasing with GA ($p < 0.001$). The rate of PDFF change with GA, PDFF at 30 weeks + 2 days of gestation and R^2 for each are given in Table 4.3. The rates of PDFF change with GA are not significantly different between the white adipose tissue compartments ($p = 0.97$), but the PDFFs at 30 weeks + 2 days of gestation are significantly different ($p < 0.0001$), with the cheeks having a much higher PDFF over the GA range studied. The perirenal brown adipose tissue compartment does not have a significantly different

rate of PDFF change over GA ($p = 0.21$) compared to the upper arm white adipose tissue compartment, but does have a significantly lower PDFF at 30 weeks + 2 days of gestation ($p < 0.0001$).

Table 4.4. Results of Pearson Correlations and ANCOVA of $R2^*$ with GA for All Compartments. R^2 gives the goodness of fit. The rate of $R2^*$ change with GA (slope \pm standard error) and $R2^*$ at 30 weeks + 2 days gestation (Y-intercept \pm standard error) are given to describe the line, and the p-value testing if the rate of $R2^*$ change with GA (slope) is different from zero is also listed.

Compartment	R^2	Rate of $R2^*$ Change with GA (s^{-1}/week)	p-value of rate of $R2^*$ change	$R2^*$ at 30 weeks + 2 days GA (s^{-1})
Cheeks	0.05	0.40 ± 0.37	0.3	25 ± 2
Thorax	0.22	0.55 ± 0.23	0.03	26 ± 1
Upper Arms	0.07	0.38 ± 0.32	0.2	28 ± 1
Forearms	0.18	0.66 ± 0.33	0.06	28 ± 2
Abdomen	0.20	0.62 ± 0.28	0.04	26 ± 1
Perirenal	0.11	-1.6 ± 1.4	0.3	35 ± 8
Thighs	0.11	0.56 ± 0.35	0.1	27 ± 2
Lower Legs	0.22	0.78 ± 0.33	0.03	27 ± 2
Whole Body	0.22	0.86 ± 0.36	0.03	24 ± 2

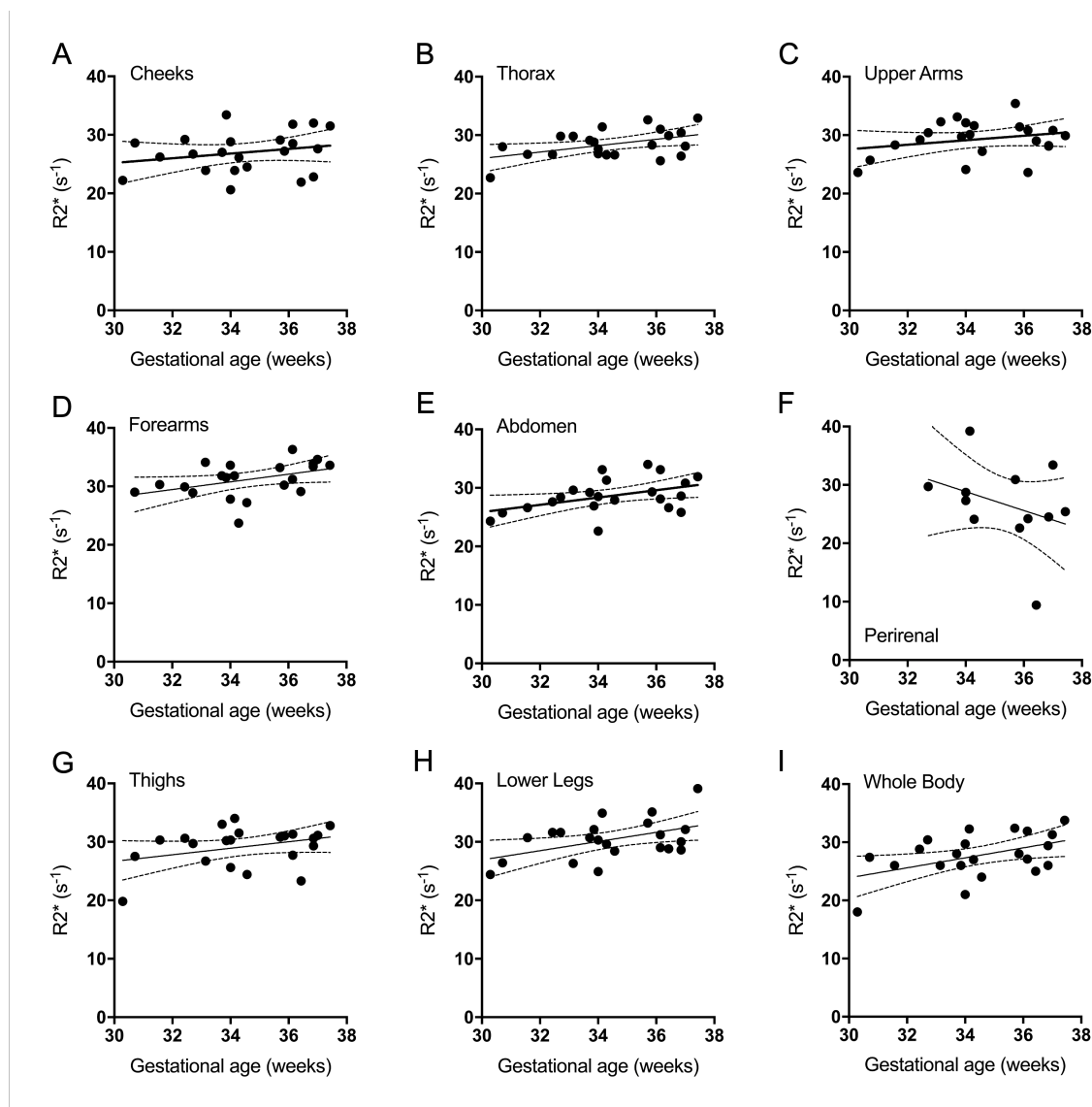


Figure 4.3. $R2^*$ versus GA. The lines of best fit and individual data points are shown for (A) cheeks, (B) thorax, (C) upper arms, (D) forearms, (E) abdomen, (F) perirenal, (G) thighs, (H) lower legs, and (I) the adipose tissue from the whole body. The thorax, abdomen, lower legs and whole body have rates of $R2^*$ change with GA significantly different from zero ($p < 0.05$). The rate of $R2^*$ change with GA, $R2^*$ at 30 weeks + 2 days of gestation and R^2 for each are given in Table 4.4. The rates of $R2^*$ change with GA are not significantly different between the white adipose tissue compartments ($p = 0.96$), and the $R2^*$ at 30 weeks + 2 days of gestation are significantly different ($p = 0.0002$). The perirenal brown adipose tissue compartment did not have a significantly different rate of $R2^*$ change with GA ($p =$

0.08) or $R2^*$ at 30 weeks + 2 days of gestation ($p = 0.16$) compared to the upper arm white adipose tissue compartment.

The rate of PDFF change with GA in the perirenal brown adipose tissue compartment was not significant (listed in Table 4.3, shown in Figure 4.2). There was no significant difference between the perirenal brown adipose tissue compartment and the upper arm white adipose tissue compartment. The PDFF at 30 weeks + 2 days gestation was significantly different between the brown adipose tissue and white adipose tissue compartments ($p < 0.0001$), with upper arm white adipose tissue having a higher PDFF. The rate of $R2^*$ change with GA for perirenal brown adipose tissue was not significant for any analysis.

4.4 Discussion

Fetal adipose tissue undergoes rapid development in mid-late gestation, and we demonstrate that water-fat MRI is sensitive to this developmental process after 30 weeks gestation in our sample of healthy pregnant women. We confirmed the result from Chapter 2 that lipid content of the adipose tissue compartments, as measured by PDFF, increases through gestation, and found that there are differences in lipid fractions in different white adipose tissue compartments at any given GA. Our results suggest that different locations accumulate fetal adipose tissue at a similar rate, as indicated by the consistent rate of PDFF change over GA.

The technique of measurement is described and can be replicated; the segmentation method could be applied to other measurements within the adipose tissue ($R1$ or $R2$, for example) or adapted to measure other soft tissues in the absence of bony landmarks (arm and leg muscle, for example). It is worth noting that this manual segmentation method is time-consuming, with segmentation of a single fetus' adipose tissue taking around 4 hours. Our interrater reliability was excellent in all compartments except the perirenal compartment, which illustrates the capacity and consistency of our method of assessing subcutaneous adipose tissue compartments. The perirenal compartment is very small and has a very low PDFF in these fetuses, making it difficult to reliably segment. This approach has the advantage of measuring PDFF and $R2^*$ in volumes of interest rather

than using small regions of interest to avoid sampling error, as well as the avoidance of sampling in heterogeneous adipose tissues (containing white adipose tissue and brown adipose tissue) such as the shoulders, back and trunk. Analyses of such “compartments” might underestimate PDFF or provide assessments of fetal lipid deposition with unclear metabolic influence. Measuring different adipose tissue compartments can be challenging due to fetal positioning and the inability to use bony landmarks. However, this method has the advantage of assessing a median lipid fraction within the compartment rather than in only one section of the compartment. Additionally, the use of PDFF rather than volume minimizes the impact of any measured changes in the boundaries of each compartment. Better resolution may improve the capacity to reliably measure the perirenal compartment, allowing assessment of brown adipose tissue changes with GA with these methods.

Adipose tissue develops at different GA in different locations, as shown from samples obtained from stillborn human fetuses, starting with the cheeks, followed by the trunk and extremities [21]. We found a similar pattern of development for all white adipose tissue compartments, with development first in cheeks, followed by proximal extremities and trunk and, lastly, the distal extremities and abdomen. Adipose tissue development starts well before the first GA at which adipose tissue lipid fraction can be accurately assessed [21]; however, it is likely that there is a consistent subcutaneous fetal adipose tissue developmental process throughout the body. This means we cannot demonstrate the GA at which adipose tissue starts to develop, but we can provide evidence regarding the sequence of subcutaneous tissue development in the human fetus. Our results also support work using T1-weighted MRI, demonstrating the developmental sequence of adipose tissue/muscle ratio beginning in the face followed by the nuchal region and then the trunk, buttocks and thighs [22]. We would postulate that PDFF provides a more accurate measure for the quantification of lipid content [4] than T1-weighted MRI, as its quantification is independent of comparison to signal intensities of different tissues, such as muscle, whose signal intensity may also be changing with GA. PDFF leaves no ambiguity in interpretation and confirms that the amount of lipid relative to the amount of lipid and water in the fetal adipose tissue compartments is increasing with GA.

The signal decay measure ($R2^*$) utilized in our work showed increases with advancing GA, as the lipid-water heterogeneity increased with increasing number and/or size of lipid vesicles. $R2^*$ values published for the upper arm in infants and children suggest that $R2^*$ will peak in infancy and then decline in childhood [5]. This is consistent with a peak in the heterogeneity of adipose tissue during infancy before developing into a more homogeneous lipid-dominated tissue in childhood. Further exploration with susceptibility-weighted imaging and biophysical modelling might enhance understanding of adipose tissue microstructural development. A method to probe the adipose tissue microstructure may help distinguish brown adipose tissue and white adipose tissue, as different types of adipose tissue have different numbers and sizes of lipid vesicles.

Methods to non-invasively identify and assess brown adipose tissue and white adipose tissue through gestation are important to understand differences, impacts and any long-term consequences of pathologic tissue development. Water-fat MRI has been used to differentiate between brown adipose tissue and white adipose tissue in one-day-old infants [5,23], but its utility to determine differences during fetal life has not been studied. Brown adipose tissue has been identified in fetuses histologically throughout the thorax and abdomen, particularly in perirenal, supra-iliac, interscapular, intercostal and retroperitoneal deposits [24]. We did not find changes in brown adipose tissue development with advancing GA in the perirenal tissue. This may reflect difficulties in getting an accurate measurement in the very thin tissue; alternatively, other measurements may best assess this lipid type and its development with GA.

Our study utilized a small sample of our obstetrical patients to generate our data. Although the results of the imaging are reliable and consistent, we recognize the limitations of using this set of 22 women to suggest that this represents a “normal distribution” of fetal adipose tissue. Several publications suggest that fetal adipose tissue development is affected by maternal obesity; however, these studies have concentrated on the volume or thickness of the fetal adipose tissue, rather than the concentration of lipid relative to water within the tissue [25-27]. While we have found no significant differences in fetal lipid fraction in women with elevated BMI, suggesting that adipose tissue develops similarly regardless of the presence of obesity (unpublished data), we

recognize that the sample size in the current study is too small to adequately assess an effect of maternal adiposity on fetal tissue compartment PDFF. Since we expect maternal obesity to have similar effects on all tissue compartments, we have included all BMI in this study. Additionally, this study would ideally be performed as a longitudinal study. Rather than imaging individual participants each at unique GA, it would be preferable to image participants multiple times over the third trimester to understand the changes in adipose tissue development during this time period.

Whether the GA sampled in this study are representative of the optimal timing during which we can reliably assess changes in fetal adipose tissue development remains uncertain. Below 30 weeks GA, low fetal adipose tissue lipid content rendered MRI uninterpretable and, therefore, we felt it was not valid. As well, examination of fetal adipose tissue in the second trimester may be complicated by more frequent fetal motion. A potential solution to address this motion is to obtain radial acquisitions with motion sorting; this technique has been used successfully in paediatric populations [28]. With radial acquisitions, each data acquisition contains low spatial frequency information, which allows for evaluation of motion in the data. This information can be used for binning into different motion states (maternal inspiration vs. expiration) and selecting data free of fetal motion. Further study using these techniques may allow assessment of fetal adipose tissue in the second trimester, confirming the GA when the lipid accumulation begins to more fully characterize development and accumulation throughout gestation.

Another important limitation is the combination of the inconsistency in the orientation of the scan plane relative to the fetus with non-isotropic voxels. The orientation of the non-isotropic voxels relative to the fetal adipose tissue compartments is not consistent and could result in different degrees of partial voluming that negatively impacts the accuracy of the segmentation. In order to minimize this problem, isotropic voxels should be used. We believe this would be more appropriate than trying to consistently orient the scan plane (e.g., axial to fetal abdomen) when multiple compartments are being investigated because the fetuses are in variable positions. It would be possible to orient the scan plane

relative to a single compartment (e.g., fetal abdomen), but that would still leave inconsistencies in the other compartments.

4.5 Conclusions

We have demonstrated that different fetal adipose tissue compartments contain different levels of lipid through late pregnancy but have, with the exception of perirenal adipose tissue, a similar rate of lipid accumulation. This study provides important data regarding lipid levels and lipid accumulation rates in fetal adipose tissue compartments in uncomplicated pregnancies; information useful for the design of studies addressing fetal adipose tissue development in relation to fetal metabolic health and development of future disease.

4.6 References

1. Wadhwa PD, Buss C, Entringer S, Swanson JM (2009) Developmental origins of health and disease: brief history of the approach and current focus on epigenetic mechanisms. *Semin Reprod Med* 27 (5):358-368. doi:10.1055/s-0029-1237424
2. Ornoy A (2011) Prenatal origin of obesity and their complications: Gestational diabetes, maternal overweight and the paradoxical effects of fetal growth restriction and macrosomia. *Reprod Toxicol* 32 (2):205-212. doi:10.1016/j.reprotox.2011.05.002
3. Ali AT, Hochfeld WE, Myburgh R, Pepper MS (2013) Adipocyte and adipogenesis. *Eur J Cell Biol* 92 (6-7):229-236. doi:10.1016/j.ejcb.2013.06.001
4. Reeder SB, Hu HH, Sirlin CB (2012) Proton density fat-fraction: a standardized MR-based biomarker of tissue fat concentration. *J Magn Reson Imaging* 36 (5):1011-1014. doi:10.1002/jmri.23741
5. Hu HH, Yin L, Aggabao PC, Perkins TG, Chia JM, Gilsanz V (2013) Comparison of brown and white adipose tissues in infants and children with chemical-shift-encoded water-fat MRI. *J Magn Reson Imaging* 38 (4):885-896. doi:10.1002/jmri.24053
6. Larciprete G, Di Pierro G, Barbati G, Deabess T, Jarvis S, Valensise H, Romanini ME, Gioia S, Arduini D (2008) Could birthweight prediction models be improved by adding fetal subcutaneous tissue thickness? *J Obstet Gynaecol Res* 34 (1):18-26. doi:10.1111/j.1447-0756.2007.00741.x
7. Larciprete G, Valensise H, Vasapollo B, Novelli GP, Parretti E, Altomare F, Di Pierro G, Menghini S, Barbati G, Mello G, Arduini D (2003) Fetal subcutaneous tissue thickness (SCTT) in healthy and gestational diabetic pregnancies. *Ultrasound Obstet Gynecol* 22 (6):591-597. doi:10.1002/uog.926

8. Larciprete G, Valensise H, Di Pierro G, Vasapollo B, Casalino B, Arduini D, Jarvis S, Cirese E (2005) Intrauterine growth restriction and fetal body composition. *Ultrasound Obstet Gynecol* 26 (3):258-262. doi:10.1002/uog.1980
9. Hu HH, Perkins TG, Chia JM, Gilsanz V (2013) Characterization of human brown adipose tissue by chemical-shift water-fat MRI. *Am J Roentgenol* 200 (1):177-183. doi:10.2214/ajr.12.8996
10. Butt K, Lim KI (2019) Guideline No. 388-Determination of Gestational Age by Ultrasound. *J Obstet Gynaecol Can* 41 (10):1497-1507. doi:10.1016/j.jogc.2019.04.010
11. Sladkevicius P, Saltvedt S, Almstrom H, Kublickas M, Grunewald C, Valentin L (2005) Ultrasound dating at 12-14 weeks of gestation. A prospective cross-validation of established dating formulae in in-vitro fertilized pregnancies. *Ultrasound Obstet Gynecol* 26 (5):504-511. doi:10.1002/uog.1993
12. Yu H, McKenzie CA, Shimakawa A, Vu AT, Brau AC, Beatty PJ, Pineda AR, Brittain JH, Reeder SB (2007) Multiecho reconstruction for simultaneous water-fat decomposition and T2* estimation. *J Magn Reson Imaging* 26 (4):1153-1161. doi:10.1002/jmri.21090
13. Reeder SB, Pineda AR, Wen Z, Shimakawa A, Yu H, Brittain JH, Gold GE, Beaulieu CH, Pelc NJ (2005) Iterative decomposition of water and fat with echo asymmetry and least-squares estimation (IDEAL): application with fast spin-echo imaging. *Magn Reson Med* 54 (3):636-644. doi:10.1002/mrm.20624
14. Reeder SB, McKenzie CA, Pineda AR, Yu H, Shimakawa A, Brau AC, Hargreaves BA, Gold GE, Brittain JH (2007) Water-fat separation with IDEAL gradient-echo imaging. *J Magn Reson Imaging* 25 (3):644-652. doi:10.1002/jmri.20831
15. Yu H, Shimakawa A, Hines CD, McKenzie CA, Hamilton G, Sirlin CB, Brittain JH, Reeder SB (2011) Combination of complex-based and magnitude-based multiecho water-fat separation for accurate quantification of fat-fraction. *Magn Reson Med* 66 (1):199-206. doi:10.1002/mrm.22840
16. Yu H, Shimakawa A, McKenzie CA, Brodsky E, Brittain JH, Reeder SB (2008) Multiecho water-fat separation and simultaneous R2* estimation with multifrequency fat spectrum modeling. *Magn Reson Med* 60 (5):1122-1134. doi:10.1002/mrm.21737
17. Fedorov A, Beichel R, Kalpathy-Cramer J, Finet J, Fillion-Robin JC, Pujol S, Bauer C, Jennings D, Fennessy F, Sonka M, Buatti J, Aylward S, Miller JV, Pieper S, Kikinis R (2012) 3D Slicer as an image computing platform for the Quantitative Imaging Network. *Magnetic resonance imaging* 30 (9):1323-1341. doi:10.1016/j.mri.2012.05.001
18. Kikinis R, Pieper SD, Vosburgh K (2014) 3D Slicer: a platform for subject-specific image analysis, visualization, and clinical support. In: Jolesz FA (ed) *Intraoperative Imaging Image-Guided Therapy*. Springer, New York,

19. Roberts NT, Hernando D, Holmes JH, Wiens CN, Reeder SB (2018) Noise properties of proton density fat fraction estimated using chemical shift-encoded MRI. *Magn Reson Med* 80 (2):685-695. doi:10.1002/mrm.27065
20. Koo TK, Li MY (2016) A Guideline of Selecting and Reporting Intraclass Correlation Coefficients for Reliability Research. *J Chiropr Med* 15 (2):155-163. doi:10.1016/j.jcm.2016.02.012
21. Poissonnet CM, Burdi AR, Garn SM (1984) The chronology of adipose tissue appearance and distribution in the human fetus. *Early Hum Dev* 10 (1-2):1-11. doi:10.1016/0378-3782(84)90106-3
22. Blondiaux E, Chougar L, Gelot A, Valence S, Audureau E, Ducou le Pointe H, Jouannic JM, Dhombres F, Garel C (2018) Developmental patterns of fetal fat and corresponding signal on T1-weighted magnetic resonance imaging. *Pediatr Radiol* 48 (3):317-324. doi:10.1007/s00247-017-4038-z
23. Hu HH, Tovar JP, Pavlova Z, Smith ML, Gilsanz V (2012) Unequivocal identification of brown adipose tissue in a human infant. *J Magn Reson Imaging* 35 (4):938-942. doi:10.1002/jmri.23531
24. Merklin RJ (1974) Growth and distribution of human fetal brown fat. *Anat Rec* 178 (3):637-645. doi:10.1002/ar.1091780311
25. Modi N, Murgasova D, Ruager-Martin R, Thomas EL, Hyde MJ, Gale C, Santhakumaran S, Doré CJ, Alavi A, Bell JD (2011) The influence of maternal body mass index on infant adiposity and hepatic lipid content. *Pediatr Res* 70 (3):287-291. doi:10.1203/PDR.0b013e318225f9b1
26. Sewell MF, Huston-Presley L, Super DM, Catalano P (2006) Increased neonatal fat mass, not lean body mass, is associated with maternal obesity. *Am J Obstet Gynecol* 195 (4):1100-1103. doi:10.1016/j.ajog.2006.06.014
27. Hull HR, Dinger MK, Knehans AW, Thompson DM, Fields DA (2008) Impact of maternal body mass index on neonate birthweight and body composition. *Am J Obstet Gynecol* 198 (4):416.e411-416. doi:10.1016/j.ajog.2007.10.796
28. Benkert T, Feng L, Sodickson DK, Chandarana H, Block KT (2017) Free-breathing volumetric fat/water separation by combining radial sampling, compressed sensing, and parallel imaging. *Magn Reson Med* 78 (2):565-576. doi:10.1002/mrm.26392

Chapter 5

5 Conclusions

This chapter will conclude the thesis by summarizing and concluding the content from Chapters 2-4, examining the limitations of the work presented, and proposing future directions for research building on the knowledge presented in this thesis.

5.1 Chapter Summaries

In Chapter 2, my co-authors and I demonstrated that it is feasible to use water-fat magnetic resonance imaging (MRI) to assess fetal adipose tissue. Additionally, it was shown that the measurement was reproducible, both between readers and between measurements taken by one reader. In this chapter, I also demonstrated that water-fat MRI is sensitive to the lipid filling of adipose tissue. This study found a correlation between gestational age (GA) and fat signal fraction (FSF) of the adipose tissue, which agrees with histological studies that demonstrated that fetal adipose tissue accumulates lipid in the third trimester [1,2]. This is a measurement that had not been performed non-invasively before and opened the door for further research into the lipid content of fetal adipose tissue and the factors that may affect it.

In Chapter 3, my co-authors and I assessed the effects of the confounding factors of the multiphase spectrum of lipid and $T2^*$ decay by comparing the FSF measured with modified two-point Dixon and the proton density fat fraction (PDFF) measured using chemical-shift encoded (CSE)-MRI on fetal adipose tissue measures. This work showed that the two measurements were reliable in fetal adipose tissue and either can be used for comparison between participants. I also demonstrated that $T2^*$ decay is an important source of bias in the fetal liver as the FSF measured with modified two-point Dixon was higher than the PDFF measured with CSE-MRI in a third of the fetuses assessed. The repeatability of the PDFF measurement with CSE-MRI was also assessed and found to be excellent both between readers and from test-retest. From this work, we concluded that while the results from modified two-point Dixon and CSE-MRI are reliable, CSE-MRI is the preferred method for assessing fetal adipose tissue. The PDFF obtained from CSE-

MRI is more accurate, as it is the validated MRI-based biomarker of tissue lipid concentration [3].

In Chapter 4, I wanted to explore the capabilities of CSE-MRI in fetal adipose tissue, and I chose to look for differences in the PDFF of different adipose tissue compartments. My co-authors and I measured the PDFF in the white adipose tissue of the cheeks, thorax, abdomen, upper arms, forearms, thighs, and lower legs, and assessed the brown adipose tissue surrounding the kidneys. I showed that all the white adipose tissue compartments accumulated lipids at a similar rate but that at 30 weeks gestation, they had different PDFF values, suggesting that their development began at different times. This agrees with histological studies [1], as those adipose tissue compartments that began accumulating lipids earliest in gestation on histology have the highest PDFF values on MRI. I also compared the perirenal brown adipose tissue to the white adipose tissue of the upper arms as these begin to accumulate lipids at a similar GA according to histology [1]. I did not find a difference in the rate of lipid accumulation, but the PDFF at 30 weeks gestation was different between the two compartments. However, more work could be done to allow water-fat MRI to differentiate between the fetus's brown and white adipose tissues.

5.2 Thesis Conclusions

From the work presented in this thesis, it is clear that water-fat MRI can be used to assess fat fraction in fetal adipose tissue. I have highlighted some major considerations one must remember when assessing fat fraction of fetal adipose tissue through Chapters 2-4, which I will summarize here.

Chapter 3 shows that CSE-MRI should be the preferred method to measure PDFF in the fetus when available. While the measurements from both modified two-point Dixon and CSE-MRI were found to be reliable between the techniques when assessing fetal adipose tissue, the fat fraction measurements were not identical. This is attributed to the additional bias corrections used with CSE-MRI that allow it to give a PDFF measurement rather than the FSF measurement obtained from modified two-point Dixon. This difference may be more important if one seeks to measure the fat fraction of other fetal

tissues, as bias from T2* may increase the estimation of lipids in a tissue. We demonstrated this effect in the liver, where a third of our participants had pseudo-fat appear in the fetal liver with modified two-point Dixon but not CSE-MRI. This is a crucial observation as the liver is a tissue of interest for lipid deposition related to metabolic disorders. Recently, it was shown that CSE-MRI could detect differences in the hepatic PDFF of fetuses of mothers with diabetes [4].

The strongest correlation with fat fraction in third trimester fetal adipose tissue is the gestational age of the pregnancy, as shown in Chapters 2 and 4. This reflects the adipose tissue accumulating lipids within the adipocytes. Combining the results from Chapters 2 and 4, we see a large increase from approximately 10% at 29 weeks to 34% at 37 weeks gestation in the fetal trunk/abdomen. Therefore, the single most important consideration when assessing the fat fraction of fetal adipose tissue must be GA. Future studies aiming to compare individuals need to account for the change in PDFF with GA, either by including it in the analysis or by imaging at a limited GA range.

One must also consider the location of PDFF measurement, as in Chapter 4 I demonstrated differences between adipose tissue compartments. Since different fetal adipose tissue compartments begin accumulating lipids at different times, compartments should be compared against themselves when looking for differences between participants.

It should be noted that water-fat MRI was not only feasible, but also repeatable for the measurement of fat fraction when either modified two-point Dixon or CSE-MRI was used. As shown in Chapters 2-4, this was true across time (intra-rater reliability, and test-retest) and raters (inter-rater reliability). Our measurements were repeatable both for total fetal adipose tissue (Chapter 3) and when individual compartments were considered (Chapters 2 and 4), even without bony landmarks to guide the segmentation.

5.3 Thesis Limitations

The population of pregnant mothers included in this study varied in comorbidities present and GA at the time of MRI and was mostly homogeneous in ethnicity. This is a

limitation as the results cannot be used to define normal adipose tissue development. Such interpretations are also limited by the sample size included in the thesis. While understanding normal fetal adipose tissue development is an admirable goal that is not reached with the work presented here, this thesis does provide the building blocks necessary for such measurements. As some of the questions addressed in this thesis concern the feasibility and limitations of the water-fat MRI to measure fetal adipose tissue, a range of comorbidities and GA gives me confidence that the techniques discussed here can be applied to most pregnancies. Pregnancies that cannot be assessed with water-fat MRI include those with contraindications to MRI and those in the first half of pregnancy when lipid accumulation may be too low to detect with the methods presented here.

A second limitation is the cross-sectional design of the studies included in this thesis. The correlation between GA and fat fraction demonstrated here demonstrates that the fat fraction increases throughout gestation. But a longitudinal study is necessary to truly understand this relationship and model that increase. We have estimated the increase in PDFF with GA to be linear. However, a more complex model is probable, with the increase in PDFF starting slowly in the second trimester, being highest in the middle to the end of the third trimester, then slowing down again sometime in infancy. Longitudinal studies should be designed to tease out the relationship between adipose tissue lipid concentrations and age. Additionally, these longitudinal studies should be used to assess differences between clinical groups, as a change in the developmental trajectory may be found rather than changes in PDFF at a given GA. Longitudinal measurements of growth are frequently used in obstetrics, and this approach should also be applied to fetal adipose tissue lipid accumulation. This is a strength of water-fat MRI over previous histological studies, as the non-invasiveness of MRI allows for multiple measurements of tissue lipid content to be made during pregnancy and beyond.

Additionally, all the work in this thesis was performed at 1.5 T. I predict the results presented here regarding feasibility, bias correction, and repeatability would also be true at higher field strengths. Indeed, the signal to noise ratio (SNR) obtained at a higher field strength would be higher than we had, which may improve the measurements made by

making the delineation of the adipose tissue easier and allowing measurements of lower PDFF values, as expected earlier in gestation, in brown adipose tissue and other tissues such as the liver.

One of the strengths of CSE-MRI is the use of a multi-peak lipid spectrum during the calculation of PDFF. This step is crucial to correctly assigning signal to water or lipid [5,6]. The lipid spectrum used in the iterative decomposition of water and fat with echo asymmetry and least squares estimation (IDEAL) reconstruction is a 6-peak model determined by spectroscopy in the liver of people with non-alcoholic fatty liver disease [7]. This is because the development of IDEAL was targeted at measuring hepatic triglycerides for monitoring hepatic steatosis. Some caution must be taken when using this spectrum for other applications [7]. The lipid spectrum reflects the fatty acid composition of the triglycerides in a sample, and the fatty acid composition is different in different tissues. Fatty acid composition is described by the chain length (CL), number of double bonds (ndb), and number of methylene-interrupted double bonds (nmidb) [7]. The liver spectrum was found to have $CL = 17.45$, $ndb = 1.92$, and $nmidb = 0.32$ [7]. Different values were found in adipose tissue when measured with spectroscopy, with adult adipose tissue having average values of: $CL = 17.5$, $ndb = 2.782$, $nmidb = 0.723$ [8]. Different fatty acid compositions were even found between superficial and deep subcutaneous adipose tissue and visceral adipose tissue [8]. It is reasonable to expect that fetal adipose tissue could also have a different fatty acid composition, and therefore lipid spectrum, from the liver, and possibly adult adipose tissue.

Using an incorrect lipid spectrum could introduce errors in the calculated PDFF [7]. While this is of some concern and represents a limitation of this thesis, there is evidence that any errors introduced using the incorrect lipid spectrum will be small [9]. The bias in PDFF measurements when using different lipid spectra was investigated by varying the spectral model to any biologically plausible combination of CL, ndb, and nmidb [9]. The maximum difference between the generated PDFFs was 1.5%, and the largest bias measured between a possible spectral model and the standard one derived from liver lipids was 1.2% [9]. These are both small errors, so I expect that using the true lipid

spectrum from fetal adipose tissue would not result in large changes in our measured fat fractions.

5.4 Future Directions

The work presented in Chapters 2-4 laid the building blocks for future studies utilizing water-fat MRI to investigate fetal adipose tissue. There are so many exciting research questions I could not address within this thesis, which will ultimately lead to a better understanding of the developmental programming of metabolic diseases and may one day lead to changes in clinical care before, during, and after pregnancy.

5.4.1 Increase the signal-to-noise ratio of water-fat MRI for fetal adipose tissue assessment

We obtained sufficient SNR to measure the fat fraction of subcutaneous adipose tissue (and, in some cases, perirenal adipose tissue) from 29 weeks onward, corresponding to fat fractions of approximately 10% or more. However, we need to increase the SNR to examine lower fat fractions. Lower fat fractions are expected earlier in gestation and possibly in brown adipose tissue. This may be why the perirenal adipose tissue compartment was only identified in fetuses after 32 weeks gestation.

There are a few ways the SNR could be increased; increasing signal or reducing noise both result in a higher SNR. Practically, there are a few ways to achieve this goal; moving to higher field strength, such as 3.0 T, increasing the acquisition time by using a motion robust sequence, or increasing the signal with a higher flip angle.

The MRI signal can be increased by moving to higher field strength since SNR increases linearly with field strength; therefore, if we increase the field strength from 1.5 T to 3.0 T, we should roughly double our SNR. 3.0 T MRI is becoming increasingly available, and many with a 70 cm or larger bore diameter would aid in making pregnant women more comfortable.

Alternatively, noise can be reduced by averaging the signal from multiple acquisitions. Obtaining more acquisitions requires more time, and with the techniques used in this thesis, we are time-limited due to motion. We obtain our images during maternal breath

hold and must keep our acquisition time within the time a pregnant woman can hold her breath (we used 16 s). Additionally, there is fetal motion to consider, and the longer you take for image acquisition, the more likely the fetus will move. Therefore, to reduce noise by averaging more image data, we need to overcome the motion sensitivity of the sequence. Utilizing a motion-robust sequence, such as a sequence with radial acquisitions and motion sorting [10-12], would allow for longer acquisition time and could ultimately provide higher SNR.

These two methods were recently implemented to measure the PDFF in the fetal liver [4]. Imaging at 3.0 T and using a radial acquisition allowed for measurements of PDFFs under 5%. This method could also be used to measure the PDFF of fetal adipose tissue, particularly in the second trimester when fat fractions will be low.

Another way to increase the signal, and thus SNR, is to use a higher flip angle. Of course, this reintroduces the T1 bias, which must be corrected to obtain an accurate measure of PDFF [13,14]. If the T1 of water and lipid in your tissue of interest is known, you can use these values, along with your flip angle and TR, to correct the T1 bias [13,14]. If we recall Eqs. 1.12 and 1.13 from Section 1.4.2.4:

$$W = \frac{M_w (1 - e^{-TR/T1_w}) \sin \alpha}{(1 - e^{-TR/T1_w} \cos \alpha)} \quad \text{Eq. 1.12}$$

$$F = \frac{M_f (1 - e^{-TR/T1_f}) \sin \alpha}{(1 - e^{-TR/T1_f} \cos \alpha)} \quad \text{Eq. 1.13}$$

Then we can rearrange to solve for the water and lipid proton densities, M_w and M_f respectively:

$$M_w = \frac{W (1 - e^{-TR/T1_w} \cos \alpha)}{(1 - e^{-TR/T1_w}) \sin \alpha} \quad \text{Eq. 5.1}$$

$$M_f = \frac{F \left(1 - e^{-TR/T1_f} \cos \alpha \right)}{\left(1 - e^{-TR/T1_f} \right) \sin \alpha} \quad \text{Eq. 5.2}$$

Using these proton densities to calculate fat fraction will give an unbiased PDFF.

A description of the T1 of water and lipid in fetal adipose tissue demonstrates that the T1 values do not change significantly with GA in the third trimester or between adipose tissue compartments [15]. The values reported are 946.6 ± 128.2 msec for water and 224.9 ± 41.9 msec for lipid [15]. After correction, an accurate PDFF would be obtained, and the images would have a higher SNR than with the low flip angle approach. This could be combined with a higher field strength and motion-robust imaging to further increase the SNR.

5.4.2 Assess the entire gestational period of lipid accumulation in fetal adipose tissue

In this thesis, I presented data showing a PDFF increase from 29 weeks to 38 weeks gestation. This does not represent the entire period of lipid accumulation in the fetal adipose tissue, as tissues begin accumulating lipids around 16 weeks gestation and, at term, have not reached adult PDFF values. In infants between 1 and 171 days old, subcutaneous adipose tissue PDFF values in the shoulder ranged from 63.2 - 88.9% [16]. Similarly, in infants between 11 and 56 days of age, subcutaneous adipose tissue in the nuchal region had a PDFF value of $67.7 \pm 4.6\%$ [17]. The values in both studies are lower than the values of 90% in adult subcutaneous adipose tissue [18].

It would be fascinating to measure PDFF earlier in gestation, starting between 16 and 18 weeks, as this is when fetal adipocytes have accumulated some lipids [1]. This would rely on the work suggested in Section 5.4.1, as the fat fraction values will be very low this early in gestation. I would expect to see a slow PDFF increase to begin at the early GA, with the increase becoming larger further into the third trimester.

We measured PDFFs in fetuses up to 37 weeks 3 days gestation, and while this is almost the end of gestation, it would be interesting to try and push further. I want to better

model the relationship between PDFF and GA, and going to later GA (and likely infancy) would be required to understand when the PDFF increase begins to slow.

The effect of birth and onset of lactation of offspring adipose tissue PDFF values would be another interesting research question. Infants lose weight after birth, as the body releases stored energy until lactation is well established, and I expect a drop in adipose tissue PDFF values would occur as a result.

Ideally, this would all be performed with longitudinal studies so that the trajectory of PDFF with GA could be appropriately modelled. An understanding of adipose tissue development in “normal” pregnancies would allow for investigation into which clinical groups have altered development.

5.4.3 Investigate differences between different clinical populations

The goal of health research is to improve clinical care. Before water-fat MRI of fetal adipose tissue can impact clinical care, we need to apply it to clinical populations and add to the knowledge obtained from other methods. We are preparing a preliminary study for publication, which used water-fat MRI to assess the development of fetal adipose tissue in populations including fetal growth restriction, macrosomia, maternal obesity and maternal diabetes as a starting point. These groups all represent individuals potentially susceptible to negative metabolic programming, and this study will be the first to assess how the adipose tissue accumulates lipids in these populations. Understanding how lipid accumulation is affected in different clinical populations may allow changes to clinical care early in life when minimizing developmental programming of metabolism could change an individual’s lifelong health trajectory.

An example of an important application is to assess the impacts of maternal diabetes treatment on fetal adipose tissue development. Metformin and insulin are commonly used to treat type 2 diabetes in pregnancy, and studies comparing the two have shown them to be equally safe and effective in controlling maternal glucose levels [19]. The two function differently and consequently can be expected to have different effects on the metabolic environment a fetus experiences when used during pregnancy, and may have

different later-life effects on the offspring's metabolic health. Metformin reduces hepatic glucose production, stimulates insulin sensitivity in the liver and skeletal muscle, inhibits gluconeogenesis and reduces lipid synthesis [20]. Insulin treatment, by comparison, works to overcome the insulin insensitivity present with type 2 or gestational diabetes. Since metformin reduces lipid synthesis [20], it is possible that fetuses exposed to metformin will have less lipid within their adipose tissue than those receiving insulin treatment. A study following children to 2 years of age suggested that *in-utero* exposure to metformin treatment may reduce lipid deposition viscerally and promote lipid storage in subcutaneous depots [21]. Water-fat MRI could determine if that difference begins during gestation.

5.4.4 Measure the fatty acid composition of fetal adipose tissue

Water-fat MRI can do more than measure the lipid content within tissues. Since it is sensitive to the lipid spectrum, it is also possible to use water-fat MRI to measure the lipid spectrum. With measurements of the lipid spectrum, it is possible to estimate the fatty acid composition of the tissues through CL, ndb, and nmdb [22,23]. Each peak within the lipid spectrum is related to specific hydrogen nuclei on the triglyceride molecule [7], as shown in Figure 1.4.

Magnetic resonance spectroscopy (MRS) could be used to obtain spectra from fetal adipose tissue, but this is not a simple measurement to make since fetal movement after selection of the MRS voxel could cause the MRS voxel to be outside of the fetal adipose tissue, especially since these tissues are small. This problem is avoided using MRI since we can image the entire uterus.

CSE-MRI has been used with a reconstruction that separates the signal into water and lipid peak components to estimate the contribution of different lipid peaks to the total signal [22-28]. The final output of this reconstruction is CL, ndb, and nmdb maps.

This technique could be applied to fetal adipose tissue to characterize its development further. I believe it would be particularly interesting to investigate fatty acid composition differences between white adipose tissue and brown adipose tissue. In Chapter 4, I found

differences in the PDFF between upper arm white adipose tissue and perirenal brown adipose tissue; however, these were small differences, and because the PDFF also varies with GA and anatomical location, I do not think PDFF alone will be sufficient to determine if an adipose tissue compartment is primarily composed of brown or white adipose tissue. A previous MRS study comparing murine white adipose tissue and brown adipose tissue found differences in the lipid spectrum, with white adipose tissue having higher amounts of unsaturated triglycerides than brown adipose tissue [29]. A combination of differences in PDFF and fatty acid composition may be sufficient to distinguish white adipose tissue from brown adipose tissue in the human fetus. There is disagreement in the literature regarding the classification of fetal adipose tissue as white adipose tissue or brown adipose tissue, and this may present a method to distinguish the tissue types non-invasively.

5.5 Significance and Impact

Although the lipid filling of fetal adipose tissue was studied with histology 40 years ago, this thesis contains the first non-invasive method to measure this process. This allows for studies involving living pregnancies and makes longitudinal assessments possible. This thesis provides the building blocks necessary to design studies utilizing this measurement to study the normal accumulation of lipids in fetal tissues and investigate abnormal development that is expected with the developmental programming of metabolic diseases.

This work also provides some advancement towards distinguishing fetal brown and white adipose tissue non-invasively. While there is still much work to be done here, there is a lot of research interest in brown adipose tissue, and it is likely that brown and white adipose tissue develop and contribute to metabolic dysfunction risk differently. Therefore, we need to be able to identify the tissues correctly to be able to study them effectively.

5.6 References

1. Poissonnet CM, Burdi AR, Garn SM (1984) The chronology of adipose tissue appearance and distribution in the human fetus. *Early Hum Dev* 10 (1-2):1-11. doi:10.1016/0378-3782(84)90106-3
2. Poissonnet CM, Burdi AR, Bookstein FL (1983) Growth and development of human adipose tissue during early gestation. *Early Hum Dev* 8 (1):1-11. doi:10.1016/0378-3782(83)90028-2
3. Reeder SB, Hu HH, Sirlin CB (2012) Proton density fat-fraction: a standardized MR-based biomarker of tissue fat concentration. *J Magn Reson Imaging* 36 (5):1011-1014. doi:10.1002/jmri.23741
4. Strobel KM, Kafali SG, Shih SF, Artura AM, Masamed R, Elashoff D, Wu HH, Calkins KL (2023) Pregnancies complicated by gestational diabetes and fetal growth restriction: an analysis of maternal and fetal body composition using magnetic resonance imaging. *J Perinatol* 43 (1):44-51. doi:10.1038/s41372-022-01549-5
5. Yu H, McKenzie CA, Shimakawa A, Vu AT, Brau AC, Beatty PJ, Pineda AR, Brittain JH, Reeder SB (2007) Multiecho reconstruction for simultaneous water-fat decomposition and T2* estimation. *J Magn Reson Imaging* 26 (4):1153-1161. doi:10.1002/jmri.21090
6. Yu H, Shimakawa A, McKenzie CA, Brodsky E, Brittain JH, Reeder SB (2008) Multiecho water-fat separation and simultaneous R2* estimation with multifrequency fat spectrum modeling. *Magn Reson Med* 60 (5):1122-1134. doi:10.1002/mrm.21737
7. Hamilton G, Yokoo T, Bydder M, Cruite I, Schroeder ME, Sirlin CB, Middleton MS (2011) In vivo characterization of the liver fat ¹H MR spectrum. *NMR Biomed* 24 (7):784-790. doi:10.1002/nbm.1622
8. Hamilton G, Schlein AN, Middleton MS, Hooker CA, Wolfson T, Gamst AC, Loomba R, Sirlin CB (2017) In vivo triglyceride composition of abdominal adipose tissue measured by (1) H MRS at 3T. *J Magn Reson Imaging* 45 (5):1455-1463. doi:10.1002/jmri.25453
9. Hong CW, Mamidipalli A, Hooker JC, Hamilton G, Wolfson T, Chen DH, Fazeli Dehkordy S, Middleton MS, Reeder SB, Loomba R, Sirlin CB (2018) MRI proton density fat fraction is robust across the biologically plausible range of triglyceride spectra in adults with nonalcoholic steatohepatitis. *J Magn Reson Imaging* 47 (4):995-1002. doi:10.1002/jmri.25845
10. Benkert T, Feng L, Sodickson DK, Chandarana H, Block KT (2017) Free-breathing volumetric fat/water separation by combining radial sampling, compressed sensing, and parallel imaging. *Magn Reson Med* 78 (2):565-576. doi:10.1002/mrm.26392

11. Armstrong T, Ly KV, Ghahremani S, Calkins KL, Wu HH (2019) Free-breathing 3-D quantification of infant body composition and hepatic fat using a stack-of-radial magnetic resonance imaging technique. *Pediatr Radiol* 49 (7):876-888. doi:10.1007/s00247-019-04384-7
12. Armstrong T, Dregely I, Stemmer A, Han F, Natsuaki Y, Sung K, Wu HH (2018) Free-breathing liver fat quantification using a multiecho 3D stack-of-radial technique. *Magn Reson Med* 79 (1):370-382. doi:10.1002/mrm.26693
13. Liu CY, McKenzie CA, Yu H, Brittain JH, Reeder SB (2007) Fat quantification with IDEAL gradient echo imaging: correction of bias from T(1) and noise. *Magn Reson Med* 58 (2):354-364. doi:10.1002/mrm.21301
14. Yang IY, Cui Y, Wiens CN, Wade TP, Friesen-Waldner LJ, McKenzie CA (2014) Fat fraction bias correction using T1 estimates and flip angle mapping. *J Magn Reson Imaging* 39 (1):217-223. doi:10.1002/jmri.24126
15. Sethi S, Giza SA, Goldberg E, Empey MET, de Ribaupierre S, Eastabrook GDM, de Vrijer B, McKenzie CA (2021) Quantification of 1.5 T T(1) and T(2)(*) Relaxation Times of Fetal Tissues in Uncomplicated Pregnancies. *J Magn Reson Imaging* 54 (1):113-121. doi:10.1002/jmri.27547
16. Hu HH, Yin L, Aggabao PC, Perkins TG, Chia JM, Gilsanz V (2013) Comparison of brown and white adipose tissues in infants and children with chemical-shift-encoded water-fat MRI. *J Magn Reson Imaging* 38 (4):885-896. doi:10.1002/jmri.24053
17. Rasmussen JM, Entringer S, Nguyen A, van Erp TG, Burns J, Guijarro A, Oveisi F, Swanson JM, Piomelli D, Wadhwa PD, Buss C, Potkin SG (2013) Brown adipose tissue quantification in human neonates using water-fat separated MRI. *PLoS One* 8 (10):e77907. doi:10.1371/journal.pone.0077907
18. Abe T, Thiebaud RS, Loenneke JP (2021) The Fat Fraction Percentage of White Adipose Tissue at various Ages in Humans: An Updated Review. *J Clin Densitom* 24 (3):369-373. doi:10.1016/j.jocd.2021.01.011
19. Zhao LP, Sheng XY, Zhou S, Yang T, Ma LY, Zhou Y, Cui YM (2015) Metformin versus insulin for gestational diabetes mellitus: a meta-analysis. *Br J Clin Pharmacol* 80 (5):1224-1234. doi:10.1111/bcp.12672
20. Sivalingam VN, Myers J, Nicholas S, Balen AH, Crosbie EJ (2014) Metformin in reproductive health, pregnancy and gynaecological cancer: established and emerging indications. *Hum Reprod Update* 20 (6):853-868. doi:10.1093/humupd/dmu037
21. Rowan JA, Rush EC, Obolonkin V, Battin M, Wouldes T, Hague WM (2011) Metformin in gestational diabetes: the offspring follow-up (MiG TOFU): body composition at 2 years of age. *Diabetes Care* 34 (10):2279-2284. doi:10.2337/dc11-0660

22. Bydder M, Girard O, Hamilton G (2011) Mapping the double bonds in triglycerides. *Magn Reson Imaging* 29 (8):1041-1046. doi:10.1016/j.mri.2011.07.004
23. Berglund J, Ahlström H, Kullberg J (2012) Model-based mapping of fat unsaturation and chain length by chemical shift imaging--phantom validation and in vivo feasibility. *Magn Reson Med* 68 (6):1815-1827. doi:10.1002/mrm.24196
24. Leporq B, Lambert SA, Ronot M, Vilgrain V, Van Beers BE (2014) Quantification of the triglyceride fatty acid composition with 3.0 T MRI. *NMR Biomed* 27 (10):1211-1221. doi:10.1002/nbm.3175
25. Leporq B, Lambert SA, Ronot M, Vilgrain V, Van Beers BE (2017) Simultaneous MR quantification of hepatic fat content, fatty acid composition, transverse relaxation time and magnetic susceptibility for the diagnosis of non-alcoholic steatohepatitis. *NMR Biomed* 30 (10). doi:10.1002/nbm.3766
26. Trinh L, Peterson P, Leander P, Brorson H, Månsson S (2020) In vivo comparison of MRI-based and MRS-based quantification of adipose tissue fatty acid composition against gas chromatography. *Magn Reson Med* 84 (5):2484-2494. doi:10.1002/mrm.28300
27. Peterson P, Trinh L, Månsson S (2021) Quantitative (1) H MRI and MRS of fatty acid composition. *Magn Reson Med* 85 (1):49-67. doi:10.1002/mrm.28471
28. Peterson P, Månsson S (2013) Simultaneous quantification of fat content and fatty acid composition using MR imaging. *Magn Reson Med* 69 (3):688-697. doi:10.1002/mrm.24297
29. Hamilton G, Smith DL, Jr., Bydder M, Nayak KS, Hu HH (2011) MR properties of brown and white adipose tissues. *J Magn Reson Imaging* 34 (2):468-473. doi:10.1002/jmri.22623

Appendices

Appendix A: Ethics approval notice. Signatures and addresses have been redacted.



**Western
Research**

Research Ethics

Use of Human Participants - Ethics Approval Notice

Principal Investigator: Dr. Barbra de Vrijer
File Number: 103845
Review Level: Full Board
Approved Local Adult Participants: 120
Approved Local Minor Participants: 0
Protocol Title: Development of Magnetic Resonance Imaging for Quantitative Assessment of Fetal Liver Fat
Department & Institution: Schulich School of Medicine and Dentistry\Obstetrics & Gynaecology, Western University
Sponsor:
Ethics Approval Date: September 03, 2013
Ethics Expiry Date: March 31, 2018

Documents Reviewed & Approved & Documents Received for Information:

Document Name	Comments	Version Date
Western University Protocol		
Letter of Information & Consent	study group	2013/07/24
Letter of Information & Consent	control group	2013/07/24

This is to notify you that the University of Western Ontario Health Sciences Research Ethics Board (HSREB) which is organized and operates according to the Tri-Council Policy Statement: Ethical Conduct of Research Involving Humans and the Health Canada/ICH Good Clinical Practice Practices: Consolidated Guidelines; and the applicable laws and regulations of Ontario has reviewed and granted approval to the above referenced study on the approval date noted above. The membership of this HSREB also complies with the membership requirements for REB's as defined in Division 5 of the Food and Drug Regulations.

The ethics approval for this study shall remain valid until the expiry date noted above assuming timely and acceptable responses to the HSREB's periodic requests for surveillance and monitoring information. If you require an updated approval notice prior to that time you must request it using the University of Western Ontario Updated Approval Request form.


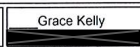

Member of the HSREB that are named as investigators in research studies, or declare a conflict of interest, do not participate in discussions related to, nor vote on, such studies when they are presented to the HSREB.

The Chair of the HSREB is Dr. Joseph Gilbert. The HSREB is registered with the U.S. Department of Health & Human Services under the IRB registration number IRB 00000940.

 _____

Signature

Ethics Officer to Contact for Further Information

 Erika Basile	 Grace Kelly	 Vikki Tran
--	---	---

This is an official document. Please retain the original in your files.

Appendix B: Waived Permission Request to reproduce paragraphs of content from the Journal of Developmental Origins of Health and Disease

CAMBRIDGE | Rights & Permissions
[Home](#) > [Rights & Permissions](#) > Permission requests from authors

Rights & Permissions

- [Rights homepage](#)
- [Permissions homepage](#)
- [Permission requests](#)
- [Permission requests from authors](#)
- [Networking requests](#)
- [Educational photocopying requests](#)
- [Links](#)

Contacts

- [Cambridge office](#)
- [New York office](#)
- [Melbourne office](#)
- [Madrid office](#)

Permission requests from authors

In certain circumstances, permission requests are not required from authors, who wish to reuse original material they have written for a Cambridge publication, provided that the subsequent use includes a full acknowledgement of the original publication together with the copyright notice and the phrase 'Reprinted with permission'.

Permission requests are waived if:

- The author wishes to reproduce a single chapter (not exceeding 20% of his/her work), journal article or shorter extract in a subsequent work (i.e. with a later publication date) of which he or she is to be the author, co-author or editor.
- The author wishes to photocopy a single chapter (not exceeding 20% of his/her work as a whole), journal article or shorter extract for his/her own teaching purposes, provided that such photocopies are not made available for sale.
- The author wishes to reproduce a single chapter (not exceeding 20% of his/her work as a whole), journal article or shorter extract on his/her personal or institution web site for teaching and research purposes.

For all other uses, permission is required, and the author or the author's publisher should refer to the [Permission requests](#) section.

© Cambridge University Press . [Copyright statement](#) | [Privacy Policy](#)

Appendix C Permission to reprint figure from the British Medical Bulletin in Chapter 1, Figure 1.2. Addresses have been redacted.

OXFORD UNIVERSITY PRESS LICENSE
TERMS AND CONDITIONS

Apr 21, 2023

This Agreement between Ms. Stephanie Giza ("You") and Oxford University Press ("Oxford University Press") consists of your license details and the terms and conditions provided by Oxford University Press and Copyright Clearance Center.

License Number	5532040008641
License date	Apr 18, 2023
Licensed content publisher	Oxford University Press
Licensed content publication	British Medical Bulletin
Licensed content title	THE STRUCTURE AND FUNCTION OF BROWN ADIPOSE TISSUE
Licensed content author	HULL, DAVID
Licensed content date	Jan 1, 1966
Type of Use	Thesis/Dissertation
Institution name	
Title of your work	Water-fat magnetic resonance imaging for the assessment of human fetal adipose tissue

Publisher of your work	The University of Western Ontario
Expected publication date	Jul 2023
Permissions cost	0.00 USD
Value added tax	0.00 USD
Total	0.00 USD
Title	Water-fat magnetic resonance imaging for the assessment of human fetal adipose tissue
Institution name	The University of Western Ontario
Expected presentation date	Jul 2023
Order reference number	13
Portions	Plate III, Figure D
Requestor Location	Ms. Stephanie Giza [REDACTED]
	[REDACTED] Attn: Ms. Stephanie Giza
Publisher Tax ID	GB125506730
Total	0.00 USD

Appendix D: Permission to reprint figure from the Magnetic Resonance in Medicine in Chapter 1, Figure 1.4. Addresses have been redacted.

JOHN WILEY AND SONS LICENSE
TERMS AND CONDITIONS

Apr 18, 2023

This Agreement between Ms. Stephanie Giza ("You") and John Wiley and Sons ("John Wiley and Sons") consists of your license details and the terms and conditions provided by John Wiley and Sons and Copyright Clearance Center.

License Number 5532080632036

License date Apr 18, 2023

Licensed
Content
Publisher John Wiley and Sons

Licensed
Content
Publication Magnetic Resonance in Medicine

Licensed
Content Title Model-based mapping of fat unsaturation and chain length by chemical shift imaging—phantom validation and in vivo feasibility

Licensed
Content Author Joel Kullberg, Håkan Ahlström, Johan Berglund

Licensed
Content Date Feb 14, 2012

Licensed
Content Volume 68

Licensed
Content Issue 6

Licensed
Content Pages 13

Type of use Dissertation/Thesis

Requestor type University/Academic

Format Print and electronic

Portion Figure/table

Number of
figures/tables 1

Will you be
translating? No

Title Water-fat magnetic resonance imaging for the assessment of human fetal
adipose tissue

Institution name The University of Western Ontario

Expected
presentation
date Jul 2023

Order reference
number 14

Portions Figure 1

Requestor
Location Ms. Stephanie Giza
[REDACTED]
[REDACTED]
Attn: Ms. Stephanie Giza

Publisher Tax
ID EU826007151

Total 0.00 USD

Appendix E: Permission to reprint article from the Journal of Maternal-Fetal and Neonatal Medicine in Chapter 2. Email addresses, addresses, and phone numbers have been redacted.

Subject: Permission to Use J Matern Fetal Neonatal Med Copyrighted Material in a Doctoral Thesis [ref:_00D0Y35Iji._5007TMVsLc:ref]
Date: Monday, June 19, 2023 at 6:02:00 AM Eastern Daylight Time
From: T&F Journal Permission Request
To: Stephanie Ann Giza

You don't often get email from [REDACTED]. [Learn why this is important](#)



Our Ref: sm/Perm/03076676

19/06/2023

Dear Stephanie Giza,

Licensed Content:

Article title: Measuring fetal adipose tissue using 3D water-fat magnetic resonance imaging: a feasibility study

Article DOI: [10.1080/14767058.2018.1506438](https://doi.org/10.1080/14767058.2018.1506438)

Author name: Stephanie A. Giza, Craig Olmstead, Daniel A. McCooeye, Michael R. Miller, Deborah A. Penava, Genevieve D. Eastabrook, Charles A. McKenzie & Barbra de Vrijer

Journal title: Maternal-Fetal & Neonatal Medicine

Volume number: 33

Issue number: 5

Year of publication: 2020

Thank you for your correspondence requesting permission to reproduce your **authors accepted manuscript** from our Journal in your thesis and to be posted in the university's repository – University of Western Ontario (London, Ontario, Canada)

We will be pleased to grant permission to reproduce your '**Accepted Manuscript**' on the sole condition that you acknowledge the original source of publication.

This is an '**Author's Accepted Manuscript**' of an article published by Taylor & Francis Group in [JOURNAL TITLE] on [DATE], available online: [https://www.tandfonline.com/\[Article DOI\]](https://www.tandfonline.com/[Article DOI])."

Using a DOI to link to the VoR on Taylor & Francis Online means that downloads, Altmetric data, and citations can be tracked and collated – data you can use to assess the impact of your work.

Please see information for sharing versions your work

<https://authorservices.taylorandfrancis.com/research-impact/sharing-versions-of-journal-articles/>

This permission does not cover any third party copyrighted work which may appear in the material requested. Please ensure you have checked all original source details for the rights holder.

Further permission will be required if your thesis is published.

Please note: This **does not allow** the use of the **Version of Record (VoR)** to be posted online, however you may include the VoR as an Appendix to the printed version of your thesis.

(VoR is the final, definitive, citable version of your paper, which has been copyedited, typeset, had metadata applied, and has been allocated a DOI (Digital Object Identifier).

This permission does not cover any third party copyrighted work which may appear in the material requested. Please ensure you have checked all original source details for the rights holder.

Please do not hesitate to let me know if I can be of further assistance.

Thank you for your interest in our Journals.


Yours sincerely

Susan McCarthy | Permissions Administrator, Journals



Taylor & Francis is a trading name of Informa UK Limited,
registered in England under no. 1072954

Disclaimer: T&F publish Open Access articles in our subscription priced journals, please check if the article you are interested in is an OA article and if so, which license was it published under.

 Before printing, think about the environment.

----- Original Message -----

From: Stephanie Ann Giza [redacted]

Sent: 17/04/2023 16:09

To: [redacted]

Subject: Permission to Use J Matern Fetal Neonatal Med Copyrighted Material in a Doctoral Thesis

Hello,

I am a graduate student at the University of Western Ontario (London, Ontario, Canada) completing my Doctoral thesis entitled "Water-fat magnetic resonance imaging for the assessment of human fetal adipose tissue". My thesis will be available in full-text on the internet for reference, study and/or copy. Except in situations where a thesis is under embargo or restriction, the electronic version will be accessible through the Western Libraries web pages, the Library's web catalogue, and also through web search engines. I will also be granting Library and Archives Canada and ProQuest/UMI a non-exclusive license to reproduce, load, distribute, or sell single copies of my thesis by any means and in any form or format. These rights will in no way restrict republication of the material in any other form by you or by others authorized by you.

I would like permission to allow inclusion of the following material in my thesis which has been published in the Journal of Maternal-Fetal and Neonatal Medicine:

SA Giza, C Olmstead, DA McCooey, MR Miller, DA Penava, GD Eastabrook, CA McKenzie, B de Vrijer. Measuring fetal adipose tissue using 3D water-fat magnetic resonance imaging: a feasibility study. J Matern Fetal Neonatal Med. 2020 Mar;33(5):831-837. <https://doi.org/10.1080/14767058.2018.1506438>.

The material will be attributed through a citation.

Please confirm in writing or by email that these arrangements meet with your approval.

Sincerely,

Stephanie Giza

Appendix F: Permission to reprint article from the Journal of Magnetic Resonance Imaging in Chapter 3. Addresses have been redacted.

JOHN WILEY AND SONS LICENSE
TERMS AND CONDITIONS

Feb 21, 2023

This Agreement between Ms. Stephanie Giza ("You") and John Wiley and Sons ("John Wiley and Sons") consists of your license details and the terms and conditions provided by John Wiley and Sons and Copyright Clearance Center.

License Number 5493810405611

License date Feb 21, 2023

Licensed
Content
Publisher John Wiley and Sons

Licensed
Content
Publication Journal of Magnetic Resonance Imaging

Licensed
Content Title Comparison of modified two-point dixon and chemical shift encoded MRI water-fat separation methods for fetal fat quantification

Licensed
Content Author Stephanie A. Giza, Michael R. Miller, Prasiddha Parthasarathy, et al

Licensed
Content Date Jan 10, 2018

Licensed
Content Volume 48

Licensed
Content Issue 1

Licensed
Content Pages 9

Type of use Dissertation/Thesis

Requestor type Author of this Wiley article

Format Print and electronic

Portion Full article

Will you be
translating? No

Title Water-fat magnetic resonance imaging for the assessment of human fetal
adipose tissue

Institution name The University of Western Ontario

Expected
presentation
date Jul 2023

Order reference
number 12

Requestor
Location Ms. Stephanie Giza
[REDACTED]
[REDACTED]
Attn: Ms. Stephanie Giza

Publisher Tax
ID EU826007151

Total 0.00 CAD

**Appendix G: Permission to reprint article from Pediatric Radiology in Chapter 4.
Addresses have been redacted.**

SPRINGER NATURE LICENSE
TERMS AND CONDITIONS

Feb 21, 2023

This Agreement between Ms. Stephanie Giza ("You") and Springer Nature ("Springer Nature") consists of your license details and the terms and conditions provided by Springer Nature and Copyright Clearance Center.

License Number	5493800209890
License date	Feb 21, 2023
Licensed Content Publisher	Springer Nature
Licensed Content Publication	Pediatric Radiology
Licensed Content Title	Water-fat magnetic resonance imaging of adipose tissue compartments in the normal third trimester fetus
Licensed Content Author	Stephanie A. Giza et al
Licensed Content Date	Jan 29, 2021
Type of Use	Thesis/Dissertation
Requestor type	academic/university or research institute
Format	print and electronic
Portion	full article/chapter

Will you be translating? no

Circulation/distribution 200 - 499

Author of this Springer Nature content yes

Title Water-fat magnetic resonance imaging for the assessment of human fetal adipose tissue

Institution name The University of Western Ontario

Expected presentation date Jul 2023

Order reference number 11

Ms. Stephanie Giza



Requestor Location



Attn: Ms. Stephanie Giza

Total 0.00 CAD

Curriculum Vitae

Name: Stephanie Giza

Post-secondary Education and Degrees: The University of Western Ontario
London, Ontario, Canada
2010-2015 B.Sc.

The University of Western Ontario
London, Ontario, Canada
2015-2023 Ph.D.

Honours and Awards: Natural Science and Engineering Research Council of Canada (NSERC)
Alexander Graham Bell Canadian Graduate Scholarship – Doctoral (105,000 CAD)
2018-2023

International Society for Magnetic Resonance in Medicine
Educational Stipend (475 USD)
2023, 2017, 2016

Imaging Network Ontario Oral Award Honorable Mention
2018

Ontario Ministry of Advanced Education and Skills Development
Queen Elizabeth II Graduate Scholarship in Science and Technology
2017-2018

London Imaging Discovery Day 2nd Poster Award (150 CAD)
2017

Ontario Ministry of Training, Colleges & Universities
Ontario Graduate Scholarship
2015-2016

International Fetal Growth Meeting
Mount Sinai Hospital Maternal Fetal Medicine Award (500 CAD)
2016

Natural Sciences and Engineering Research Council of Canada (NSERC)
Industrial Undergraduate Student Research Award (4,500 CAD)

2015, 2014, 2013

Natural Sciences and Engineering Research Council of Canada
(NSERC)

Undergraduate Student Research Award (declined)
2015

The University of Western Ontario
Dean's Honour List

2014-2015, 2012-2013, 2011-2012, 2010-2011

The University of Western Ontario
Entrance Scholarship (2,000 CAD)
2010-2011

**Related Work
Experience:**

Teaching Assistant
The University of Western Ontario
2017-2018, 2020, 2022

Research Intern
A&L Biologicals
2013-2014, 2015

Publications:

1. Simran Sethi, Stephanie A. Giza, Estee Goldberg, Mary-Ellen E.T. Empey, Sandrine de Ribaupierre, Genevieve D. Eastabrook, Barbra de Vrijer, Charles A. McKenzie. Quantification of T1 and T2* Relaxation Times of Fetal Tissues at 1.5T. *Journal of Magnetic Resonance Imaging*. 2021 Jul;54(1):113-121. doi: 10.1002/jmri.27547
2. Stephanie A. Giza, Tianna L. Koreman, Simran Sethi, Michael R. Miller, Debbie A. Penava, Genevieve D. Eastabrook, Charles A. McKenzie, Barbra de Vrijer. Water-Fat MRI of Adipose Tissue Compartments in the Normal, Third Trimester Fetus. *Pediatric Radiology*. 2021 Jun;51(7):1214-1222. doi: 10.1007/s00247-020-04955-z
3. Stephanie A. Giza, Simran Sethi, Lauren M. Smith, Mary-Ellen E.T. Empey, Lindsay E. Morris, Charles A. McKenzie. The Application of *In-Utero* Magnetic Resonance Imaging in the Study of Developmental Origins of Health and Disease. *Journal of Developmental Origins of Health and Disease*. 2021 Apr;12(2):193-202. doi: 10.1017/S2040174420001154
4. Stephanie A. Giza, Craig Olmstead, Daniel McCooeye, Michael R. Miller, Debbie Penava, Genevieve Eastabrook, Charles A. McKenzie, Barbra de Vrijer. Measuring fetal adipose tissue growth using 3D water-fat magnetic resonance

imaging: A feasibility study. *Journal of Maternal-Fetal & Neonatal Medicine*. 2020 Mar; 33(5):831-837. doi: 10.1080/14767058.2018.1506438

5. Flavien Delhaes*, Stephanie A. Giza*, Tianna Koreman, Genevieve Eastabrook, Charles A. McKenzie, Samantha Bedell, Timothy R.H. Regnault, Barbra de Vrijer. Altered Maternal and Placental Lipid Metabolism and Fetal Fat Development in Obesity: Current Knowledge and Advances in Non-Invasive Assessment. *Placenta*. 2018 Sep; 69:118-124. doi: 10.1016/j.placenta.2018.05.011
* authors contributed equally to this work
6. Stephanie A. Giza, Michael R. Miller, Prasiddha Parthasarathy, Barbra de Vrijer, Charles A. McKenzie. Comparison of modified two-point Dixon and chemical shift encoded MRI water-fat separation methods for fetal fat quantification. *Journal of Magnetic Resonance Imaging*. 2018 Jul; 48(1):274-282. doi: 10.1002/jmri.25929
7. Stephanie A. Giza, Tianna L. Koreman, Michael R. Miller, Simran Sethi, Genevieve D. Eastabrook, Debbie A. Penava, Charles A. McKenzie, Barbra de Vrijer. Clinical Correlations with Fetal Adipose Tissue as Quantified by Magnetic Resonance Imaging. Revisions submitted to *Pediatric Radiology*. PRAD-D-23-00059

Research Funding Applications:

Children's Health Research Institute Translational Research Grant Fund (*Successful*)
Impact of Metformin and Insulin on Fetal Fat Development in Diabetic Pregnancies
30,000 CAD
2018

Abstracts and Presentations:

1. Stephanie A. Giza, Simran Sethi, Genevieve Eastabrook, Barbra de Vrijer, Charles A. McKenzie. (2023) Increasing Signal of Water-Fat MRI for Imaging Fetal Adipose Tissue. Canadian National Perinatal Research Meeting.
Abstract presented as poster presentation in Montebello, Quebec, Canada (2023)
2. Stephanie A. Giza, Charles A. McKenzie, Barbra de Vrijer. (2023) Using new technologies to assess fetal adipose tissue development and programming: Water-fat MRI. Canadian National Perinatal Research Meeting.
Abstract presented as poster presentation in Montebello, Quebec, Canada (2023)
3. Stephanie A. Giza, Simran Sethi, Genevieve Eastabrook, Barbra de Vrijer, Charles A. McKenzie. (2022) High Flip Angle Chemical-Shift Encoded MRI for Imaging Fetal Adipose Tissue. International Society for Magnetic Resonance in Medicine.
Abstract presented as poster presentation in Toronto, Ontario, Canada (2023)

Published in Proceedings of the International Society for Magnetic Resonance in Medicine

4. Stephanie A. Giza, Tianna L. Koreman, Michael R. Miller, Simran Sethi, Genevieve Eastabrook, Debbie Penava, Charles A. McKenzie, Barbra de Vrijer. (2020) Maternal Obesity, Excess Gestational Weight Gain and Gestational Diabetes do not Predict Fetal Subcutaneous Adipose Tissue Measurements by Water-Fat MRI. Canadian National Perinatal Research Meeting. *Abstract presented as poster presentation at virtual meeting (2021)*
5. Simran Sethi, Stephanie A. Giza, Mary-Ellen E. Empey, Liz Lorusso, Barbra de Vrijer, Charles A. McKenzie. (2020) Quantification of T1 and T2* Relaxation Times of Fetal Adipose Tissue & Fetal Muscles at 1.5 T. Wavelengths 2020. *Abstract presented as poster presentation by Simran Sethi (2020)*
6. Simran Sethi, Stephanie A. Giza, Mary-Ellen E. Empey, Barbra de Vrijer, Charles A. McKenzie. (2020) Quantification of T1 and T2* Relaxation Times of Fetal Adipose Tissue & Fetal Muscles at 1.5 T. Imaging Network of Ontario. *Abstract presented as poster presentation by Simran Sethi (2020)*
7. Stephanie A. Giza, Simran Sethi, Barbra de Vrijer, Charles A. McKenzie. (2019) Challenges of Identifying Human Fetal Brown Adipose Tissue using MRI. In-Utero MRI 2020. *Abstract presented as oral and poster presentation in Oxford, United Kingdom (2020)*
8. Simran Sethi, Stephanie A. Giza, Mary-Ellen E. Empey, Barbra de Vrijer, Charles A. McKenzie. (2019) Quantification of T1 and T2* Relaxation Times of Fetal Fat & Fetal Muscles at 1.5 T. In-Utero MRI 2020. *Abstract presented as PowerPitch (poster) presentation by Simran Sethi (2020)*
9. Stephanie A. Giza, Genevieve Eastabrook, Barbra de Vrijer, Charles A. McKenzie. (2019) Challenges of Identifying Human Fetal Brown Adipose Tissue using MRI. ISMRM Workshop on MRI of Obesity & Metabolic Disorders. *Abstract presented as PowerPitch (Poster) presentation by Charles McKenzie (2019)*
10. Simran Sethi, Stephanie A. Giza, Mary-Ellen E. T. Empey, Barbra de Vrijer, Charles A. McKenzie. (2019) Quantification of T1 and T2* Relaxation Times of Fetal Tissues at 1.5 T. London Imaging Discovery Day. *Abstract presented as oral presentation by Simran Sethi (2019)*
11. Simran Sethi, Stephanie A. Giza, Mary-Ellen E. T. Empey, Barbra de Vrijer, Charles A. McKenzie. (2019) Quantification of T1 and T2* Relaxation Times of Fetal Tissues at 1.5 T. London Health Research Day. *Abstract presented as poster presentation by Simran Sethi (2019)*

12. Simran Sethi, Stephanie A. Giza, Mary-Ellen E. T. Empey, Barbra de Vrijer, Charles A. McKenzie. (2019) Quantification of T1 and T2* Relaxation Times of Fetal Tissues at 1.5 T. Imaging Network Ontario.
Abstract presented as oral presentation by Simran Sethi (2019)

13. Simran Sethi, Stephanie A. Giza, Mary-Ellen E. Empey, Barbra de Vrijer, Charles A. McKenzie. (2019) Quantifying T1 and T2* Relaxation Times of Fetal Fat, Fetal Liver, Fetal Kidney, and Amniotic Fluid at 1.5T. International Society for Magnetic Resonance in Medicine.
Abstract presented as oral presentation by Simran Sethi (2019)
Published in Proceedings of the International Society for Magnetic Resonance in Medicine

14. Stephanie A. Giza, Tianna Koreman, Barbra de Vrijer, Charles A. McKenzie. (2018) 3D Water-Fat MRI Detection of Developmental Maturity in Fetal Adipose Tissue Compartments. Paul Harding Research Awards Day.
Abstract presented as oral presentation in London, Ontario, Canada (2018)

15. Tianna L Koreman, Stephanie A Giza, Genevieve Eastabrook, Debbie Penava, Charles A McKenzie, Barbra de Vrijer. (2017) Fetal subcutaneous fat by 3D Water-fat MRI is independent of maternal obesity, excessive pregnancy weight gain and diabetes. Paul Harding Research Awards Day.
Abstract presented as poster presentation by Tianna Koreman (2018)

- Stephanie A. Giza, Simran Sethi, Takashi Hashimoto, Barbra de Vrijer, Charles A. McKenzie. (2018) Non-alcoholic Fatty Liver Disease Assessment in Obese and Non-obese Pregnant Women with Water-Fat MRI. Imaging Network Ontario.
Abstract presented as poster presentation in Toronto, Ontario, Canada (2018)

16. Stephanie A. Giza, Tianna Koreman, Barbra de Vrijer, Charles A. McKenzie. (2018) 3D Water-Fat MRI Detection of Developmental Maturity in Fetal Adipose Tissue Compartments. Imaging Network Ontario.
Abstract presented as oral presentation in Toronto, Ontario, Canada (2018) and awarded Oral Award

17. Tianna L Koreman, Stephanie A Giza, Genevieve Eastabrook, Debbie Penava, Charles A McKenzie, Barbra de Vrijer. (2017) Fetal subcutaneous fat by 3D Water-fat MRI is independent of maternal obesity, excessive pregnancy weight gain and diabetes. Society of Obstetricians and Gynaecologists of Canada
Abstract presented as poster presentation by Tianna Koreman (2018)

18. Stephanie A. Giza, Simran Sethi, Takashi Hashimoto, Barbra de Vrijer, Charles A. McKenzie. (2017) Non-alcoholic Fatty Liver Disease Assessment in Obese and Non-obese Pregnant Women with Water-Fat MRI. International Society for

Magnetic Resonance in Medicine.

Abstract presented as poster presentation by Simran Sethi (2018)

Published in Proceedings of the International Society for Magnetic Resonance in Medicine

19. Stephanie A. Giza, Tianna L. Koreman, Barbra de Vrijer, Charles A. McKenzie. (2017) 3D Water-Fat MRI Detection of Developmental Maturity in Fetal Adipose Tissue Compartments. International Society for Magnetic Resonance in Medicine.
Abstract presented as poster presentation by Charles McKenzie (2018)
Published in Proceedings of the International Society for Magnetic Resonance in Medicine

20. Stephanie A Giza, Craig Olmstead, Daniel McCooye, Conrad P Rockel, Alireza Akbari, Trevor P Wade, Debbie Penava, Timothy RH Regnault, Genevieve E Eastabrook, Charles A McKenzie, Barbra de Vrijer. (2017) Quantification of Fetal Fat Development in Mid-Late Gestation using 3D Water-Fat MRI. London Imaging Discovery Day.
Abstract presented as oral presentation in London, Ontario, Canada (2017) and awarded Poster Award

21. Stephanie A Giza, Craig Olmstead, Daniel McCooye, Conrad P Rockel, Alireza Akbari, Trevor P Wade, Debbie Penava, Timothy RH Regnault, Genevieve E Eastabrook, Charles A McKenzie, Barbra de Vrijer. (2017) Quantification of Fetal Fat Development in Mid-Late Gestation using 3D Water-Fat MRI. Paul Harding Research Awards Day.
Abstract presented as oral presentation in London, Ontario, Canada (2017)

22. Stephanie Giza, Barbra de Vrijer, Charles McKenzie. (2017). Comparison between 2-point Dixon and Quantitative IDEAL for Magnetic Resonance Imaging of Fetal Adipose Tissue. London Health Research Day.
Abstract presented as poster presentation in London, Ontario, Canada (2017)

23. Daniel McCooye, Stephanie Giza, Craig Olmstead, Barbra de Vrijer, Charles McKenzie. (2017). Impact of Motion and Maternal BMI on Segmentation in Fetal MRI. London Health Research Day.
Abstract presented as poster presentation by Daniel McCooye (2017)

24. Stephanie Giza, Barbra de Vrijer, Charles McKenzie. (2017). Comparison between 2-point Dixon and Quantitative IDEAL for Magnetic Resonance Imaging of Fetal Adipose Tissue. Imaging Network Ontario.
Abstract presented as oral presentation in London, Ontario, Canada (2017)

25. Daniel McCooye, Stephanie Giza, Craig Olmstead, Barbra de Vrijer, Charles McKenzie. (2017). Impact of Motion and Maternal BMI on Segmentation in Fetal MRI. Imaging Network Ontario.

Abstract presented as poster presentation by Daniel McCooeye (2017)

26. Barbra de Vrijer, Stephanie Giza, Craig Olmstead, Debbie Penava, Genevieve Eastabrook, Timothy Regnault, Charles A McKenzie. (2016). Insight Inside: Imaging fetal adipose tissue development with 3D water-fat MRI. Sociedad Latinoamericana de Investigaciones Materno-fetales y Placenta
Invited Oral Presentation for Dr. de Vrijer (2017)
27. Barbra de Vrijer, Stephanie Giza, Craig Olmstead, Debbie Penava, Genevieve Eastabrook, Timothy Regnault, Charles McKenzie. (2016). Imaging fetal subcutaneous fat development using 3D water-fat MRI. Society of Obstetricians and Gynaecologists of Canada
Abstract presented as oral presentation by Barbra de Vrijer (2017)
28. Stephanie Giza, Craig Olmstead, Timothy Regnault, Debbie Penava, Genevieve Eastabrook, Charles McKenzie, Barbra de Vrijer. (2016). 3D Water-Fat MRI of Fetal Fat Development. Canadian National Perinatal Research Meeting.
Abstract presented as oral presentation in Montebello, Quebec, Canada (2017)
29. Stephanie A Giza, Barbra de Vrijer, Charles A McKenzie. (2016). Pseudo-fat in the fetal liver with two-point Dixon water-fat separation. Journal of Magnetic Resonance Imaging, Magnetic Resonance in Medicine. International Society for Magnetic Resonance in Medicine
Abstract presented as poster presentation in Honolulu, Hawaii, USA (2017)
Published in Proceedings of the International Society for Magnetic Resonance in Medicine
30. Stephanie Giza, Craig Olmstead, Debbie Penava, Genevieve Eastabrook, Charles A McKenzie, Barbra de Vrijer. (2016). A Quantitative Tool for the Study of Adipose Tissue Development *in Utero*: 3D Water-Fat MRI. International Fetal Growth Meeting
Abstract presented as oral presentation in Toronto, Ontario, Canada (2016) and awarded Trainee Award
31. Stephanie Giza, Craig Olmstead, Charles McKenzie, Barbra de Vrijer. (2016). Feasibility of Fetal Fat Quantification in High BMI Patients using MRI. London Imaging Discovery Day
Abstract presented as oral presentation in London, Ontario, Canada (2016)
32. Stephanie Giza, Craig Olmstead, Charles McKenzie, Barbra de Vrijer. (2016). Feasibility of Fetal Fat Quantification in High BMI Patients using MRI. London Health Research Day
Abstract presented as poster presentation in London, Ontario, Canada (2016)
33. Stephanie Giza, Craig Olmstead, Kevin Sinclair, Charles A McKenzie, Barbra de Vrijer. (2015). Feasibility of Fetal Fat Volume Assessment using 3D Water-Fat

MRI. *Journal of Magnetic Resonance Imaging, Magnetic Resonance in Medicine. International Society for Magnetic Resonance in Medicine*
Abstract presented as poster presentation in Singapore (2016)
Published in Proceedings of the International Society for Magnetic Resonance in Medicine

34. Stephanie Giza, Craig Olmstead, Charles McKenzie, Barbra de Vrijer. (2015).
Feasibility of Fetal Fat Quantification in High BMI Patients using MRI.
Reproductive Sciences. Society for Reproductive Investigation
Abstract presented as poster presentation in Montreal, Quebec, Canada (2016)
Published in Reproductive Sciences

Invited Presentations:

1. “Characterizing Fetal Adipose Tissue Development with Water-Fat MRI”
A.C. Burton Day, Department of Medical Biophysics, University of Western Ontario (2021)
2. “An Introduction to MRI for Clinicians”
Fetal and Neonatal Neuroimaging Rounds, London Health Sciences Centre